Technische Universität München
TUM Campus Straubing für Biotechnologie und Nachhaltigkeit

Process engineering of *Vibrio natriegens* for the production of organic acids

Clarissa Viktoria Scheuchenegger

Vollständiger Abdruck der von dem TUM Campus Straubing für Biotechnologie und Nachhaltigkeit der Technischen Universität München zur Erlangung einer

Doktorin der Naturwissenschaften (Dr. rer. nat)

genehmigten Dissertation.

Vorsitz: Prof. Dr. Henrike Niederholtmeyer

Prüfende der Dissertation:

1. Prof. Dr. Bastian Blombach
2. Prof. Dr.-Ing. Michael Zavrel

Die Dissertation wurde am 03.07.2024 bei der Technischen Universität München eingereicht und durch den TUM Campus Straubing für Biotechnologie und Nachhaltigkeit am 19.11.2024 angenommen.

Motivation and objective

A sustainable lifestyle and the green production of goods are increasingly becoming the focus of society, which is confronted with the rapidly advancing climate change coupled with the dependency on finite resources and environmental pollution. Microbial biotechnology is part of the solution as it focuses on the sustainable production of chemicals and fuels from renewable resources using tailor-made production strains.

This work deals with the production of succinate and pyruvate from glucose using engineered *Vibrio natriegens* strains and with obstacles arising from byproducts such as exopolysaccharides.

Succinate belongs to the group of C4-dicarboxylates and has been ranked by the U.S. Department of Energy among the top twelve building block chemicals that can be converted into high-value bio-based chemicals, including biodegradable plastic (Werpy and Petersen, 2004; Cao *et al.*, 2013). Its manufacture is mainly satisfied by chemical synthesis from fossil fuels, and hence its production is dependent on finite resources and comes with high environmental costs, mainly in the form of CO_2 (Okino *et al.*, 2008). Thus, microbial production is preferable, and furthermore, CO_2 is assimilated during the anaerobic formation of succinate (Sauer *et al.*, 2008).

V. natriegens is an attractive host for biotechnology due to its high growth and substrate consumption rates, and in addition, the marine bacterium has attracted much attention by demonstrating exceptionally high volumetric productivities (Hoffart *et al.*, 2017; Thoma *et al.*, 2021). This makes *V. natriegens* the perfect candidate to realize the aim of this work: the development of a suitable production process for succinate that does not rely on the addition of expensive supplements such as yeast extract or vitamins.

Another target of this study was the establishment of a production process for pyruvate. Pyruvate is an important key element of the central metabolism and is therefore the optimal precursor for a huge variety of different products, including carbohydrates, amino and fatty acids, as well as alcohols. Due to this diversity, many applications are possible, but the pharmaceutical, cosmetic and food industries in particular benefit from the valuable properties of pyruvate. Pyruvate is regarded as safe by the European Food Safety Authority and is mainly applied as a dietary supplement for weight loss or as a cosmetic agent for skin treatments (EFSA, 2009; Maleki and Eiteman, 2017; Yuan *et al.*, 2022). However, there are many downsides to its production. Pyruvate is mainly generated by chemical synthesis from tartaric acid, which is accompanied by serious environmental issues in addition to being cost-inefficient. A sustainable approach with the greatest potential for a clean and cost-effective production of pyruvate is direct fermentation, and the establishment of such a production process for *V. natriegens* was precisely the aim of this work.

Funding and scientific contribution

The experimental work for this manuscript was performed under the direction and supervision of Prof. Dr. Bastian Blombach at the Professorship Microbial Biotechnology at the Technical University of Munich, Campus Straubing for Biotechnology and Sustainability in the time frame of 2019 to 2023.
This work was funded by the German Research Foundation (DFG) as part of the project “VPower” (grant BL1408/2-1).
Parts of this work have already been published in peer-reviewed journals or made available to the public in the form of talks or poster presentations at international conferences and have been partially incorporated identically in this manuscript.

Peer-reviewed scientific articles

Schulze C, Hädrich M, Borger J, Rühmann B, Döring M, Sieber V, Thoma F, Blombach B. Investigation of exopolysaccharide formation and its impact on anaerobic succinate production with *Vibrio natriegens*. Microbial Biotechnology 2024 Jan;17(1):e14277. doi: 10.1111/1751-7915.14277

Thoma F, **Schulze C**, Gutierrez-Coto C, Hädrich M, Huber J, Gunkel C, Thoma R, Blombach B. Metabolic engineering of *Vibrio natriegens* for anaerobic succinate production. Microbial Biotechnology 2022 Jun;15(6):1671-1684. doi: 10.1111/1751-7915.13983

Conference talks

Schulze C, Hädrich M, Borger J, Rühmann B, Thoma F, Blombach B. Impact of exopolysaccharide formation on succinate production with *Vibrio natriegens*. 1st Minisymposium UNESP-TUM, 14.11.2023. Araraquara, Brazil.

Schulze C, Hädrich M, Borger J, Rühmann B, Thoma F, Blombach B. Impact of exopolysaccharide formation on succinate production with *Vibrio natriegens*. Vnat 2023 conference, 14.03.2023. web conference, Germany.

Schulze C, Hädrich M, Thoma F, Blombach B. Investigation of exopolysaccharide formation in *Vibrio natriegens*. Vnat 2022 conference, 03.03.2022. web conference, Germany.

Poster presentation

Schulze C, Hädrich M, Borger J, Rühmann B, Döring M, Sieber V, Thoma F, Blombach B. Investigation of exopolysaccharide formation and its impact on anaerobic succinate production with *Vibrio natriegens*. VAAM annual conference, 11.09.2023. Göttingen, Germany.

Schulze C, Hädrich M, Borger J, Rühmann B, Döring M, Sieber V, Thoma F, Blombach B. Investigation of exopolysaccharide formation and its impact on anaerobic succinate production with *Vibrio natriegens*. DECHEMA Himmelfahrtstagung, 15.05.2023. Weimar, Germany.

Schulze C, Hädrich M, Borger J, Rühmann B, Sieber V, Thoma F, Blombach B. Investigation of exopolysaccharide formation in *Vibrio natriegens*. Key Technologies in the Bioeconomy 2022, 27 – 29.09.2022. Straubing, Germany.

Schulze C, Hädrich M, Borger J, Rühmann B, Sieber V, Thoma F, Blombach B. Domestication of *Vibrio natriegens* for industrial biotechnology. DECHEMA Himmelfahrtstagung on Bioprocess Engineering, 23.05.2022. Mainz, Germany.

Hädrich M, **Schulze C**, Thoma F, Blombach B. Low-biomass concept for industrial biotechnology with engineered *Vibrio natriegens*. VAAM annual conference. 22.02.2022. web conference, Germany.

Author´s contribution and involved associates

The manuscript presented here was written by myself, and most of the experiments were designed, conducted, and analyzed by me. However, within the framework of the project VPower, several people were involved, and their contributions are outlined below.

Prof. Dr. Bastian Blombach and Dr. Felix Thoma supported the planning of experiments and the interpretation of the results. Maurice Hädrich was responsible for the strain engineering and constructed the majority of the strains with the exception of two strains (*V. natriegens* Succ1 and *V. natriegens* Succ1 Δ*ackA*) that were provided by Dr. Felix Thoma. In addition, Maurice Hädrich generated the data for the characterization of pyruvate strains in shaking flasks (3.5.1), provided HPLC data for peak areas of parapyruvate, and created Figure 1 and Table A1, which have already been published by Schulze *et al.* (2023). Some of the sampling and OD measurements during pyruvate processes as well as HPLC measurements for Pyr1 – Pyr4 were carried out by him. Dr. Broder Rühmann performed the EPS measurements (concentration and composition) with the help of Manuel Döring, provided the data and assisted with the interpretation.

In the context of this work, several internships and theses were carried out, and some of the data for this thesis was generated with the help of the following students:

- Jennifer Borger (2022): Master thesis ”Process development for exopolysaccharide characterization and succinate production using *Vibrio natriegens*”
- Jennifer Borger (2022): Research internship ”Process development in a bioreactor for pyruvate production using *Vibrio natriegens*”
- Phillip Weinzierl (2022): Internship about process development of high cell density cultivations and pyruvate formation with *Vibrio natriegens.*
- Fiona Nothaaß (2021): Research practical “Formate tolerance of *Vibrio natriegens* Δ*vnp12* Δ*aceE*”
- Alexander Wastl (2020): Research internship “Verbesserung der Succinatproduktion in *Vibrio natriegens*“
- Christoph Gunkel (2020): Bachelor thesis “Succinate production in fed-batch process and analysis of the acetate metabolism in *Vibrio natriegens*”.

Acknowledgements

More than four years of work have come to an end with this dissertation, and during this exciting time I have received the support from many people, whom I would like to thank at this point.

First of all, I would like to thank my doctoral supervisor Prof. Dr. Bastian Blombach for giving me the opportunity to work on this exciting and promising project. His guidance provided a supportive and productive working environment, and I am especially grateful for the long scientific discussions that helped me progress in my research. I would also like to thank Dr. Felix Thoma, who introduced me to the laboratory work and with whom I had productive exchanges about this project.

Special thanks go to the entire MIB team, who created a constructive and pleasant working atmosphere and with whom I enjoyed being together both during working hours as well as in my free time. In particular, I would like to thank my project partner Maurice Hädrich for the close cooperation over the years, his contribution to this work, as well as the good discussions about our joint project. I would also like to thank my office colleague Dr. Felix Werner, with whom I have shared many professional and private conversations and who has brightened my long fermentation days. I would also like to thank Marc Schmollack, with whom I especially enjoyed our shared outdoor breaks, and Simon Grieshaber, to whom I could always turn to, regardless of the topic. Many thanks also go to Janine Petzenhauser and Annette Weiske, who kept the lab running and were always ready to help when needed. Further, I would like to thank my students who contributed to this work.

Last but not least, I would like to thank my family for their support over the years. Furthermore, I would like to express my gratitude to my fiancé Bazi, who has always looked after me and helped me to concentrate fully on my work.

Thank you!

Table of Content

List of tables and figures

List of figures

List of tables

Abbreviation

Abbreviation	Description
αKGDHC	α-Ketoglutarate dehydrogenase complex
AAA	Amino Acid Analysis
Ace	Acetate
Acetyl-coenzyme A	Acetyl-CoA
Acetyl-P	Acetyl phosphate
AckA	Acetate kinase
ACN	Aconitase
AcS	Acetyl-CoA synthetase
ADP	Adenosine diphosphate
AHL	Acyl-homoserine lactone
AI	Autoinducers
Ald	Alanine dehydrogenase
AMP	Adenosine monophosphate
ARTP	Atmospheric and room temperature plasma
ATCC	American type culture collection
ATP	Adenosine triphosphate

Abbreviation	Description
B. subtilis	*Bacillus subtilis*
BLAST	Basic local alignment search tool
bp	Base pair / nucleotide
c	Concentration, mol L^{-1} (M), g L^{-1}
C. glabrata	*Candida glabrata*
C. glutamicum / Cg	*Corynebacterium glutamicum*
CAI-1	Cholera autoinducer 1
C-balance	Carbon balance
CDW	Cell dry weight
CILC	Cold-induced loss of culturability
CoA	Coenzyme A
CPS	Capsular polysaccharides
CS	Citrate synthase
Dldh	D-lactate dehydrogenase
DNA	Deoxyribonucleic acid
DO	Dissolved oxygen

Abbreviation	Description
DSM	German collection of microorganisms
E. coli	*Escherichia coli*
E. scolopes	*Euprymna scolopes*
EFSA	European Food Safety Authority
EMP	Embden–Meyerhof–Parnas
EPS	Exopolysaccharides
et al.	And others
F	Gassing rate
F_0	Feeding rate at the start of the fed-batch phase
F(t)	Time-dependent feeding rate
FH	Fumarate hydratase
FLD	Fluorescence detector
Frd	Fumarate reductase
g	Gram
GAP	Glyceraldehyde 3-phosphate
GEM	Genome-scale metabolic model
Glc	Glucose
Gly	Glycerol
h	Hours
H^+	Proton
HAI-1	Harveyi autoinducer 1
HCDC	High cell density cultivation
HPLC	High-performance liquid chromatography
HT-PMP	High throughput 1-phenyl-3-methyl-5-pyrazolone
ICDH	Isocitrate dehydrogenase
ICL	Isocitrate lyase
ID	Identification
IM	Inner membrane
ISPR	In-situ product recovery
L	Liter
Lldh	L-lactate dehydrogenase
Kan^{50}	Kanamycin (50 µg mL^{-1})
KEGG	Kyoto Encyclopedia of Genes and Genomes
KPIs	Key Performance Indicators

Abbreviation	Description
m	Meter / milli (10^{-3})
M	Molar
Mb	Megabase
m_S	Substrate uptake for cell maintenance
M. succiniciproducens	*Mannheimia succiniciproducens*
Mae	Mailc enzyme
Mdh	Malate dehydrogenase
min	Minutes
MM_{HCDC}	Minimal medium for high cell density cultivations
Mqo	Malate:quinone oxidoreductase
MS	Malate synthase
MSHA	Mannose-sensitive hemagglutinin
n	Nano (10^{-9})
n.d.	Not determined
NAD^+	Nicotinamide adenine dinucleotide (oxidized)
NADH	Nicotinamide adenine dinucleotide (reduced)

Abbreviation	Description
$NADP^+$	Nicotinamide adenine dinucleotide phosphate (oxidized)
NADPH	Nicotinamide adenine dinucleotide phosphate (reduced)
OD_{600}	Optical Density at 600 nm
Odc	Oxaloacetate decarboxylase
OM	Outer membrane
O/N	Overnight
OTR	Oxygen transfer rate
P	Product
Pa	Pascal / Nm^{-2}
PA	Pyruvic acid
P_i	Phosphate
P_{tac}	*Tac* promoter
Pck	Phosphoenolpyruvate carboxykinase
Pdc	Pyruvate decarboxylase
PDHC	Pyruvate dehydrogenase complex
PEPC	Phosphoenolpyruvate carboxylase

Abbreviation	Description
PEP	Phosphoenolpyruvate
Pfl	Pyruvate formate lyase
pH	Negative decimal logarithm of the proton concentration
PHB	Poly-β-hydroxybutyrate
PMT	Photomultiplier tube
PP_i	Pyrophosphate
PPP	Pentose phosphate pathway
PPS	Phosphoenolpyruvate synthase
Pta	Phosphate acetyltransferase
Pyc	Pyruvate carboxylase
Pyk	Pyruvate kinase
Pyr	Pyruvate
Q^{ox}	Quinone
q_P	Biomass-specific product formation rate
Q_P	Volumetric productivity
Q^{red}	Quinol
Qrrs	Quorum regulatory RNAs
q_S	Biomass-specific substrate uptake rate
$q_{S,P}$	Substrate uptake required for product formation
R	Bioreactor
RID	Refractive index detector
RNA	Ribonucleic acid
ROS	Reactive oxygen species
rpm	Revolutions per minute
RT	Room temperature
s	Seconds
S	Substrate
S. cerevisiae	*Saccharomyces cerevisiae*
SA	Succinic acid
Sdh	Succinate dehydrogenase
SF	Shaking flasks
Suc	Succinate / Succinyl-CoA synthetase
t	Time
TCA	Tricarboxylic acid cycle
TCA_{ox}	Oxidative pathway of the tricarboxylic acid cycle

Abbreviation	Description
TCA_{red}	Reductive pathway of the tricarboxylic acid cycle
TCE	Trace element solution
UHPLC-UV-ESI-MS/MS	Ultra high-performance liquid chromatography with ultra violet and electrospray ionization ion trap tandem mass spectrometry
U.S.	United States
V	Volume
V_m	Molar gas volume
V. alginolyticus	*Vibrio alginolyticus*
V. cholerae	*Vibrio cholerae*
V. diabolicus	*Vibrio diabolicus*
V. fischeri	*Vibrio fischeri*
V. furnissii	*Vibrio furnissii*
V. harveyi	*Vibrio harveyi*
V. natriegens	*Vibrio natriegens*
V. parahaemolyticus	*Vibrio parahaemolyticus*
V. vulnificus	*Vibrio vulnificus*
VBNC	Viable but non-culturable
VN_c	Concentrated VN medium
VN_{mc}	Multi-concentrated VN medium
vvm	Gas volume per medium volume per minute
wt	Wildtype
X	Biomass
×g	Relative centrifugal force
y_{O2}	Oxygen content in gas
Y. lipolytica	*Yarrowia lipolytica*
$Y_{P/S}$	Substrate-specific product yield
$Y_{X/S}$	Substrate-specific biomass yield
Ø	Diameter
η	Viscosity
µ	Specific growth rate / micro (10^{-6})
°C	Degree Celsius
% (v v^{-1})	Percent volume per volume
% (w v^{-1})	Percent weight per volume
% (w w^{-1})	Percent weight per weight

Chemicals	
1,3-PDO	1,3-propanediol
2,3-BDO	2,3-butanediol
3-HP	3-hydroxypropionate
Ca^{2+}	Calcium ion
$CaCl_2$ x 2 H_2O	Calcium chloride dihydrate
$CaCO_3$	Calcium carbonate
CO_2	Carbon dioxide
$CoCl_2$ x 6 H_2O	Cobalt chloride hexahydrate
$CuSO_4$ x 5 H_2O	Copper sulfate pentahydrate
EDTA	Ethylenediaminetetraacetic acid
Fe(III) citrate × H_2O	Iron(III) citrate monohydrate
$FeSO_4$ x 7 H_2O	Iron sulfate heptahydrate
H_3BO_3	Boric acid
HCl	Hydrochloric acid
HCO_3^-	Hydrogen carbonate / Bicarbonate
H_2O	Water
H_3PO_4	Phosphoric acid
H_2SO_4	Sulfuric acid
IPTG	Isopropyl-β-D-thiogalactopyranosid
$KHCO_3$	Potassium hydrogen carbonate

Chemicals	
KH_2PO_4	Potassium dihydrogen phosphate
K_2HPO_4	Dipotassium hydrogen phosphate
KIO_3	Potassium iodate
KOH	Potassium hydroxide
L-DOPA	L-3,4-dihydroxyphenyl-L-alanine
$MgCl_2$ x 6 H_2O	Magnesium chloride hexahydrate
$MgSO_4$ x 7 H_2O	Magnesium sulfate heptahydrate
$MnSO_4$ x H_2O	Manganese sulfate monohydrate
MOPS	3-(N-morpholino)propanesulfonic acid
$Na_2B_4O_7$ x 10 H_2O	Sodium tetraborate decahydrate
NaCl	Sodium chloride
$NaHCO_3$	Sodium bicarbonate
Na_2HPO_4	Sodium hydrogen phosphate
Na_2MoO_4 x 2 H_2O	Sodium molybdate dihydrate
Na_2SeO_3	Sodium selenite
Na_2SO_4	Sodium sulfate
NH_4OH	Ammonium hydroxide
$(NH_4)_2SO_4$	Ammonium sulfate
Na_2WO_4 x 2 H_2O	Sodium tungstate dihydrate
$NiCl_2$ x 6 H_2O	Nickel chloride hexahydrate

Chemicals	
O_2	Oxygen
Tris	Tris(hydroxymethyl)aminomethane
$ZnSO_4$ x 7 H_2O	Zinc sulfate heptahydrate

Abstract

The high growth and substrate uptake rates of *Vibrio natriegens* render this marine bacterium an emerging host for biotechnology. For industrial processes, key performance indicators need to be maximized and typically fed-batch processes are applied to obtain high space-time yields. This work deals with the establishment of a glucose-limited fed-batch process for *V. natriegens* wildtype that yielded 28.4 g biomass L^{-1}. During this process, 157 mg exopolysaccharides (EPS) L^{-1} were secreted, resulting in an approximately 800-fold increase in the viscosity of the bioreactor broth. Multiple strains lacking EPS-related genes were constructed to target this issue. Nevertheless, all mutant strains still secreted EPS in varying amounts, but the monomeric composition differed for all of them compared to the wildtype strain. However, the inactivation of the transcriptional biofilm regulator CpsR resulted in a consistently low viscosity throughout the process. Furthermore, two mutant strains lacking the EPS gene clusters *syp* and *cps* did not increase the viscosity either, and both secreted the least amount of EPS (about 80 mg L^{-1}).

An anaerobic two-stage process was developed for the succinate producer *V. natriegens* Δ*lldh* Δ*dldh* Δ*pfl* Δ*ald* Δ*dns*::*pyc*$_{Cg}$ (Succ1) using minimal medium without expensive supplements. A titer of 60.4 g succinate L^{-1} was achieved along with an exceptionally high maximum productivity of 20.8 g_{Suc} L^{-1} h^{-1} and an overall productivity of 8.6 g_{Suc} L^{-1} h^{-1}. However, only 62% of the carbon from glucose was recovered at the end of the process. In addition, an elevated viscosity was observed as well, and it was speculated that EPS formation was at least partially responsible for the carbon sink. The additional deletion of *cpsR* and *cps* in *V. natriegens* Succ1 resulted in a consistently low viscosity throughout the fermentation. Furthermore, about 80% of the carbon was recovered and the product yield was improved to 1.4 mol_{Suc} mol_{Glc}^{-1}, which corresponds to 81% of the theoretical maximum.

Besides the development of a production process for succinate, an aerobic fed-batch process for the acetate auxotrophic pyruvate producer *V. natriegens* Δ*vnp12* Δ*aceE* was established. Usually, high biomass concentrations are required to meet the process demands for volumetric productivities. However, this also means that most of the carbon is converted into the catalyst rather than the product, and that a large amount of biomass waste is generated that needs to be dealt with once the process is complete. Due to the high substrate consumption rates of *V. natriegens*, high productivities are achievable even at low biomass concentrations, and the process presented in this work takes advantage of this. The pyruvate process was performed in minimal medium with glucose and, due to the auxotrophy of the pyruvate strain, acetate was provided. A final titer of 22 g pyruvate L^{-1} was obtained with a productivity of 2.2 g_{Pyr} L^{-1} h^{-1}. The addition of an 8 mM acetate h^{-1} feed increased the titer by 85% to 41 g pyruvate L^{-1} and the volumetric productivity was enhanced to 4.1 g_{Pyr} L^{-1} h^{-1}, which is one of the highest productivities reported to date.

Zusammenfassung

Vibrio natriegens ist aufgrund seiner hohen Wachstums- und Substrataufnahmeraten ein vielversprechender Produktionswirt für die industrielle Biotechnologie. Die Evaluierung industrieller Prozesse erfolgt häufig anhand von Leistungsindikatoren wie dem Produkttiter, der Produktausbeute und der volumetrischen Produktivität. Das Ziel industrieller Prozesse liegt in der Maximierung dieser Parameter, wobei häufig Fed-Batch-Prozesse eingesetzt werden, um hohe Raum-Zeit-Ausbeuten zu erhalten. Die folgende Arbeit befasst sich mit der Etablierung eines Glukose-limitierten Fed-Batch-Prozesses für den *V. natriegens* Wildtyp. Während des Prozesses wurden 28 g Biomasse L^{-1} erreicht, allerdings wurden dabei ebenfalls 157 mg Exopolysaccharide (EPS) L^{-1} in das Medium sekretiert, was zu einer Erhöhung der Viskosität um das 800-fache führte. Daraufhin wurden mehrere Mutantenstämme konstruiert, denen EPS-bezogene Gene fehlten. Alle Stämme produzierten weiterhin EPS in variierenden Mengen, allerdings unterschied sich die monomere Zusammensetzung der einzelnen EPS im Vergleich zum Wildtyp. Die Inaktivierung des transkriptionellen Biofilmregulators CpsR resultierte in einer konstant niedrigen Viskosität während des gesamten Prozesses. Zwei weitere Mutanten, denen die EPS-Gencluster *syp* und *cps* fehlten, wiesen die geringste EPS Produktion auf (circa 80 mg L^{-1}) und erhöhten die Viskosität ebenfalls nicht.

Für den Succinatproduzenten *V. natriegens* Δ*lldh* Δ*dldh* Δ*pfl* Δ*ald* Δ*dns*::*pyc*$_{Cg}$ (Succ1) wurde ein zweistufiger anaerober Prozess unter Verwendung von Minimalmedium ohne teure Zusätze entwickelt. Dabei wurde ein Titer von 60,4 g Succinat L^{-1} und eine außergewöhnlich hohe maximale Produktivität von 20,8 g_{Suc} L^{-1} h^{-1} erzielt. Die Gesamtproduktivität betrug 8,6 g_{Suc} L^{-1} h^{-1}. Am Ende des Prozesses konnten jedoch nur 62 % des Kohlenstoffs aus Glucose identifiziert werden. Zudem wurde eine erhöhte Viskosität beobachtet, was zu der Annahme führte, dass die Bildung von EPS zumindest teilweise für den fehlenden Kohlenstoff verantwortlich ist. Durch die zusätzliche Deletion von *cpsR* und *cps* in *V. natriegens* Succ1 gelang es, die Viskosität während der Fermentation konstant niedrig zu halten und es konnten anschließend etwa 80 % des Kohlenstoffs zugeordnet werden. Des Weiteren konnte die Produktausbeute auf 1,4 mol_{Suc} mol_{Glc}^{-1} verbessert werden. Dies entspricht bereits 81 % des theoretischen Maximums.

Zusätzlich zur Entwicklung eines Succinatprozesses wurde ein aerober Fed-Batch-Prozess für den acetatauxotrophen Pyruvatproduzenten *V. natriegens* Δ*vnp12* Δ*aceE* etabliert. In der Regel sind hohe Biomassekonzentrationen erforderlich, um die Prozessanforderungen an die volumetrische Produktivität zu erfüllen. Dies hat jedoch zur Folge, dass ein Großteil des Kohlenstoffs in den Katalysator und nicht in das Produkt umgewandelt wird und zudem eine erhebliche Menge an Biomasseabfällen entsteht, die nach Abschluss des Prozesses abgetrennt und entsorgt werden müssen. Aufgrund der hohen Substrataufnahme von *V. natriegens* sind hohe Produktivitäten selbst bei geringen

Biomassekonzentrationen möglich, was sich der in dieser Arbeit vorgestellte Prozess zu Nutze macht. Der Pyruvatprozess wurde in Minimalmedium mit Glukose durchgeführt und aufgrund der Auxotrophie des Pyruvatstammes wurde zusätzlich Acetat supplementiert. Zunächst wurde ein Titer von 22 g Pyruvat L^{-1} mit einer Produktivität von 2,2 g_{Pyr} L^{-1} h^{-1} erreicht. Durch die Verwendung eines 8 mM Acetat h^{-1} Feeds konnte der Titer um 85 % auf 41 g Pyruvat L^{-1} gesteigert und die volumetrische Produktivität auf 4,1 g_{Pyr} L^{-1} h^{-1} erhöht werden. Dies entspricht einer der höchsten bisher berichteten Produktivitäten.

1. Introduction

1.1. Intrinsic properties of *Vibrio natriegens*

Vibrio natriegens was first isolated in 1958 from marsh mud from the coast of Sapelo Island in Georgia (Payne, 1958). The Gram-negative γ-proteobacterium is rod-shaped and has one to three polar flagella, with a single flagellum being the most common (Austin *et al.*, 1978). It is prototrophic, but requires Na^+ for proliferation, substrate utilization, and protein expression, although it remains metabolically active in the absence of Na^+ (Payne, 1958, 1960; Payne *et al.*, 1961; Webb and Payne, 1971; Thoma and Blombach, 2021). The marine bacterium tolerates a wide pH range between 6.0 and 9.5 with an optimum at pH 7.5 (Payne *et al.*, 1961). *V. natriegens* has received much attention due to its outstandingly high growth and biomass-specific substrate uptake rates (Hoffart *et al.*, 2017). With a doubling time of less than 10 min in complex medium at 37 °C, it is the fastest growing non-pathogenic bacterium known to date (Eagon, 1962). In minimal medium containing glucose, *V. natriegens* exhibits growth rates of approximately 1.7 h^{-1} and 0.9 h^{-1} under aerobic and anaerobic conditions, respectively (Hoffart *et al.*, 2017; Long *et al.*, 2017), which are at least twice as high as the growth rates reported for other industrially relevant organisms such as *Escherichia coli*, *Corynebacterium glutamicum*, *Bacillus subtilis*, and *Saccharomyces cerevisiae* (Varma and Palsson, 1994; Albers *et al*., 1996; Sauer *et al*., 1996; Gombert *et al*., 2001; Blombach *et al*., 2013; Michel *et al*., 2015; Gonzalez *et al*., 2017; Hoffart *et al*., 2017; Long *et al*., 2017).

V. natriegens shows remarkable flexibility with respect to carbon sources under aerobic conditions, and furthermore, the substrates D-gluconate, D-glucose, D-mannitol, and D-ribose support biomass formation even under anaerobic conditions (Hoff *et al.*, 2020; Thoma and Blombach, 2021). ^{13}C metabolic flux analysis revealed that *V. natriegens* and *E. coli* share a similar core carbon metabolism when grown on glucose. Under aerobic conditions, glucose is mainly metabolized via the Embden-Meyerhof-Parnas (EMP) pathway and to a lesser extent via the pentose phosphate pathway (PPP), whereby the flux through the latter is reduced by 33% compared to *E. coli* (Long *et al.*, 2017). The resulting nicotinamide adenine dinucleotide phosphate (NADPH) deficiency is compensated by transhydrogenase activity, which accounts for 56% of NADPH formation (Long *et al*., 2017; Thoma and Blombach, 2021). The genome of *V. natriegens* has been fully sequenced and is divided into two circular chromosomes of approximately 3.24 Mb (chromosome 1) and 1.92 Mb (chromosome 2) (Maida *et al.*, 2013; Wang *et al.*, 2013; Lee *et al.*, 2016). *V. natriegens* meets biosafety level 1 standards and a genetic toolbox is already available that has been applied to modify the bacterium for the production of various

compounds (Weinstock *et al.*, 2016; Hoff *et al.*, 2020; Stukenberg *et al.*, 2021; Thoma and Blombach, 2021; Teufel *et al.*, 2022).

1.1.1. Exopolysaccharide formation

Exopolysaccharides (EPS) are high-molecular-weight carbohydrate polymers secreted by various organisms, such as bacteria, yeast, and fungi, into their surrounding environment without any attachment to the cell or as capsular polysaccharides (CPS) that are still associated with the cell surface (Cescutti, 2010; Barcelos *et al.*, 2020). Further, they can be categorized as homopolysaccharides, which are built from only one type of monosaccharide, and the more common form, heteropolysaccharides, which consist of several different types of monomeric sugars (Barcelos *et al.*, 2020). The structure of heteropolysaccharides is often composed of hexoses, pentoses, amino sugars, as well as uronic acids. In addition, non-sugar organic and inorganic substituents such as succinic and acetic acids, sulfates and phosphates may be present (Kenne and Lindberg, 1983, Nichols *et al.*, 2005). EPS serve many important functions. They are crucial for the formation of biofilms and protect the cell from biotic and abiotic stress factors by altering the physical and chemical microenvironment around the cell. Furthermore, EPS can mediate pathogenicity and are essential for the adhesion to surfaces or the colonization of other organisms (Nichols *et al.*, 2005; Moradali and Rehm, 2020). In addition, EPS synthesis is often closely linked to biofilm formation and quorum sensing, the cell-to-cell communication (Yildiz and Visick, 2009). Due to the great chemical diversity of EPS, a wide range of applications is possible in the medical, pharmaceutical, waste water, and food industries, among others. Their biosynthesis is being studied in detail in order to identify valuable EPS and to engineer production hosts towards tailor-made EPS with valuable physicochemical properties (Barcelos *et al.*, 2020; Schilling *et al.*, 2020). Prominent examples include xanthan gum, which is widely used as an emulsifier and food thickener in the food industry (Lopes *et al.*, 2015), or hyaluronic acid, a popular cosmetic ingredient (Yao *et al.*, 2021). Some promising EPS for *Vibrio* species in the medical and cosmetic fields have also been described, such as the EPS formed by *Vibrio alginolyticus* and *Vibrio diabolicus* (Zanchetta *et al.*, 2003; Goudenège *et al.*, 2014; Drouillard *et al.*, 2015, 2018). Although there are many possible applications for EPS, they are often secreted as an unwanted byproduct during production processes and negatively affect them. The synthesis can be growth or non-growth associated and the fundamental challenge of EPS formation to the operation of bioreactors is the shift in rheology from a non-viscous Newtonian to a high-viscous non-Newtonian bioreactor broth, which ultimately leads to a heterogeneous system causing several negative effects. Due to the resulting shear-thinning nature of the bioreactor broth, a small area near the impeller (high shear zone) still exhibits a low viscosity and this area remains well mixed and aerated (Freitas *et al.*, 2011; Seviour *et al.*, 2011; Freitas *et al.*, 2017). However, the mass

transfer is reduced for the major part of the bioreactor, resulting in a poor heat transfer and an insufficient oxygen supply. The latter cannot be remedied by increasing the aeration rate, as the gas would simply flood the impeller as it flows through the well-mixed, low viscosity region (Seviour *et al.*, 2011). In addition, the heterogenicity complicates the monitoring and control of the process parameters and negatively affects the subsequent downstream processing, particularly the recovery and purification of the product (McNeil and Harvey, 1993; Freitas *et al.*, 2011; Seviour *et al.*, 2011; Freitas *et al.*, 2017).

Vibrio species are well known for their ability to produce EPS and biofilms, and colonization of metallic surfaces by a *V. natriegens* biofilm using EPS as adhesives has already been described (Cheng *et al.*, 2010; Dong *et al.*, 2016). Several genes and gene clusters potentially involved in the synthesis of EPS have been identified (Figure 1). In total, a remarkable 0.7% of the genome of *V. natriegens* consists of such genes (Schulze *et al.*, 2023). In 2018, Lebellenger *et al.* examined 103 genome sequences of Vibrionaceae and identified genetic elements similar to the *syp* cluster of *V. diabolicus* in 70% of them. *Syp* stands for symbiosis polysaccharides, and this gene cluster is best known from *Vibrio fischeri*, where it is required for biofilm formation and the symbiotic colonization of the Hawaiian bobtail squid *Euprymna scolopes* (Yip *et al.*, 2005). Moreover, the *syp* cluster was linked to the synthesis of the valuable hyaluronic acid-like EPS HE800 produced by *V. diabolicus*, which attracted attention for its bone-healing properties (Zanchetta *et al.*, 2003; Goudenège *et al.*, 2014). Homologous clusters were also present in *Vibrio parahaemolyticus* and *Vibrio vulnificus* (Yip *et al.*, 2005). BLASTP analysis of SypK from *V. fischeri* VF_A1030 revealed a 35% identity hit with PN96_04625, and the genomic region showed a *syp*-like cluster in *V. natriegens* (Ruby *et al.*, 2005; Schulze *et al.*, 2023) (Figure 1). Furthermore, it has already been reported that *sypK* encodes for an oligosaccharide translocase and that its deletion could significantly reduce EPS formation in *V. diabolicus* (Goudenège *et al.*, 2014). Another EPS cluster, *cps*, is required for the synthesis of CPS in *V. parahaemolyticus* (Güvener and McCarter, 2003). In *V. natriegens*, a gene PN96_14980 has been detected that shares 79% identity with the nucleotide sequence of *cpsA,* which is part of the *cps* cluster in *V. parahaemolyticus* (Jensen *et al.*, 2013, Schulze *et al.*, 2023). In addition, the genomic region around PN96_14980 resembled the *cps* cluster in *V. natriegens* (Schulze *et al.*, 2023) (Figure 1). Furthermore, the gene PN96_10960 showed a 71% and 81% identity to the nucleotide sequence of *vpsR* of *Vibrio cholerae* VC_0665 (Heidelberg *et al.*, 2000) and *cpsR* of *V. parahaemolyticus* AY216912 (Güvener and McCarter, 2003), respectively, which are described as positive transcriptional regulators of EPS formation (Yildiz *et al.*, 2001), and hence the gene PN96_10960 is hereinafter referred to as *cpsR* (Schulze *et al.*, 2023). Another gene involved in CPS synthesis is the gene *wbfF* (Dalia *et al.*, 2017), which is also present in *V. natriegens*. Several genes annotated for polysaccharide and lipopolysaccharide synthesis are located in the vicinity of this gene, including sugar transferases and a type II secretion system for polysaccharides (Ali *et al.*, 2000; Johnson *et al.*, 2014; Schulze *et al.*, 2023).

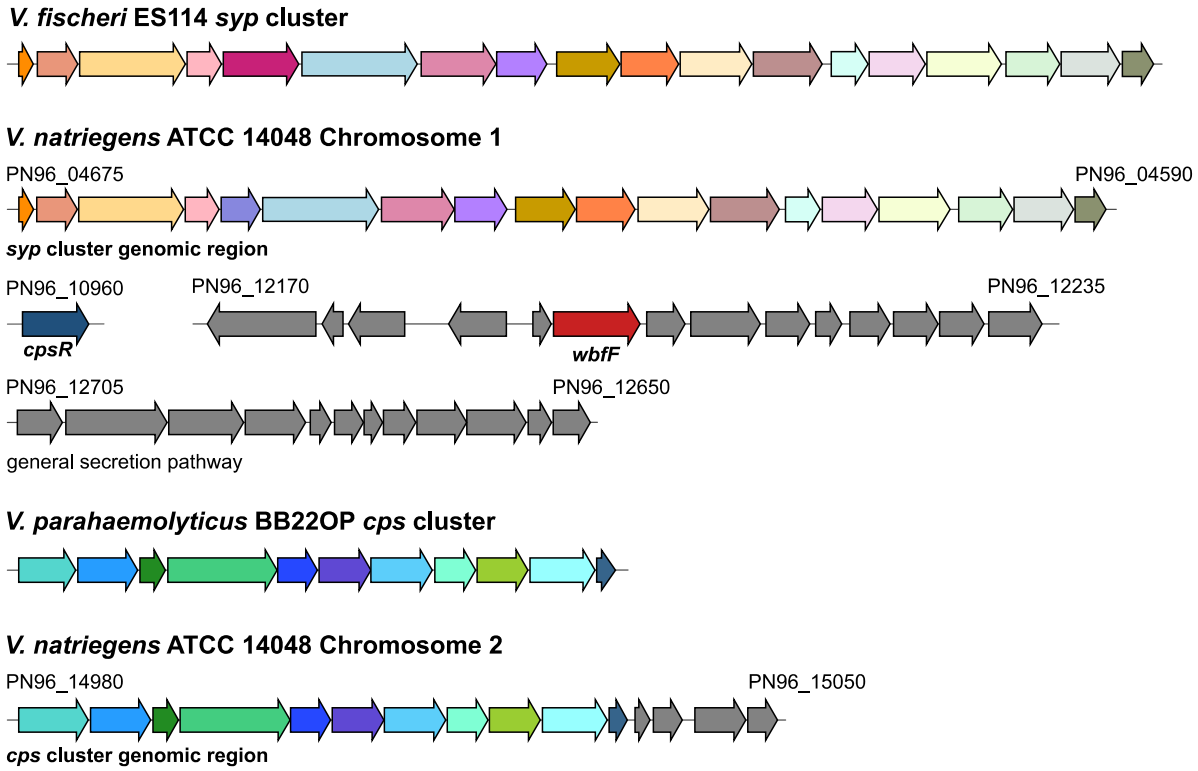

Figure 1: Genetic regions and genes potentially related to polysaccharide biosynthesis in *V. natriegens*. Genes are represented by arrows in scale. Positions are ordered by their locations on the chromosomes and labeled with their respective gene identifiers. Similarities of the *syp* and *cps* regions to published clusters of *V. fischeri* (VF_A1020-VF_A1037) (Yip et al., 2005) and *V. parahaemolyticus* (VPBB_A1276-VPBB_A1286) (Güvener and McCarter, 2003) are shown by matching colors for genes displaying over 60% sequence identity by BLASTN. (Schulze *et al.*, 2023)

1.1.2. Quorum sensing and viable but non-culturable cells

The formation of EPS and biofilms is often tightly regulated by quorum sensing (Yildiz and Visick, 2009). Quorum sensing is the cell-to-cell communication that regulates gene expression in response to the cell population density. The transfer of information between cells of either the same or different species is mediated by chemical signal molecules known as autoinducers (AI). The chemical communication includes the production, release, detection, and response of the small hormone-like AI (Waters and Bassler, 2005). Once a critical threshold is exceeded, a change in cell metabolism is triggered and coordinated gene expression of an entire cell population is enabled, allowing bacteria to function as a multicellular organism (Waters and Bassler, 2005). Quorum sensing occurs in many *Vibrio* species such as *Vibrio harveyi* (Henke and Bassler, 2004), *V. cholerae* (Jung *et al.*, 2016), *V. parahaemolyticus* (Kalburge *et al.*, 2017), and *V. fischeri* (Ball *et al.*, 2017). *V. fischeri* forms a symbiotic relationship with the Hawaiian bobtail squid *E. scolopes*. The bacterium colonizes the nutrient-rich light organ where it

grows to high cell densities while inducing bioluminescence. The light emission serves the squid as a defense against predators by mimicking moonlight, thus preventing a telltale shadow on the ocean floor (Visick and McFall-Ngai, 2000). *V. fischeri* uses a LuxIR signaling circuit for quorum sensing (Waters and Bassler, 2005). LuxI is an AI synthase that produces the AI acyl-homoserine lactone (AHL) and LuxR serves as a cytoplasmatic AI receptor/DNA binding transcriptional activator. The external concentration of the AI rises with an increasing cell-population density. Once a critical concentration has been reached, AHL is bound by LuxR and the complex activates the transcription of the luciferase operon *luxICDABE*, which is required for light emission. In addition, LuxR-AHL also induces the expression of *luxI,* since it is encoded in the luciferase operon, resulting in the flooding of the environment with AHL, thus creating a positive feedback loop (Waters and Bassler, 2005). The LuxIR system is widely spread among Gram-negative bacteria (Ball *et al.*, 2017). However, membrane-bound AI receptors are more common in other *Vibrio* species. These receptors initiate a signaling cascade resulting in the expression of a TetR-type transcription factor that regulates quorum sensing genes. This master quorum sensing regulator is highly conserved among many *Vibrio* species (e.g., HapR in *V. cholerae*, SmcR in *V. vulnificus*, LitR in *V. fischeri*, and OpaR in *V. parahaemolyticus*). The regulator in *V. harveyi* has been named LuxR as well, although it differs structurally, biochemically, and genetically from the LuxR protein of *V. fischeri* (Ball *et al.*, 2017). *V. harveyi* utilizes multiple quorum sensing signaling systems that regulate bioluminescence and EPS production, among other things (Milton, 2006). The bacterium possesses three AI-synthases, LuxM, CqsA, and LuxS, which produce harveyi autoinducer 1 (HAI-1), cholera autoinducer 1 (CAI-1), and autoinducer 2 (AI-2), respectively (Figure 2). At a low cell density (Figure 2A), the extracellular concentration of AI is not sufficient to bind to the respective membrane receptors LuxN, CqsS, and LuxPQ (Ball *et al.*, 2017). The latter is a complex consisting of the periplasmic receptor LuxP, which binds AI-2 and regulates the activity of the inner membrane sensor LuxQ, which transmits AI-2 information into the cytoplasm (Neiditch *et al.*, 2005). The membrane receptors act as kinases and phosphorylate the protein LuxU (Figure 2A). LuxU transfers the phosphate to the regulator LuxO, and LuxO~P in turn activates the quorum regulatory RNAs (Qrrs). The Qrrs activate the transcription factor AphA, while the production of LuxR is negatively regulated (Figure 2A). As AI accumulate in the surrounding environment of the bacterial cell, the membrane-bound receptors bind the AI and subsequently, function as phosphatases by removing phosphate from LuxO-P (Figure 2B). Thus, Qrrs are no longer expressed, AphA is no longer produced, and expression of LuxR is high, which regulates quorum sensing related genes responsible for the uniform behavior of a cell population (Ball *et al.*, 2017) (Figure 2B). Multiple feedback loops ensure the precise expression of the master regulators AphA (for low cell densities) and LuxR (for high cell densities). Qrrs activates AphA expression and represses the expression of LuxR, LuxM, and LuxO, while LuxR activates *qrr* transcription. AphA and LuxR auto-repress their own expression, and in addition, AphA represses LuxR and vice versa (Ball *et al.*, 2017) (Figure 2).

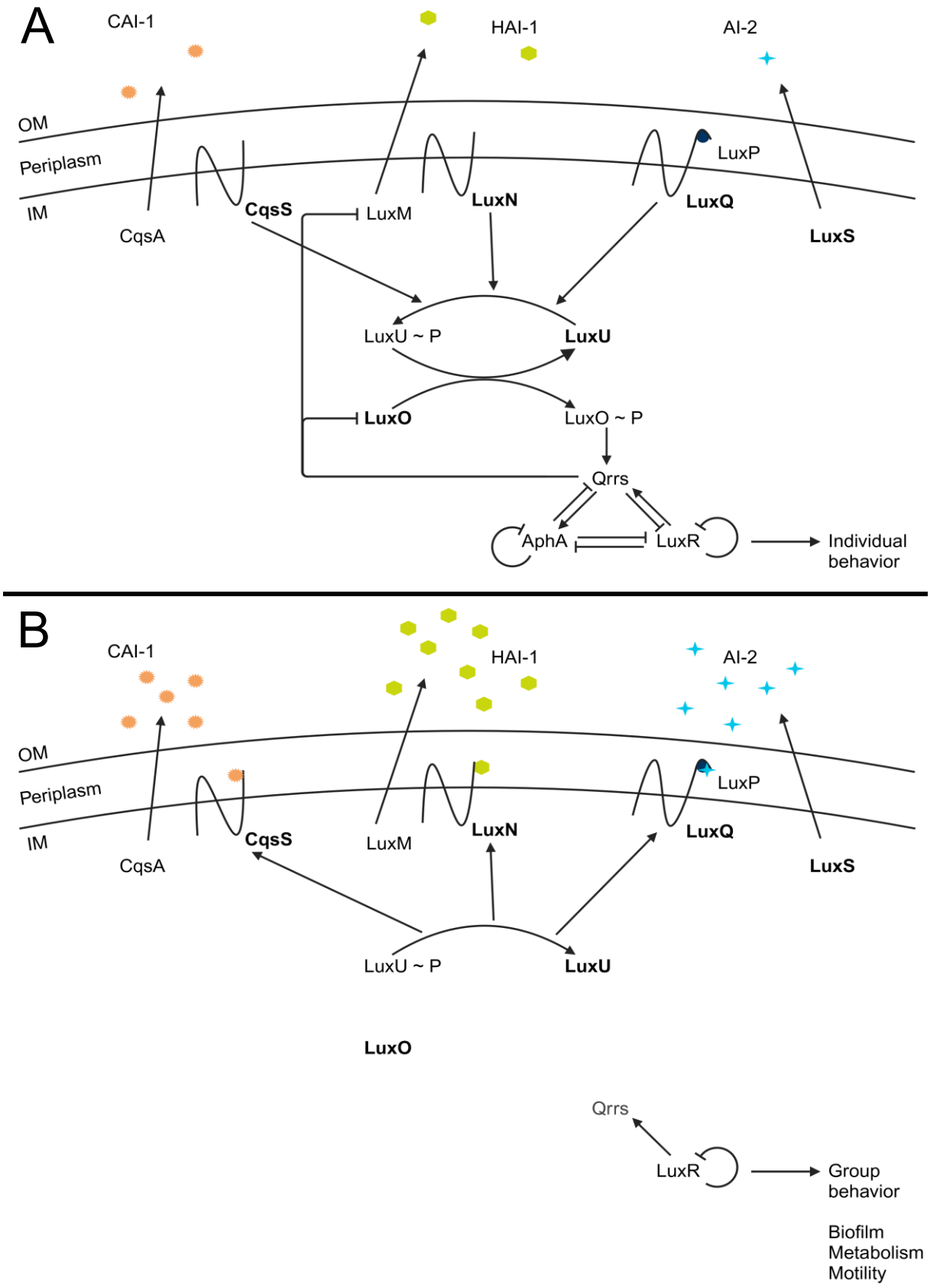

Figure 2: Quorum sensing system of *V. harveyi*. Activation mechanisms are indicated by arrows and repression mechanisms by lines with a bar at the end. The autoinducer synthases CqsA, LuxM, and LuxS produce the autoinducers (AI) CAI-1, HAI-1, and AI-2, respectively. At low cell densities (A), the concentration of the AI is not sufficient to bind to the membrane receptors CqsS, LuxN, and LuxPQ.

LuxU gets phosphorylated and then transfers the phosphate to the regulator LuxO. LuxO ~ P activates quorum regulatory RNAs (Qrrs), which in turn activate the expression of the low cell density regulator AphA. Simultaneously, Qrrs repress LuxR, LuxM, and LuxO. AphA represses the expression of LuxR, Qrrs, and itself. LuxR auto-represses its own expression as well as that of AphA and activates Qrrs. At high cell densities (B), the AI bind to the receptors, which then dephosphorylate LuxU. Thus, LuxO is not phosphorylated and Qrrs and AphA are not expressed. LuxR is expressed at high levels and regulates genes involved in group behavior. The high cell density regulator activates *qrr* transcription and represses *aphA* transcription. In addition, LuxR auto-represses its expression. Regulators and receptors in bold are annotated by KEGG database for *V. natriegens*. Qrrs written in gray indicate that they are not active. OM stands for outer membrane and IM for inner membrane.

Quorum sensing has not been studied in *V. natriegens* so far. However, some genes potentially involved in quorum sensing have been annotated by KEGG (Table A1), and essential components of the quorum sensing system of *V. harveyi* have also been identified in *V. natriegens*, such as the membrane-bound receptors CqsS, LuxN, and LuxQ for the signaling molecules CAI-1, HAI-1, and AI-2. Furthermore, the regulators LuxU, LuxO and HapR, which is a homolog of LuxR, as well as the AI-synthase LuxS have been identified (Figure 2) (Waters and Bassler, 2005; Ball *et al.*, 2017; Schulze *et al.*, 2023).

Apart from biofilm and EPS formation, quorum sensing is also involved in other biological processes, such as the mediation of the viable but non-culturable state (VBNC) (Li and Zhao, 2020). Under adverse environmental conditions, such as limitations and changes in nutrient availability, salinity, temperature, solar radiation, and oxygen saturation, some bacteria can enter the VBNC state to improve their chances of survival. In this state, the cells cannot be cultured on routine growth media. Once the stress factors are no longer present and the conditions are again favorable for growth, the cells can be resuscitated (McDougald *et al.*, 1998; Zhang *et al.*, 2021a). The transition to the VBNC state is usually accompanied by morphological alterations, such as shrinkage and a change to a coccoid form. Additionally, differences in the composition of the cell wall, genetic expression, and metabolism have been reported, including the reduction in nutrient transport, respiration, and macromolecular synthesis (Oliver, 2005; Asakura *et al.*, 2007; Du *et al.*, 2007). Du *et al.* (2007) reported that the morphological changes are reversible for resuscitated cells of *V. alginolyticus* VIB283 and almost no morphological differences were observed compared to normal cells.

VBNC was first discovered in 1982 by Xu *et al.* for *E. coli* and *V. cholerae* and has since been reported for many other bacteria, including some *Vibrio* species, such as *V. fischeri* (Ramaiah *et al.*, 2002), *V. harveyi* (Sun *et al.*, 2008), *V. alginolyticus* (Du *et al.*, 2007), and *V. vulnificus* (Oliver, 1995). *V. natriegens* has also been listed as one of approximately 60 bacteria capable of entering the VBNC state (Oliver, 1995, 2005). The initiation of the VBNC state in *Vibrio* species is often cold-related, and a temperature upshift has been reported to promote resuscitation (Xu *et al.*, 1982; Oliver, 1995; Wong *et*

al., 2004; Du *et al.*, 2007; Sun *et al.*, 2008). Other resuscitation-promoting factors, such as the supplementation of sodium pyruvate, amino acids, vitamins, and many others, have been reported for various bacteria (Zhang *et al.*, 2021a). Among these are also quorum sensing molecules. Ayrapetyan *et al.* (2014) discovered that AI-2 can induce the resuscitation of *V. vulnificus*. Mutants unable to produce AI-2 could not be resuscitated unless exogenous AI-2 was provided. Furthermore, it was shown that cinnamaldehyde, a quorum sensing inhibitor, could delay the resuscitation of wildtype (wt) cells, confirming the importance of quorum sensing in resuscitation. A similar study for *V. cholerae* reported that the addition of CAI-1 and AI-2 to environmental samples could enhance the recovery of dormant cells (Bari *et al.*, 2013). In addition, it was shown that *V. cholerae* O1 uses quorum sensing to prevent the transition into the VBNC state and, in particular, that the upregulation of *hapR* resulted in a prolonged culturability in artificial seawater at 4 °C (Wu *et al.*, 2020).

1.2. *Vibrio natriegens* – a new industrial host

Key performance indicators (KPIs) are used to assess the suitability of microbial processes. To be competitive for industrial applications, conventional production processes for bulk chemicals must be improved and the KPIs must be pushed to their maximum. High product titers of 100 g L^{-1}, product yields $Y_{P/S}$ of around 80 – 90%, and productivities of at least 2.5 g L^{-1} h^{-1} are demanded (Werpy and Petersen, 2004; Thoma and Blombach, 2021). The volumetric productivity Q_P is determined by the biomass-specific product formation rate q_P, which in turn depends on the biomass-specific substrate uptake rate q_S, as this parameter defines the amount of carbon that can be converted into the desired product. The q_S is directly related to the growth rate μ, rendering the fastest growing non-pathogenic bacterium *V. natriegens* a promising candidate to exploit its potential as a new industrial host (Hoffart *et al.*, 2017).

1.2.1. **Bioprocess engineering with *V. natriegens***

To meet the requirements for KPIs, high biomass (X) concentrations are often essential and fed-batch processes are usually applied to achieve high space-time yields. Thiele *et al.* (2021) conducted a fed-batch process with *V. natriegens* wt using a combination of an exponential and a constant glucose feeding strategy. The DO was regulated above 40% via agitation rate, air flow, and oxygen content in the gas mix. A beneficial effect of reducing the cultivation temperature from 37 to 30 °C was reported and a cell dry weight (CDW) of 55 g_X L^{-1} was achieved. *V. natriegens* requires sodium for proliferation and its demand is mostly satisfied with sodium chloride. This can pose a challenge, since high salt loads complicate downstream processing and chloride can cause corrosion on metal surfaces, such as those

used in bioreactors. Therefore, a medium containing only traces of chloride has been developed that maintains the growth rate at 91% (Hoffart *et al.*, 2017). Recently, Biener *et al.* (2023) reported the highest CDW of approximately 60 g_X L^{-1} for *V. natriegens* during a fed-batch process at 30 °C using a minimal medium in which sodium chloride was completely replaced by disodium hydrogen phosphate, disodium sulfate, and sodium citrate.

Although high salt loads may negatively impact downstream processing, the halotolerance of *V. natriegens* can also be used to advantage. Typically, large amounts of sterile fresh water are required for media and feedstock preparation, contributing to the overall production costs (Chen, 2012). Due to the halotolerance of *V. natriegens*, fresh water can be replaced by less expensive high salinity water such as seawater or even wastewater streams. In addition, sterilization is no longer required, saving time and costs, as the growth of a vast number of microorganisms is inhibited or abolished under these conditions. The production of 2,3-butanediole (2,3-BDO) and poly-β-hydroxybutyrate (PHB) under non-sterile conditions has already been reported for *V. natriegens*. In general, PHB production is accompanied by high substrate and sterilization costs, which account for up to 50% of the total production cost (Li *et al.*, 2023b). *V. natriegens* p15A-*phaBAC* was able to produce 2.4 g PHB L^{-1} from glycerol (Gly) under non-sterile conditions, outperforming the genetically engineered *E. coli* MG1655 p15A-*phaBAC* strain (Li *et al.*, 2023b). For 2,3-BDO production with *V. natriegens* Δ*frdA* Δ*ldhA*-pETRABC, a non-sterile process using seawater-based minimal medium was performed, achieving 41 g 2,3-BDO L^{-1} within 12 h (Meng *et al.*, 2022).

1.2.2. **Biotechnological applications**

Over the past 10 years, *V. natriegens* has attracted a lot of attention due to its unique features and numerous publications have appeared on this bacterium. First chassis strains have already been developed for biotechnological applications. To obtain a robust platform strain, Pfeifer *et al.* (2019) identified and consequently deleted two prophage regions (VNP1 and VNP2) from the genome, which can be activated under stress but also spontaneously under standard cultivation conditions. Further, two commercially available strains, Vmax™ Express and the next generation strain Vmax™ X2 (Synthetic Genomics Inc., La Jolla, CA, U.S.A.), have been modified for improved protein expression and the incorporation of noncanonical α-amino acids (González et al., 2021; Mojica et al., 2024). Both strains have a reduced genome and a genomically integrated and inducible T7 RNA polymerase system, allowing the usage of pET and pET-like vectors (Weinstock et al., 2016; Xu et al., 2021).

V. natriegens has been engineered for a variety of different products, including alcohols, organic and amino acids, polyesters, as well as pigments such as melanin. Conventionally, melanin is produced by chemical synthesis or by isolation from natural sources such as sepia ink (Smith *et al.*, 2023). Wang *et*

al. (2020) overexpressed the tyrosinase gene *tyr1* from *Priestia megaterium* in *V. natriegens*. The resulting strain *V. natriegens* pJV-Tyr1 formed 0.5 g melanin L^{-1} from L-tyrosine within 2 h. Recently, Smith *et al.* (2023) optimized the minimal medium M9v2 for *V. natriegens* pJV-Tyr1 and were able to further enhance the titer to 7.6 g melanin L^{-1} from overnight (O/N) cultures, achieving the highest reported volumetric productivity to date of 473 mg L^{-1} h^{-1}.

Li *et al.* (2023a) presented a strategy for carbon-negative biosynthesis of several products. In a phototrophic community, *Synechococcus elongatus* was used to produce sucrose from carbon dioxide (CO_2), and *V. natriegens* successfully metabolized the sugar to various products (313 mg lactic acid L^{-1}, 137 mg 2,3-BDO L^{-1}, 25 mg p-coumaric acid L^{-1}, and 9 mg melanin L^{-1}). A remarkably high productivity of 34 g L^{-1} h^{-1} for alanine production was reported by Hoffart *et al.* (2017). Therefore, *V. natriegens* was engineered to eliminate byproduct formation of lactate, acetate, formate, succinate, and ethanol. The resulting strain, *V. natriegens* Δ*dldh* Δ*lldh* Δ*pfl* Δ*mdh,* produced 17 g alanine L^{-1} from glucose using an anaerobic resting cell approach in minimal medium. Zhang *et al.* (2021b) engineered *V. natriegens* for the production of 1,3-propanediol (1,3-PDO) and 3-hydroxypropionate (3HP) by removing byproduct related genes and by introducing a high-copy plasmid pTrc99a for gene overexpression. Further, the gene *glpD*, which is essential for glycerol degradation, was shifted from the chromosome to the plasmid to increase plasmid stability. High final concentrations of 65 g 3-HP L^{-1} and 70 g 1,3-PDO L^{-1} were obtained from glycerol. In 2023, Zhang *et al.* reported a strategy to systematically engineer *V. natriegens* for 1,3-PDO production using a genome-scale metabolic model (GEM) based on AutoKEGGRec. By analyzing the product pathway from glycerol together with the metabolic flux distribution, a strategy to improve the production from glycerol was developed. Therefore, the synthetic production pathway and the glycerol oxidation pathway were balanced, the intracellular reducing environment was optimized, e.g., by improving NADPH availability, and byproduct-related genes encoding for ethanol, lactate, acetate, formate, and 3-HP were deleted. Further, the dissolved oxygen (DO) levels were adjusted during the cultivation. This resulted in a final concentration of approximately 70 g 1,3-PDO L^{-1} with a product yield of 0.61 $mol_{1,3\text{-}PDO}$ mol_{Gly}^{-1} and a volumetric productivity of 2.4 $g_{1,3\text{-}PDO}$ L^{-1} h^{-1}. For the production of 2,3-BDO and acetoin, a pulsed microaerobic fed-batch process was performed with *V. natriegens* harboring the plasmid p455-Ediss containing genes (*budA*, *budB*, and *budC* from *Enterobacter cloacae* subsp. *dissolvens*) for the 2,3-BDO synthetic pathway. A combined diol titer of 50 g L^{-1} and an overall productivity of 3.9 g_{Diol} L^{-1} h^{-1} were obtained (Erian *et al.*, 2020). Meng *et al.* (2022) utilized *V. natriegens* Δ*frdA* Δ*ldhA*-pETRABC for 2,3-BDO production and achieved 41 g 2,3-BDO L^{-1} with an overall productivity of 3.4 $g_{2,3\text{-}BDO}$ L^{-1} h^{-1} using a non-sterilized fed-batch process. Wu *et al.* (2023) attenuated the translation of the *aceE* gene encoding for the E1 subunit of the pyruvate dehydrogenase complex (PDHC), fine-tuned *ppc* encoding for phosphoenolpyruvate carboxylase (PEPC), and removed the prophage regions VNP12 along with genes required for the biosynthesis of byproducts to obtain a suitable pyruvate producer strain. The final

strain *V. natriegens* Δ*VPN1* Δ*VPN2* Δ*pflB* Δ*lldh* Δ*dldh* Δ*pps1* Δ*pps2* P2-*aceE*^{TTG} P2-*ppc*^{ATG} produced 54 g pyruvate (Pyr) L^{-1} from glucose within 16 h using a fed-batch process. Most recently, the high tolerance of *V. natriegens* to formate and its capability to efficiently utilize the promising C1 feedstock was proven (Tian *et al.*, 2023). To further improve formate assimilation, the serine synthesis and formate utilization pathways were coupled and subsequently adaptive laboratory evolution experiments were conducted. Finally, the genes *idgs* from *Streptomyces lividans* and *sfp* from *B. subtilis* were integrated to establish an indigoidine production pathway. The resulting strain S-TCA-2.0-IE consumed 165 g formate L^{-1} and formed 29 g indigoidine L^{-1} within 72 h (Tian *et al.*, 2023). Other examples of successful applications of *V. natriegens* include the production of PHB (Dalia *et al.*, 2017; Li *et al.*, 2023b), selenium and selenium nanoparticles (Fernández-Llamosas *et al.*, 2017), darobactin A (Wuisan *et al.*, 2021), ß-carotene (Ellis *et al.*, 2019), violacein (Ellis *et al.*, 2019), and L-3,4-dihydroxyphenyl-L-alanine (L-DOPA) (Liu *et al.*, 2022).

1.2.2.1. Succinate production

Succinate is an intermediate of the tricarboxylic acid (TCA) cycle and a fermentative end product. It can be formed by several pathways starting from glycolysis (Thoma *et al.*, 2021). The oxidative pathway of the TCA (TCA_{ox}) and the glyoxylate shunt both yield 1 mol of succinate (Suc) per mol of glucose (Glc) and thereby generating 3 mol of nicotinamide adenine dinucleotide (NADH) and 2 mol of CO_2. The highest theoretical product yield of 2 mol_{Suc} mol_{Glc}^{-1} is obtained when succinate is produced by the reductive arm of the TCA (TCA_{red}). Therefore, 1 mol of pyruvate together with 2 mol of NADH and 1 mol of CO_2 are required to obtain 1 mol of succinate. However, the redox state of the cell is not balanced regardless of the pathway used. If the carbon is routed via TCA_{red}, more reducing power is required. NADH can be generated when pyruvate is decarboxylated by the PDHC to acetyl-CoA, which in turn is converted to 1 mol of acetate (Ace), yielding 1 mol of adenosine triphosphate (ATP) and 1mol of NADH. The usage of the TCA_{ox} creates a surplus of NADH that cannot be recycled by the respiratory chain under anaerobic conditions and no other electron acceptors are available. If all pathways are fully operational under anaerobic conditions, the redox state and carbon flux of the cell can be balanced and a maximum yield of 1.71 mol_{Suc} mol_{Glc}^{-1} is possible when 71% of the carbon is channeled via the TCA_{red} and 29% via the TCA_{ox}/glyoxylate shunt (Vuoristo *et al.*, 2016; Thoma *et al.*, 2021).

Succinate belongs to the group of 1,4-dicarboxylates and has been ranked by the U.S. Department of Energy as one of the top twelve building block chemicals that can be converted from sugar to high-value biobased chemicals through biological conversion (Werpy and Petersen, 2004). Succinate serves as precursor for numerous chemicals including tetrahydrofuran, 1,4-butanediol, γ-butyrolactone, pyrrolidones, and hydroxybutyric acid, which can be used directly or converted into valuable compounds

for various industrial sectors (Werpy and Petersen, 2004). Further, succinate functions as a platform compound for the synthesis of polyesters and biodegradable materials, such as the plastic polybutylene succinate. In addition, it can be used as an anticarcinogenic and insulinotropic agent in the pharmaceutical industry (Cao *et al.*, 2013). In the agricultural sector, succinate is used for seed treatment and as a growth regulator. Moreover, it is used in the food industry as a bread-softening agent and flavor enhancer, among other things (Yang *et al.*, 2020). The market potential for succinic acid (SA) and its direct derivatives is expected to be 245,000 tons per year, while the market potential for succinic acid-derived polymers is estimated at 25,000,000 tons per year (Bozell and Petersen, 2010).

To date, the demand for succinate has been met mainly by petrochemical synthesis from the precursor n-butane/butadiene via maleic anhydride (Bechthold *et al.*, 2008). Traditional chemical processes cause serious environmental problems, often require high temperatures and pressures, and are confronted with declining global fossil fuel resources and their increasing prices (Cao *et al.*, 2013). Therefore, sustainable and environmentally friendly biobased processes must be established. However, the overall cost of biobased fermentations must first be reduced in order to become more competitive with existing petrochemical processes. High product titers of 100 g L^{-1}, yields of around 80 – 90% and minimum productivities of 2.5 g L^{-1} h^{-1} are required (Werpy and Petersen, 2004; Thoma and Blombach, 2021). Moreover, to cut fermentation costs, the usage of minimal media without the addition of expensive components such as yeast extract is necessary. The costs of substrate and downstream processing must be considered and carefully weighed. For instance, refined sugar is an expensive carbon source, but natural carbon sources often contain a large number of substances that may interfere with the process and increase the cost of product purification (Sauer *et al.*, 2008). The purification costs for fermentative-based products typically account to more than 60% of the overall cost, and hence it is crucial to minimize downstream-related costs to enhance competitiveness with petrochemical processes (Bechthold *et al.*, 2008, Dai *et al.*, 2020). Ideally, the pH value of the bioreactor broth should be low and pH adjustment should be avoided throughout the fermentation to reduce the costs of neutralization (Werpy and Petersen, 2004). In addition, succinate is present in the undissociated form, which is advantageous since the free acid form rather than the salt form is required for most applications (Bechthold *et al.*, 2008). Finally, the accumulation of byproducts needs to be reduced, as the subsequent separation from the product adds to the overall cost.

Many efforts have been made to optimize succinate production using natural succinate overproducers like *Actinobacillus succinogenes*, *Anaerobiospirillum succiniproducens*, and *Mannheimia succiniciproducens*, as well as with metabolically engineered bacteria and yeasts, such as *E. coli*, *C. glutamicum*, and *S. cerevisiae*. Various strategies have been applied to either improve existing metabolic pathways or to introduce new ones (Cheng *et al.*, 2013). Common approaches include the elimination of byproduct formation through gene knockouts and the overexpression of genes directly involved in the succinate production pathway. In addition, strategies to alter the substrate and

product transport and to improve the internal NADH and ATP formation have been employed, and often a combination of all of the above has been used. Acetate, formate, lactate, and pyruvate have been repeatedly reported as common byproducts and are thus the main targets for metabolic engineering. Lee *et al.* (2006) disrupted the *ldhA*, *pflB*, *pta*, and *ackA* genes in *M. succiniciproducens* and obtained a strain that produced 52 g SA L^{-1} with almost no formation of acetate, formate, and lactate. *C. glutamicum* Δ*ldhA* - pCRA717 was engineered to overexpress the *pyc* gene encoding for the pyruvate carboxylase (Pyc) to increase the anaplerotic flux towards oxaloacetate and to limit lactate production. A final titer of 146 g SA L^{-1} was achieved within 46 h (Okino *et al.*, 2008). *C. glutamicum* BOL-3/pAN6-*gap* was successfully modified to eliminate byproducts such as acetate and lactate. Furthermore, the redox balance was improved by chromosomal integration of an NAD^+-coupled formate dehydrogenase from *Mycobacterium vaccae*. Thus, formate could be used as a donor for reducing equivalents and CO_2. Moreover, pyruvate carboxylation was enhanced by integration of the *pyc* gene from *C. glutamicum* DM1727. A titer of 134 g succinate L^{-1} was obtained with a volumetric productivity of 2.6 g_{Suc} L^{-1} h^{-1} (Litsanov *et al.*, 2012). Sánchez *et al.* (2005) engineered *E. coli* SBS550MG (pHL413) by deleting genes belonging to the lactate, ethanol, and acetate pathways to conserve NADH and/or carbon. Further, heterologous overexpression of *pyc* from *Lactococcus lactis* was conducted and the gene *iclR,* which encodes for a transcriptional repressor protein of the glyoxylate shunt, was deleted. This strategy was used to construct a dual succinate synthesis pathway in which the carbon flux is directed simultaneously through the TCA_{red} and the glyoxylate shunt to improve NADH availability, since the glyoxylate shunt requires less NADH for succinate formation, thus increasing the overall yield of succinate. A high average product yield of 1.5 mol_{Suc} mol_{Glc}^{-1} was reported. Zhu *et al.* (2014) showed that the overexpression of the succinate exporter SucE and the overexpression of enzymes belonging to the glyoxylate shunt could improve the succinate yield from glucose. Using an anaerobic fed-batch process, a final titer of 109 g succinate L^{-1} with a final yield of 1.32 mol_{Suc} mol_{Glc}^{-1} was achieved with *C. glutamicum*. Besides bacteria, the yeast *S. cerevisiae* is an established succinate producer that has been used for aerobic succinate production since the reductive pathway is thermodynamically unfavorable and the corresponding enzymes are subject to glucose repression (Raab and Lang, 2011). The high acid- and osmotolerance of *S. cerevisiae* allows fermentation at a low pH value without the necessity for pH titration, which facilitates downstream processing by eliminating the need for salt neutralization, thus reducing production costs (Raab and Lang, 2011).

Dual phase or two-stage processes are often used for succinate production. These processes have the advantage of decoupling the growth from the production phase, allowing ideal conditions to be applied to each phase. In a dual-phase system, a transition is made from aerobiosis to anaerobiosis, while in a two-stage process, the different stages are performed in two different vessels (Lange *et al.*, 2017). The timing of the transition has to be chosen carefully, as the productivity of the cells is highly dependent on their physiological state at that time. Furthermore, enzymes that are expressed during aerobic growth

can remain active throughout the production phase, and thus have a strong influence on productivity. Vemuri *et al.* (2002) used oxygen-dependent changes in fermentation parameters, such as the respiratory quotient and the DO content, to test different transition times with *E. coli* AFP111/pTrc99A-*pyc* in a dual-phase process, as oxygen is considered an important regulator for facultative anaerobes due to a variety of alternative enzymes that are expressed at different oxygen levels. The highest titer of 98 g succinate L^{-1} was reached when the transition to the anaerobic phase occurred at a DO value of around 90%. Wang *et al.* (2011) chose a different approach and tested different cell densities to determine the transition time. A positive correlation was found between higher CDWs and the overall process performance in terms of titer, yield, and productivity. The highest titer of 116 g succinate L^{-1} was achieved with 20 g_X L^{-1} at the transition time with *E. coli* SD121. The strain showed a productivity of 1.55 g_{Suc} L^{-1} h^{-1} and a remarkable product yield of 1.7 mol_{Suc} mol_{Glc}^{-1}. Jiang *et al.* (2010) discovered that the applied growth rate and the chosen glucose supply have an influence on succinate production as well. A beneficial effect of a glucose-limited growth compared to a stable glucose concentration of 20 g glucose L^{-1} was observed for a two-stage process, and the reduction of the growth rate from 0.15 to 0.07 h^{-1} further increased the final concentration by 36% to 101 g SA L^{-1}.

In some cases, triple-phase processes with an oxygen-limited interface between aerobic biomass formation and zero-growth product formation are applied to adapt the enzymatic machinery towards anaerobiosis (Lange *et al.*, 2017). Zhu *et al.* (2011) investigated the difference in the length of the microaerobic phases using *E. coli* SBS550MG (pHL413) and reported that the duration of the microaerobic phase greatly affects the cell viability when switching to anaerobic conditions. An optimum of 2 – 5 h was found. Furthermore, the DO regulated by the agitation rate during the aerobic and microaerobic phases had an effect on cell viability, succinate production, and byproduct formation, and it was shown that more pyruvate accumulation occurred in high DO experiments. Depending on the chosen agitation rate, yields between 1.24 and 1.60 mol_{Suc} mol_{Glc}^{-1} were obtained. The effect of the pH regulation was studied as well, and a negative effect was shown in regard of specific succinate production rate and yield when a pH control was applied during the aerobic and microaerobic phases as long as the value did not drop below pH 5.5. By applying the best conditions, a titer of 62 g succinate L^{-1} was obtained. Martínez *et al.* (2010) investigated the impact of different aeration rates in a dual-phase system with *E. coli* SB550MG (pHL413) using a 1 L bioreactor. At a high aeration rate of 150 L h^{-1}, a productivity of 0.9 g_{Suc} L^{-1} h^{-1} and a yield of 1.25 mol_{Suc} mol_{Glc}^{-1} were obtained. Pyruvate accumulation was observed during the production phase. Reducing the aeration rate to 90 L h^{-1} resulted in a three-hour microaerobic phase. Almost no pyruvate formation was observed and, in addition, the productivity and yield were increased to 1.3 g_{Suc} L^{-1} h^{-1} and 1.55 mol_{Suc} mol_{Glc}^{-1}, respectively.

The following Table 1 provides an overview of the KPIs achieved by bacterial fermentation. The data generated in this work for *V. natriegens* will be discussed in more detail below.

Table 1: Overview of bacterial succinate production processes. Reported values for succinic acid production have been recalculated for succinate and are marked with the symbol *.

Organism	Substrate	Complex/organic supplements	Q_P | g L^{-1} h^{-1}	Titer | g L^{-1}	Yield | g g^{-1}	Time | h	Reference
Actinobacillus succinogenes	Sucrose + CO_2 + Na_2CO_3	Yeast extract + Corn steep liquor	2.1*	59.5*	0.82*	28	Jiang *et al.* (2014)
Corynebacterium glutamicum	Glucose + $NaHCO_3$	Biotin + Thiamine	3.1*	144*	0.90*	46	Okino *et al.* (2008)
	Glucose + Formate + $NAHCO_3$	/	2.5	134	1.08	53	Litsanov *et al.* (2012)
	Glucose + $NAHCO_3$	/	1.1	109	0.85	98	Zhu *et al.* (2014)
Escherichia coli	Glucose + CO_2 + Na_2CO_3	Yeast extract + Tryptone + Biotin + Thiamine	1.3	98	1.14	75	Vemuri *et al.* (2002)
	Glucose + CO_2 + Na_2CO_3	Yeast extract + Tryptone	/	40	0.97	/	Sánchez *et al.* (2005)
	Glucose + CO_2	Tryptone + Yeast extract + Thiamine + Biotin	1.3	19	1.55	15	Martínez *et al.* (2010)
	Glucose + CO_2 + $NAHCO_3$ Citric acid + Fe(III) citrate + $Mg_5(CO_3)_4$	Thiamine HCl + Biotin	1.9*	99*	1.05*	/	Jiang *et al.* (2010)
	Glucose + $NAHCO_3$ + CO_2	Tryptone + Yeast extract	1.6	116	1.1	75	Wang *et al.* (2011)

Organism	Substrate	Complex/organic supplements	Q_P | g L^{-1} h^{-1}	Titer | g L^{-1}	Yield | g g^{-1}	Time | h	Reference
Mannheimia succiniciproducens	Glucose + Glycerol + $NaHCO_3$ + CO_2	Biotin + Ca-pantothenate + Pyridoxine-HCl + Thiamine + Ascorbic acid + Nicotinic acid + Amino acids	10.2*	132*	0.80*	13	Ahn *et al.* (2020)
	Glucose + CO_2	Yeast extract	1.8*	52*	0.73*	29	Lee *et al.* (2006)
Vibrio natriegens	Glucose + $KHCO_3$	/	8.6	60	0.74	7	Thoma *et al.* (2021) This work
	Glucose + $KHCO_3$	/	8.5	51	0.90	6	Schulze *et al.* (2023) This work

For *V. natriegens*, it has already been shown that both the TCA_{red} as well as the TCA_{ox}/glyoxylate shunt contribute to succinate formation under anaerobic conditions (Figure 3) (Thoma et al., 2021). Genes for a PEPC and a PEP carboxykinase (Pck) are annotated in contrast to a Pyc, and thus it is possible that the anaerobic flux to oxaloacetate is only provided via PEP carboxylation (Thoma *et al.*, 2021). In 2021, *V. natriegens* was already engineered for anaerobic succinate production based on a strain lacking the genes for a D- and L-lactate dehydrogenase (*dldh* and *lldh*) and for a pyruvate formate lyase (*pfl*) (Hoffart *et al.*, 2017) (Figure 3). To eliminate other competing pathways and to increase the availability of precursors, the *ald* gene, annotated for alanine dehydrogenase, was removed (Figure 3). These genetic modifications were intended to increase the pyruvate pool. In addition, the *pyc* gene from *C. glutamicum* was integrated to support the anaplerotic flux from pyruvate (Figure 3). The resulting strain *V. natriegens* Δ*lldh* Δ*dldh* Δ*pfl* Δ*ald* Δ*dns*::pyc_{Cg} (Succ1) formed 60 g succinate L^{-1} from glucose during a zero-growth process in VN medium that did not require the addition of vitamins, amino acids, or other expensive supplements. A product yield of 1.14 mol_{Suc} mol_{Glc}^{-1} was obtained, and an exceptionally high overall

productivity of 8.6 g_{Suc} L^{-1} h^{-1} was achieved. During the initial production phase, a maximum productivity of 20.8 g_{Suc} L^{-1} h^{-1} was reported (Thoma et al., 2021).

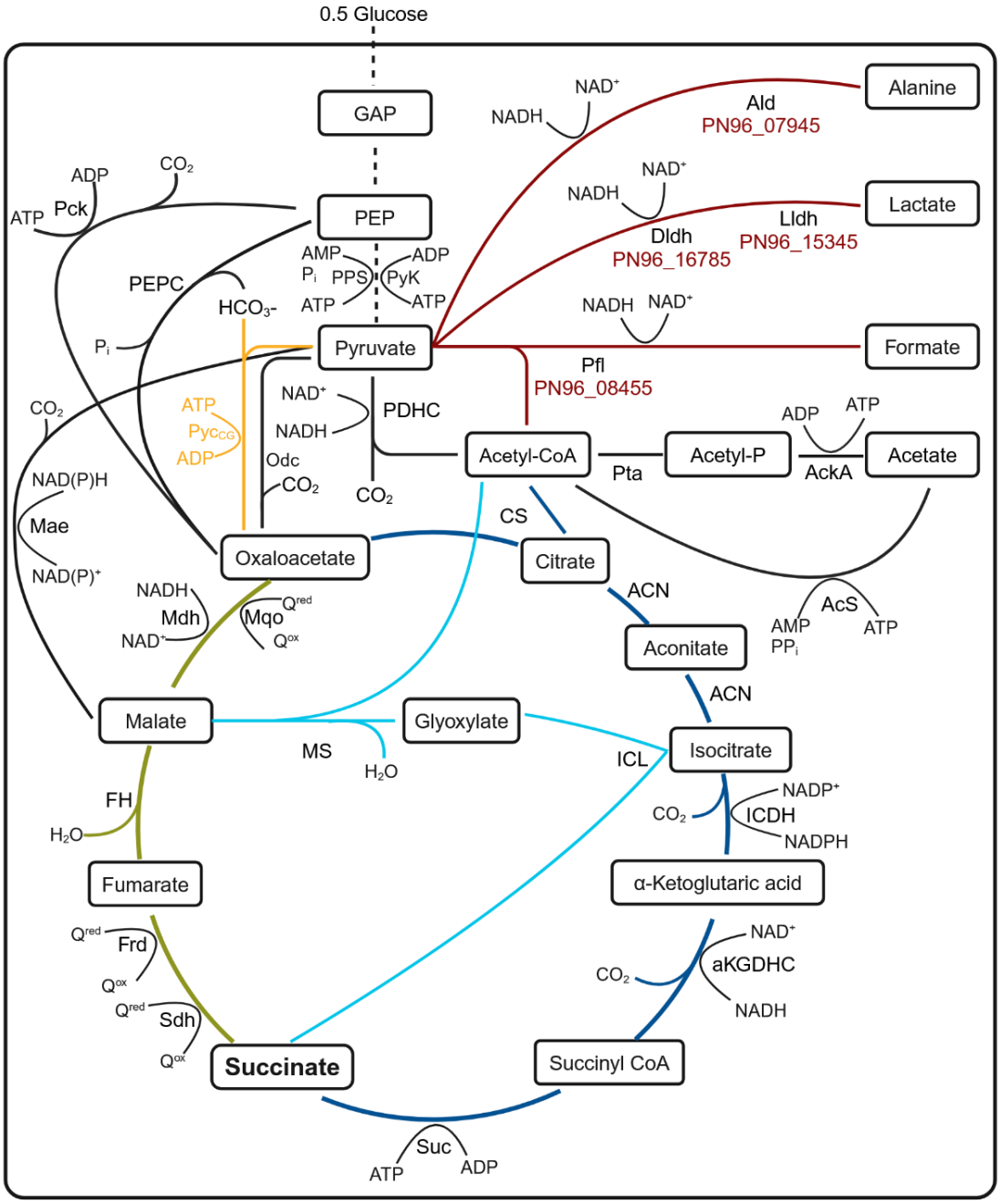

Figure 3: Pathways for succinate formation in *V. natriegens.* Dashed lines indicate multistep reactions. The reductive branch of the TCA cycle is highlighted in green and the oxidative branch in dark blue. The glyoxylate shunt is depicted in light blue. Red lines indicate that the metabolism has been engineered and the corresponding red written genes have been deleted. A yellow path represents the genomic integration of an enzyme. Metabolites are boxed and the corresponding enzymes and cofactors are written underneath or next to them. Abbreviations for metabolites and cofactors: Acetyl-CoA – acetyl-coenzyme A, Acetyl-P – acetyl phosphate, ADP – adenosine diphosphate, AMP – adenosine

monophosphate, ATP – adenosine triphosphate, CO_2 – carbon dioxide, GAP – glyceraldehyde 3-phosphate, HCO_3^- – hydrogen carbonate, H_2O – water, NAD^+ – nicotinamide adenine dinucleotide (oxidized), NADH – nicotinamide adenine dinucleotide (reduced), $NADP^+$ – nicotinamide adenine dinucleotide phosphate (oxidized), NADPH – nicotinamide adenine dinucleotide phosphate (reduced), P_i – phosphate, PEP – phosphoenolpyruvate, PP_i – pyrophosphate, Q^{ox} – quinone, Q^{red} – quinol; Abbreviations for enzymes: αKGDHC – α-ketoglutarate dehydrogenase complex, AckA – acetate kinase, ACN – aconitase, AcS – acetyl-CoA synthetase, Ald – alanine dehydrogenase, CS – citrate synthase, Dldh – D-lactate dehydrogenase, FH – fumarate hydratase, Frd – fumarate reductase, ICDH – isocitrate dehydrogenase, ICL – isocitrate lyase, Lldh – L-lactate dehydrogenase, Mae – malic enzyme, Mdh – malate dehydrogenase, MS – malate synthase, Mqo – malate:quinone oxidoreductase, Odc – oxaloacetate decarboxylase, Pck – PEP carboxykinase, PDHC – pyruvate dehydrogenase complex, PEPC – PEP carboxylase, Pfl – pyruvate formate lyase, PPS – PEP synthase, Pta – phosphate acetyltransferase, Pyc_{CG} – pyruvate carboxylase from *C. glutamicum*, PyK – pyruvate kinase, Sdh – succinate dehydrogenase, Suc – succinyl-CoA synthetase.

1.2.2.2. Pyruvate production

Pyruvate is a three-carbon 2-oxo-monocarboxylic acid and the final product of glycolysis (Maleki and Eiteman, 2017). Located in the central metabolism, it is an important intermediate for various products like carbohydrates, alanine, ethanol, fatty acids, and energy (via TCA) (Yuan *et al.*, 2022).

Pyruvate and its derivatives find many applications in the pharmaceutical, cosmetic, and food industries. It is used as a dietary supplement for weight loss and for the enhancement of the physical condition. Other health benefits include an improvement of the myocardial function or a reduction of the HDL cholesterol. Moreover, it possesses antioxidant effects and could be used as nutraceutical for diabetes II (Maleki and Eiteman, 2017; Yuan *et al.*, 2022). In the cosmetic industry, pyruvic acid (PA) is used as a potent chemical peeling agent for the treatment of acne, superficial scars, photodamage, and pigmentary disorders (Berardesca *et al.*, 2006). Furthermore, pyruvate serves as a precursor for various chemicals, including L-tyrosine, L-tryptophan, N-acetylneuraminic acid (sialic acid), and L-DOPA (Yuan *et al.*, 2022). Additionally, it has been used for butanol production via a three-enzyme cascade and has been proposed as a starting material for the enzymatic synthesis of propionate (Maleki and Eiteman, 2017). Pyruvate is mainly produced by chemical synthesis through dehydration and decarboxylation of tartaric acid. This process is easy to implement, but requires high temperatures, causes serious environmental issues, and is also not cost efficient (Li *et al.*, 2001a; Yuan *et al.*, 2022). Another method uses lactic acid as a raw material and causes it to react with oxygen under the action of catalysts. This method is being investigated as an environmentally friendly alternative to the tartaric acid method.

However, biotechnological production offers a promising alternative for the cost-efficient production of pyruvate (Li *et al.*, 2001a; Yuan *et al.*, 2022). There are three options for biotechnological production of pyruvate: the resting cell approach, which decouples the growth and production phases, the enzymatic conversion, and the direct fermentation method. The latter shows the greatest potential in terms of cost-effectiveness and product purity (Li *et al.*, 2001a).

Early metabolic engineering approaches for microbial processes focused on increasing the rate of glycolysis (Maleki and Eiteman, 2017). From 1 mol of glucose, 2 mol of pyruvate are formed, accompanied by the generation of 2 mol of NADH and ATP. When ATP production decreases, the cells attempt to compensate for the reduced ATP availability by increasing the rate of glycolysis (Maleki and Eiteman, 2017). The deletion of *atpFH* resulted in an inactivation of F0 of the (F1F0)H+-ATP synthase complex in an *E. coli* strain that also contained mutations in *aceEF*, *pfl*, *poxB*, *pps*, and *ldhA*. This additional deletion significantly increased the specific glucose consumption rate by 36% and the specific pyruvate production rate by 49% compared to the parental strain. The deletion of the respiratory repressor ArcA further increased the KPIs, and the final strain *E. coli* ALS1059 strain reached 90 g pyruvate L^{-1} with a volumetric productivity of 2.1 g_{Pyr} L^{-1} h^{-1} in a fed-batch process and yielded 0.68 g_{Pyr} g_{Glc}^{-1} (Zhu *et al.*, 2008). Another possibility to enhance pyruvate formation is to increase the oxidation of NADH and thus the availability of NAD^+. Overexpression of a water-forming NADH oxidase from *Streptococcus pneumoniae* increased the glucose uptake rate in *E. coli* by 70% (Vemuri *et al.*, 2006). The introduction of the NADH oxidase in *E. coli* ALS1059 could further improve the specific glucose uptake and pyruvate formation rate by about 10% (Zhu *et al.*, 2008).

Due to the central position of pyruvate in aerobic and anaerobic microbial metabolism and its involvement in many subsequent reactions, byproducts such as acetate, lactate, and ethanol frequently accumulate during fermentations. This consumes a large amount of carbon that is not channeled into the desired product and further, it complicates the subsequent product separation. Thus, metabolic engineering is required to eliminate competing pathways and to promote pyruvate accumulation. Biobased production is mainly performed with *E. coli* and yeasts. Many studies on vitamin-auxotroph yeasts, e.g., *Candida glabrata*, *Yarrowia lipolytica* (formerly known as *Torulopsis glabrata* and *Candida lipolytica*), and *S. cerevisiae* have been reported (Li *et al.*, 2001a). For instance, Li *et al.* (2001b) utilized a multivitamin auxotrophic *C. glabrata* strain (WSH-IP303) for pyruvate production in a batch culture. The accumulation of large amounts of pyruvate requires a specific balance of thiamine, nicotinic acid, biotin, riboflavin, and pyridoxine. It has been shown that thiamine, a cofactor of the PDHC and pyruvate decarboxylase (Li *et al.*, 2001a), had the greatest influence on pyruvate production. By combining the optimal vitamin concentrations, a titer of 69 g pyruvate L^{-1} and a product yield of 0.62 g_{Pyr} g_{Glc}^{-1} were achieved within 56 h (Li *et al.*, 2001b). Yuan *et al.* (2020) utilized the yeast *Y. lipolytica* for the formation of PA from glycerol. Osmotic stress is known to limit cell growth as well as biomass yield and it strongly affects the product synthesis in *Y. lipolytica*. Therefore, mutations were

induced by the atmospheric and room temperature plasma (ARTP) method and a subsequent screening of mutants with elevated NaCl tolerance was conducted. The resulting mutant strain A4 was able to resist the osmotic pressure caused by NaCl and survived concentrations of up to 160 g NaCl L^{-1}. Further, it achieved a final titer of 97 g PA L^{-1} and a yield of 0.8 g_{PA} g_{Gly}^{-1}, which was about 30% higher compared to the parental strain. In a fed-batch process, *Y. lipolytica* SKO 6 produced 126 g PA L^{-1} and 124 g PA L^{-1} with yields of 0.68 g_{PA} g_{Gly}^{-1} and 0.62 g_{PA} g_{Gly}^{-1} from pure and crude glycerol, respectively (Cybulski *et al.*, 2019). Van Maris *et al.* (2004) utilized a pyruvate decarboxylase-negative (Pdc^-) *S. cerevisiae* strain for aerobic pyruvate production in batch cultures. Pdc^- strains require C2 compounds such as acetate or ethanol for growth, and further, they are not able to grow on defined medium with glucose even in the presence of a C2 source. Therefore, a selection pressure was applied in a chemostat culture to obtain a C2-independent strain, and in a subsequent selection round it was screened for glucose tolerance in batch cultures. The selected strain TAM produced 135 g pyruvate L^{-1} within 100 h with a product yield of 0.54 g_{Pyr} g_{Gly}^{-1}.

In *E. coli*, a common strategy to limit or block the carbon flux from glycolysis to TCA is the deletion or downregulation of a component of the PDHC (Figure 3). The PDHC is responsible for the oxidative decarboxylation of pyruvate to acetyl-CoA, and thus represents a key element between glycolysis and TCA. Tomar *et al.* (2003) studied different *E. coli* strains, each containing a mutation of a gene involved in the PDHC (*aceE*, *aceF*, and *lpd*) or in the acetate synthesis pathway (*ack*, *pta*, and *rpoS*). In addition, the gene *ppc*, which encodes for PEPC, was deleted in each mutant strain. Manipulation of the PDHC resulted in the cessation of the flux to acetyl-CoA, which is necessary for cell growth, and thus additional carbon in the form of acetate was provided for the synthesis of acetyl-CoA. During the initial screening for a high product yield, it was shown that the *ppc* mutation decreased pyruvate yield in all strains except for the lowest producer strain (*rpoS* mutant), which obtained 0.09 g_{Pyr} g_{Glc}^{-1}. The highest yields were obtained for the *aceE* and *aceF* mutants (0.54 and 0.47 g_{Pyr} g_{Glc}^{-1}, respectively), and batch fermentations for pyruvate production were subsequently conducted with these strains. The best results were obtained for the *aceF* mutant. A titer of approximately 35 g pyruvate L^{-1} was achieved with a productivity of 1.5 g_{Pyr} L^{-1} h^{-1} and a high yield of 0.72 g_{Pyr} g_{Glc}^{-1}. Zelić *et al.* (2003) used the acetate auxotrophic *E. coli* strain YYC202 *ldhA::Kan* strain for pyruvate production in a fed-batch process. Therefore, the correlation between the CO_2 production rate and the acetate consumption rate was determined experimentally and was subsequently used for on-line regulation of the acetate feed. A final concentration of 62 g pyruvate L^{-1} was obtained with a yield of 1.11 mol_{Pyr} mol_{Glc}^{-1} and a productivity of 1.8 g_{Pyr} L^{-1} h^{-1}. In a subsequent study, several process alternatives were investigated. Using a continuous process with cell retention, a high productivity of 4.6 g_{Pyr} L^{-1} h^{-1} was achieved. However, this approach was not pursued further, since long-term production instabilities were observed. Moreover, an in-situ product recovery process (ISPR) was tested. The integration of on-line product recovery is crucial for inhibiting products and this could be the case at high pyruvate concentrations above 500 mM pyruvate L^{-1} (Zelić

et al., 2003; Zelić *et al.*, 2004). During this ISPR process, electrodialysis was used for product separation and a final (calculated) titer of 79 g pyruvate L^{-1} was obtained. The highest yield of 1.78 mol_{Pyr} mol_{Glc}^{-1} together with a high productivity of 6.0 g_{Pyr} L^{-1} h^{-1} was achieved using a repetitive fed-batch approach (Zelić *et al.*, 2004).

Besides *E. coli* and yeasts, other bacteria have been utilized for pyruvate production. *C. glutamicum* was engineered to accumulate pyruvate. The PDHC and the pyruvate:quinone oxidoreductase were inactivated. In addition, the gene *ldhA* encoding for a NAD^+-dependent L-lactate dehydrogenase (LldhA) was deleted and the native acetohydroxyacid synthase was replaced by an attenuated variant (ΔC-T IlvN) to abolish L-valine overflow. Furthermore, the genes *alaT* and *avtA* encoding for transaminases were deleted to reduce L-alanine formation. The resulting strain *C. glutamicum* Δ*aceE* Δ*pqo* Δ*ldhA* ΔC–T *ilvN* Δ*alaT* Δ*avtA* produced approximately 45 g pyruvate L^{-1} with a yield of 0.97 mol_{Pyr} mol_{Glc}^{-1} using a fed-batch process with oxygen deprivation during the mid- and late-growth phases (Wieschalka *et al.*, 2012).

Halophilic microbes have gained attention for the production of organic acids (Li *et al.*, 2001a; Yin *et al.*, 2015) and the halophilic, alkaliphilic *Halomonas* sp. KM-1 was studied for pyruvate production. The bacterium secreted 63 g pyruvate L^{-1} within 48 h using an aerobic batch cultivation with sodium nitrate- and glucose-rich medium without sterilization (Kawata *et al.*, 2016).

Recently, *V. natriegens* has been engineered for pyruvate production as well (Wu *et al.*, 2023). The two prophage regions VNP1 and VNP2 were deleted to improve cell robustness. Furthermore, it has already been shown that prophage-free *V. natriegens* exhibits an increased pyruvate production (Pfeifer *et al.*, 2019). In a next step, essential genes for the synthesis of byproducts such as formate, lactate, and PEP were removed by deleting the genes encoding for pyruvate formate lyase (*pflB*), L-lactate dehydrogenase (*lldh*), D-lactate dehydrogenase (*dldh*), and PEP synthase (*pps1* and *pps2*). Further, the *aceE* gene encoding for the E1 subunit of the PDHC was downregulated and the expression of the *ppc* gene encoding for the PEPC was fine-tuned to balance the formation of biomass and pyruvate. The resulting strain PYR32 achieved a titer of 54 g pyruvate L^{-1}, a yield of 1.17 mol_{Pyr} mol_{Glc}^{-1}, and a total volumetric productivity of 3.4 g_{Pyr} L^{-1} h^{-1} in a fed-batch process at 30 °C (Wu *et al.*, 2023). Moreover, high titers were obtained when pyruvate was produced from sucrose (34 g L^{-1}) or gluconate (57 g L^{-1}) with yields around 1.3 mol_{Pyr} mol_{S}^{-1}. However, the productivity decreased to 1.6 g_{Pyr} L^{-1} h^{-1} from sucrose and to 1.8 g_{Pyr} L^{-1} h^{-1} from gluconate (Wu *et al.*, 2023).

Besides the typical fermentative byproducts, e.g., acetate, lactate, and ethanol that can occur during pyruvate production, the molecule parapyruvate, also known as 4-hydroxy-4-methyl-2-oxogluterate and 2-hydroxy-2-methyl-4-oxopentanedioic acid, is a less studied compound responsible for impurities in PA or PA salts (Montgomery and Webb, 1956; Margolis and Coxon, 1986; Chang *et al.*, 2018). Parapyruvate is the result of an aldol-type condensation that can occur under strongly acidic and basic conditions. It can be present as dicarboxylic acid and cyclic lactone derivate as well as linear polymers.

Solutions of sodium pyruvate are unstable and the instability is greater at higher temperatures, at basic pH values, or in the presence of Tris or ammonium salts. The solution is also not suitable for storage at -20 °C or above (Margolis and Coxon, 1986). Parapyruvate inhibits the enzyme lactate dehydrogenase and it can react with transaminases to form amino acids (Margolis and Coxon, 1986). Further, it is an analog of α-ketoglutarate and may therefore be a competitive inhibitor of the α-ketoglutarate dehydrogenase complex (αKGDHC) and consequently of the TCA (Montgomery and Webb, 1956). Inhibition of the enzyme complex is associated with functional abnormalities in mitochondria, and a decreased activity is implicated in age-related neurodegenerative diseases such as Alzheimer´s or Parkinson´s disease (Chang *et al.*, 2018). In a study using human fibroblastic Hs68 cells, it was shown that parapyruvate can inhibit αKGDHC activity and induce senescence in Hs68 cells. This effect can be reversed by the supplementation with high levels of calcium ions (Ca^{2+}), which are an activator of the αKGDHC (Chang *et al.*, 2018).

Pyruvate is an approved food supplement by the European Food Safety Authority (EFSA, 2009). The industrial production of calcium pyruvate requires alkaline treatment, which promotes the formation of parapyruvate. Chang *et al.* (2018) detected parapyruvate between 1.4 and 10.6% in all five tested commercially available supplements from the U.S. market. Stability tests of parapyruvate at pH 2 suggested that the compound remains stable in acidic environments, such as the stomach, and thus the authors concluded that parapyruvate content should be an important issue for the food safety of pyruvate supplements.

2. Material & Methods

This chapter provides an overview of the bacterial strains used in this work and their various cultivation methods, ranging from small-scale shaking flasks and test tubes up to bioreactor cultures and the associated operating methods, such as batch, fed-batch, and two-stage processes. Furthermore, the composition of the media used is given. Sample processing, the subsequent analytical evaluation, as well as the determination of growth parameters and KPIs are stated. The chemicals, devices, software and materials used in this work alongside the corresponding manufacturers are listed in Table A2, Table A3, and Table A4. Figures 2 – 7 were generated with Biorender.com.

2.1. Bacterial strains

All bacterial strains used in this work are summarized in Table 2. For long-term storage, the strains were preserved at -80 °C as 30% (v v^{-1}) glycerol stocks. For stock preparation, cells were cultivated O/N in 5 mL 2×YTN (adapted from Sambrook and Russell (2001)), and then an appropriate amount of the cell suspension was transferred and mixed with glycerol. Thereafter, the stock was immediately frozen.

Table 2: Bacterial strains

Strain	Relevant characteristic(s)	Source or reference
V. natriegens wt	Wildtype strain DSM 759 (ATCC 14048)	German Collection of Microorganisms and Cell Cultures
V. natriegens Δ*luxS*	*V. natriegens* wt with deletion of the *luxS* gene (PN96_01245)	provided by Maurice Hädrich
V. natriegens Δ*sypK*	*V. natriegens* wt with deletion of the *sypK* gene (PN96_04625)	provided by Maurice Hädrich
V. natriegens Δ*cpsR*	*V. natriegens* wt with deletion of the *cpsR* gene (PN96_10960)	Schulze *et al.* (2023)
V. natriegens Δ*wbfF*	*V. natriegens* wt with deletion of the *wbfF* gene (PN96_12195)	Schulze *et al.* (2023)
V. natriegens Δ*cps*	*V. natriegens* wt with deletion of the genomic region PN96_14980 to PN96_15050	Schulze *et al.* (2023)
V. natriegens Δ*syp* Δ*cps*	*V. natriegens* Δ*cps* with additional deletion of the genomic region PN96_04590 to PN96_04675	Schulze *et al.* (2023)
V. natriegens Succ1	*V. natriegens* Δ*lldh* Δ*dldh* Δ*pfl* Δ*ald* Δ*dns*::*pyc*$_{Cg}$ (locus tags: PN96_16785, PN96_16800, PN96_08455, PN96_09745 and genomic integration of *pyc* gene from *C. glutamicum* ATCC 13032 into the *dns* gene (PN96_00865))	Thoma *et al.* (2021)
V. natriegens Succ1 Δ*ackA*	*V. natriegens* Succ1 with deletion of an *ackA* gene (PN96_21510)	Thoma *et al.* (2021)
V. natriegens Succ1 Δ*cpsR*	*V. natriegens* Succ1 with deletion of the *cpsR* gene (PN96_10960)	Schulze *et al.* (2023)
V. natriegens Succ1 Δ*cps*	*V. natriegens* Succ1 with deletion of the genomic region PN96_14980 to PN96_15050	Schulze *et al.* (2023)
V. natriegens Δ*aceE*	*V. natriegens* wt with deletion of the gene PN96_01335	provided by Maurice Hädrich
V. natriegens Δ*vnp12* Δ*aceE*	*V. natriegens* Δ*aceE* with the additional deletion of the *vnp12* gene clusters (Pfeifer *et al.*, 2019)	provided by Maurice Hädrich
V. natriegens Δ*vnp12* Δ*aceE* Δ*papA*	*V. natriegens* Δ*vnp12* Δ*aceE* with the additional deletion of the gene PN96_18530	provided by Maurice Hädrich
V. natriegens Δ*vnp12* Δ*aceE* pEKEx2-*papA*	*V. natriegens* Δ*vnp12* Δ*aceE* with the plasmid pEKEx2 with the gene *papA* under the control of the tac-promotor P_{tac}	provided by Maurice Hädrich

2.2. Cultivation media

An overview of all media, including supplements, is provided below. Media and supplements were prepared with deionized water unless otherwise stated. The sterilization of the media was performed by autoclaving, and the supplements were sterilized by passing the solutions through a 0.2 µm filter (Filtropur S plus 0.2, SARSTEDT, Nümbrecht, Germany). Sterile liquid media were stored at room temperature (RT), and sterile supplements were aliquoted and then frozen at -20 °C. Supplements were thawed shortly before usage and added to the already autoclaved medium.
Cultivations were performed using 2×YTN medium (Table 3 and 4).

Table 3: 2×YTN agar plates (adapted from Sambrook and Russell (2001))

Compound	Concentration
Tryptone	16 g L^{-1}
Yeast extract	10 g L^{-1}
NaCl	15 g L^{-1}
Agar-Agar	15 g L^{-1}

Agar plates were stored at 4 °C.

Table 4: 2×YTN medium for liquid cultures (adapted from Sambrook and Russell (2001))

Compound	Concentration
Tryptone	16 g L^{-1}
Yeast extract	10 g L^{-1}
NaCl	15 g L^{-1}
$MgCl_2 \times 6\ H_2O$	50 mM

Minimal cultures were conducted with VN medium supplemented with $CaCl_2$, $MgSO_4 \times 7\ H_2O$, and trace element solution 1 (TCE1) (Table 5). For shaking flask cultures, the pH was adjusted to 7.5 with 5 M KOH before the medium was autoclaved. The pH of all TCE solutions was adjusted to 1 with 32% hydrochloric acid (HCl) to ensure the complete dissolution of all compounds prior to filtration.

Table 5: VN minimal medium (Hoffart *et al.*, 2017). No MOPS was added for bioreactor cultures.

Compound	Concentration
$(NH_4)_2SO_4$	5 g L^{-1}
NaCl	15 g L^{-1}
K_2HPO_4	1 g L^{-1}
KH_2PO_4	1 g L^{-1}
MOPS	21 g L^{-1}
$CaCl_2 \times 2\ H_2O$	0.01 g L^{-1}
$MgSO_4 \times 7\ H_2O$	0.25 g L^{-1}
TCE1 (1000× stock)	1 mL L^{-1}
TCE1 (1000× stock)	
$FeSO_4 \times 7\ H_2O$	16.4 g L^{-1}
$MnSO_4 \times H_2O$	10 g L^{-1}
$CuSO_4 \times 5\ H_2O$	0.31 g L^{-1}
$ZnSO_4 \times 7\ H_2O$	1 g L^{-1}
$NiCl_2 \times 6\ H_2O$	0.02 g L^{-1}

The medium was slightly modified for fed-batch processes to accumulate high biomass concentrations (Table 6).

Table 6: VN minimal medium for fed-batch processes (adapted from Hoffart *et al.* (2017)).

Compound	Concentration
$(NH_4)_2SO_4$	5 g L^{-1}
NaCl	15 g L^{-1}
K_2HPO_4	1 g L^{-1}
KH_2PO_4	1 g L^{-1}
$CaCl_2 \times 2\ H_2O$	0.01 g L^{-1}
$MgSO_4 \times 7\ H_2O$	1.2 g L^{-1}
Fe(III) citrate $\times H_2O$	0.1 g L^{-1}
TCE1 (1000× stock)	1 mL L^{-1}
TCE1 (1000× stock)	
$FeSO_4 \times 7\ H_2O$	16.4 g L^{-1}
$MnSO_4 \times H_2O$	10 g L^{-1}
$CuSO_4 \times 5\ H_2O$	0.31 g L^{-1}
$ZnSO_4 \times 7\ H_2O$	1 g L^{-1}
$NiCl_2 \times 6\ H_2O$	0.02 g L^{-1}

As an alternative to a chloride-containing medium, the following medium VN_{V2} (Table 7) was used.

Table 7: VN_{V2} minimal medium without chloride (adapted from Hoffart *et al.* (2017)). No MOPS was used for bioreactor cultures.

Compound	Concentration
$(NH_4)_2SO_4$	5 g L^{-1}
Na_2SO_4	18 g L^{-1}
K_2HPO_4	1 g L^{-1}
KH_2PO_4	1 g L^{-1}
MOPS	21 g L^{-1}
$CaCl_2 \times 2\ H_2O$	0.01 g L^{-1}
$MgSO_4 \times 7\ H_2O$	0.25 g L^{-1}
TCE1 (1000× stock)	1 mL L^{-1}
TCE1 (1000× stock)	
$FeSO_4 \times 7\ H_2O$	16.4 g L^{-1}
$MnSO_4 \times H_2O$	10 g L^{-1}
$CuSO_4 \times 5\ H_2O$	0.31 g L^{-1}
$ZnSO_4 \times 7\ H_2O$	1 g L^{-1}
$NiCl_2 \times 6\ H_2O$	0.02 g L^{-1}

During the establishment of a fed-batch process for *V. natriegens* wt, media optimization was performed and a tabular summary of the media used is presented below (Table 8).

Table 8: Tested media and supplements for the optimization of fed-batch processes

Medium	Compound	Concentration
Concentrated VN medium (VN_c)	$(NH_4)_2SO_4$	10 g L^{-1}
	NaCl	15 g L^{-1}
	K_2HPO_4	3 g L^{-1}
	KH_2PO_4	3 g L^{-1}
	$CaCl_2 \times 2\ H_2O$	0.01 g L^{-1}
	$MgSO_4 \times 7\ H_2O$	1.20 g L^{-1}
	TCE1 (1000× stock)	1 mL L^{-1}
Multi-concentrated VN medium (VN_{mc}) (adapted from Thiele *et al.* (2021))	$(NH_4)_2SO_4$	20 g L^{-1}
	NaCl	15 g L^{-1}
	K_2HPO_4	20 g L^{-1}
	KH_2PO_4	20 g L^{-1}
	$MgSO_4 \times 7\ H_2O$	5 g L^{-1}
	TCE1 (1000× stock)	1 mL L^{-1}
Minimal medium for high cell density cultivations (MM_{HCDC}) (adapted from Riesenberg *et al.* (1991))	$(NH_4)_2SO_4$	4 g L^{-1}
	NaCl	15 g L^{-1}
	KH_2PO_4	13.3 g L^{-1}
	Citric acid	1.7 g L^{-1}
	$CaCl_2 \times 2\ H_2O$	0.01 g L^{-1}
	$MgSO_4 \times 7\ H_2O$	1.20 g L^{-1}
	TCE3 (1000× stock)	1 mL L^{-1}
Supplements	**Compound**	**Concentration**
Trace Element Solution 2 (TCE2) (1000× stock) (adapted from Erian *et al.* (2018) and Nimbalkar *et al.* (2018))	H_3BO_3	0.4 g L^{-1}
	Na_2SeO_3	0.4 g L^{-1}
	$Na_2WO_4 \times 2\ H_2O$	0.4 g L^{-1}
	$Na_2MoO_4 \times 2\ H_2O$	0.4 g L^{-1}
Trace Element Solution 3 (TCE3) (1000× stock) (adapted from Riesenberg *et al.* (1991))	$CoCl_2 \times 6\ H_2O$	2.5 g L^{-1}
	EDTA	8.4 g L^{-1}
	H_3BO_3	3.0 g L^{-1}
	$Na_2MoO_4 \times 2\ H_2O$	2.5 g L^{-1}

During fed-batch fermentations a glucose-feed was applied with the following composition (Table 9):

Table 9: Feeding solution

Compound	Concentration
Glucose	550 g L^{-1}
NaCl	15 g L^{-1}
$MgSO_4 \times 7\ H_2O$	1.2 g L^{-1}

Each medium for the pyruvate producer strain *V. natriegens* Δ*vnp12* Δ*aceE* pEKEx2-*papA* was additionally supplemented with 1mM isopropyl β-D-1-thiogalactopyranosid (IPTG) and 50 µg Kanamycin mL^{-1} (Kan^{50}).

2.3. Shaking flask cultures

All cultivations started from a glycerol stock, from which cells were streaked out on a 2×YTN agar plate. After an O/N incubation at 37 °C, a single colony was used to inoculate a glass tube filled with 5 mL of 2×YTN. The preculture was again left to grow O/N on an orbital shaker (Ø 25 mm, Multitron®2, INFORS GmbH, Einsbach, Germany) at 37 °C and 180 rpm. Subsequently, 500 µL of the cell suspension was used to inoculate a 500 mL baffled shaking flask preculture containing 50 mL of VN minimal medium supplemented with 10 g glucose L^{-1}. During the exponential growth phase, an appropriate amount of the preculture was harvested to inoculate the main culture to an optical density measured at 600 nm (OD_{600}) of 0.1. Therefore, the preculture was centrifuged (10 min, RT, 4,347×g), the supernatant was discarded, and the remaining cell pellet was resuspended in 1 mL of 0.9% NaCl (w v^{-1}). The suspension was used to inoculate a second shaking flask containing VN medium with 10 g glucose L^{-1} (Figure 4). All shaking flask cultures had an initial pH of 7.5 and cultivation was performed on an orbital shaker at 37 °C and 180 rpm, unless otherwise stated. For pyruvate production, shaking flask were supplemented with 7.5 g glucose L^{-1} and 1 g acetate L^{-1} instead of 10 g glucose L^{-1}. Acetate was added by a 25% (w/v^{-1}) potassium acetate solution, and the glucose stock solution used (50% (w/v^{-1})) was prepared with D(+)-glucose monohydrate. The pH of the stock solutions was not adjusted.

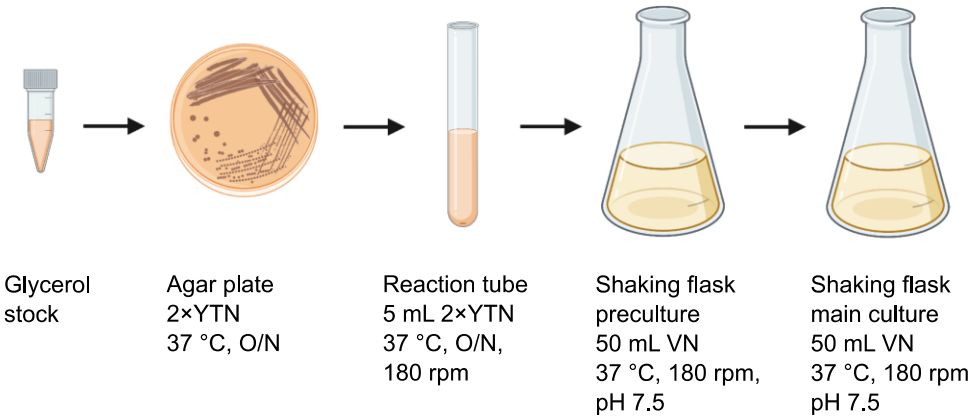

Figure 4: Seed train for shaking flask cultures.

2.4. Batch process

A seed train similar to the one used for shaking flask cultivations was applied for batch processes (Figure 5). The shaking flask preculture was harvested by centrifugation (10 min, RT, 4,347×g) during the exponential growth phase. The cell pellet was resuspended in 1 mL of 0.9% NaCl (w v^{-1}) and the volume was filled up to 50 mL with VN medium. The suspension was used to inoculate a bioreactor with 1 L of VN minimal medium supplemented with 10 g glucose L^{-1} to an OD_{600} of 0.1. All bioreactor processes were performed using a DASGIP Parallel Bioreactor System (Eppendorf, Jülich, Germany) with a vessel volume of 2 L. The antifoam agent Struktol® J 647 (Schill+Seilacher GmbH, Hamburg, Germany) was manually added as required through a septum port.

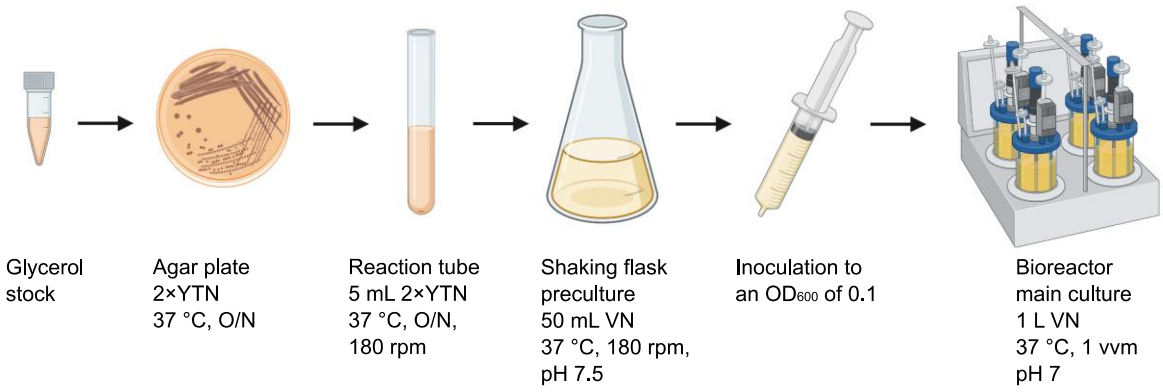

Figure 5: Seed train for batch processes.

Cultivations were conducted at 37 °C. Pressurized air at 1 vvm was used for aeration. The DO was controlled at 50% via the agitation rate (between 400 and 1,500 rpm) and the DO was monitored with a polarographic probe (DO Sensor InPro®6800, Mettler Toledo, Giessen, Germany). The DO sensors were calibrated after the bioreactors were autoclaved and all supplements were added to the medium. Subsequently, the temperature, the agitation and aeration rate were adjusted to the initially set process parameters and a one-point calibration to 100% was performed once the set parameters were stable. The content of oxygen (O_2) and CO_2 in the exhaust gas was detected with the gas analyzer GA4 (Eppendorf, Jülich, Germany). A one-point calibration with pressurized air was performed before usage. The pH value was determined with a standard pH probe (405-DPAS-SC-K8S/325, Mettler Toledo, Giessen, Germany) and it was maintained at 7 using a two-sided pH regulation with 13.3 M NH_4OH and 1.1 M H_3PO_4. Prior to installing the pH sensors in the bioreactors, a two-point calibration was conducted with buffer solutions at a pH of 4 and 7. Acids, bases and feeds were added as required during the process using peristaltic pumps controlled by the DASGIP MP8 module. The module was calibrated at regular intervals according to the manual provided by Eppendorf. For this purpose, a defined volume of a liquid of known density was pumped into a container and the value was compared to the theoretically calculated volume. The deviation was used to adjust the calibration factor. The monitoring of the process parameters and the calibration procedures were the same for all subsequent processes, unless otherwise indicated.

2.5. Glucose-limited fed-batch process

For glucose-limited fed-batch process, an identical seed train as shown in Figure 5 was applied. Bioreactor cultivation was performed with 1 L of VN minimal medium (Table 6). The process was divided into two phases. Initially, 6 g glucose L^{-1} were provided and during this first batch phase the cells grew unlimited with a maximum growth rate μ_{max}. Shortly before glucose depletion, an exponentially increasing glucose feed (Table 9) was started at the beginning of the fed-batch phase to limit the growth rate μ_{set} in order to avoid an overflow metabolism, which would occur above a critical growth rate μ_{crit}. The process parameters were set and controlled according to 2.4. The feeding rate over time F(t) was calculated by using Equation (1).

$$F(t) = F_0 \times e^{\mu_{set} t} \mid L\ h^{-1} \quad (1)$$

$F(t) \mid L\ h^{-1}$	Time-dependent feeding rate
$F_0 \mid L\ h^{-1}$	Feeding rate at the start of the fed-batch phase
$\mu_{set} \mid h^{-1}$	Set growth rate
$t \mid h$	Process time

The initial feeding rate F_0 was determined with the following Equation (2).

$$F_0 = \frac{V_R \times q_s \times c_{X,fed}}{c_{Feed}} \mid L\ h^{-1} \quad (2)$$

$V_R \mid L$	Initial bioreactor volume (medium)
$q_S \mid g_S\ g_X\ h^{-1}$	Biomass-specific substrate uptake rate
$c_{X,fed} \mid g_X\ L^{-1}$	Biomass concentration at the beginning of the fed-batch phase
$c_{Feed} \mid g_S\ L^{-1}$	Substrate concentration in the feeding solution

The bioreactor contained a volume V_R of 1 L VN minimal medium. The biomass-specific substrate uptake rate q_S is based on the substrate requirements for biomass formation, cell maintenance, and product formation (Equation (3)).

$$q_S = \frac{\mu_{set}}{Y_{X/S}} + m_S + q_{S,P} \mid g_S\ g_X^{-1}\ h^{-1} \quad (3)$$

$Y_{X/S} \mid g_X\ g_S^{-1}$	Biomass yield
$m_S \mid g_S\ g_X\ h^{-1}$	Substrate uptake required for cell maintenance
$q_{S,P} \mid g_S\ g_P\ h^{-1}$	Substrate uptake required for product formation

The growth rate μ_{set} was defined as 0.1 h^{-1} and the biomass yield $Y_{X/S}$ was adopted from Hoffart *et al.* (2017) with 0.38 $g_X\ g_{Glc}^{-1}$. During the process, no product formation should occur, and hence the term for $q_{S,P}$ can be set to zero. The required glucose uptake for maintenance metabolism was already determined by Linton *et al.* (1977) with 0.063 $g_{Glc}\ g_X^{-1}\ h^{-1}$.

The biomass concentration at the beginning of the fed batch phase $c_{X,fed}$ was calculated by converting Equation (4).

$$Y_{X/S} = \frac{\Delta c_X}{\Delta c_S} = \frac{c_{X,fed} - c_{X,0}}{c_{S,0} - c_{S,fed}} \mid g_X\ g_S^{-1} \quad (4)$$

$c_{X,0} \mid g_X\ L^{-1}$	Initial biomass concentration
$c_{S,0} \mid g_{Glc}\ L^{-1}$	Initial glucose concentration
$c_{S,fed} \mid g_{Glc}\ L^{-1}$	Substrate concentration at the beginning of the fed-batch phase

The substrate concentration $c_{S,0}$, and the biomass concentration $c_{X,0}$ were set to 6 g glucose L^{-1} and 0.03 $g_X\ L^{-1}$, respectively, at the beginning of the process. It was assumed that glucose was (almost) depleted at the transition to the fed-batch phase and therefore $c_{S,fed}$ was defined as 0 g glucose L^{-1}. The substrate concentration in the feeding solution c_{Feed} contained 550 g glucose L^{-1} (Table 9). Thus, all parameters for the calculation of F_0 are known.

A detailed summary of all fed-batch processes, including deviations from the conditions described in this section, is provided in Table 10.

Table 10: Overview of all glucose-limited fed-batch processes. Only deviations from the reference process are mentioned. Reference: Fed-batch process with *V. natriegens* wildtype in 1 L of VN medium initially containing 6 g glucose L^{-1}. After 2.6 h, shortly before glucose depletion, a feed containing 550 g glucose L^{-1}, 1.2 g $MgSO_4 \times 7\ H_2O$ L^{-1}, and 15 g NaCl L^{-1} was started to limit the growth rate μ_{set} to 0.1 h^{-1}. The temperature was set at 37 °C and the pH was adjusted to 7. The gassing rate F was kept constant at 1 vvm of pressurized air (≙ 60 L h^{-1}). The dissolved oxygen (DO) was controlled at 50% with the agitation rate (400 – 1,500 rpm), and three Rushton impellers were installed. A slash indicates that there were no deviations from the reference. The start of the feed is displayed with t_{Feed}.

Identification	Bioreactor	Deviation process	Deviation feed
V1	R1	0.25 $g_{MgSO4 \times 7\ H2O}$ L^{-1} no Fe(III) citrate × H_2O two Rushton impellers	450 g_{Glc} L^{-1} 0.25 $g_{MgSO4 \times 7\ H2O}$ L^{-1} feed was calculated without m_S t_{Feed} = 2.9 h
	R2	μ_{set} = 0.3 h^{-1} 0.25 $g_{MgSO4 \times 7\ H2O}$ L^{-1} no Fe(III) citrate × H_2O two Rushton impellers	450 g_{Glc} L^{-1} 0.25 $g_{MgSO4 \times 7\ H2O}$ L^{-1} feed was calculated without m_S t_{Feed} = 2.9 h
	R3	μ_{set} = 0.5 h^{-1} 0.25 $g_{MgSO4 \times 7\ H2O}$ L^{-1} no Fe(III) citrate × H_2O two Rushton impellers	450 g_{Glc} L^{-1} 0.25 $g_{MgSO4 \times 7\ H2O}$ L^{-1} feed was calculated without m_S t_{Feed} = 2.9 h
	R4	μ_{set} = 0.7 h^{-1} 0.25 $g_{MgSO4 \times 7\ H2O}$ L^{-1} no Fe(III) citrate × H_2O two Rushton impellers	450 g_{Glc} L^{-1} 0.25 $g_{MgSO4 \times 7\ H2O}$ L^{-1} feed was calculated without m_S t_{Feed} = 2.9 h

Identification	Bioreactor	Deviation process	Deviation feed
V2	R1	0.25 $g_{MgSO4 \times 7\ H2O}$ L^{-1} no Fe(III) citrate × H_2O two Rushton impellers	450 g_{Glc} L^{-1} 0.25 $g_{MgSO4 \times 7\ H2O}$ L^{-1} t_{Feed} = 2.9 h
	R2	0.4 mg_{TCE2} L^{-1} 0.25 $g_{MgSO4 \times 7\ H2O}$ L^{-1} no Fe(III) citrate × H_2O two Rushton impellers	450 g_{Glc} L^{-1} 0.25 $g_{MgSO4 \times 7\ H2O}$ L^{-1} t_{Feed} = 2.9 h
	R3	2.5 $g_{Yeast\ extract}$ L^{-1} 0.25 $g_{MgSO4 \times 7\ H2O}$ L^{-1} no Fe(III) citrate × H_2O two Rushton impellers	450 g_{Glc} L^{-1} 0.25 $g_{MgSO4 \times 7\ H2O}$ L^{-1} t_{Feed} = 2.9 h
	R4	0.06 mg_{KIO3} L^{-1} two Rushton impellers	450 g_{Glc} L^{-1} 0.25 $g_{MgSO4 \times 7\ H2O}$ L^{-1} t_{Feed} = 2.9 h
V3	R1	0.06 mg_{KIO3} L^{-1} two Rushton impellers F = 60 – 90 L h^{-1}	450 g_{Glc} L^{-1} 0.25 $g_{MgSO4 \times 7\ H2O}$ L^{-1}
	R2	0.25 $g_{MgSO4 \times 7\ H2O}$ L^{-1} no Fe(III) citrate × H_2O 0.06 mg_{KIO3} L^{-1} two Rushton impellers	450 g_{Glc} L^{-1} 0.25 $g_{MgSO4 \times 7\ H2O}$ L^{-1}
	R3	no Fe(III) citrate × H_2O two Rushton impellers F = 60 – 90 L h^{-1}	450 g_{Glc} L^{-1} 0.25 $g_{MgSO4 \times 7\ H2O}$ L^{-1}
	R4	0.25 $g_{MgSO4 \times 7\ H2O}$ L^{-1} two Rushton impellers F = 60 – 90 L h^{-1}	450 g_{Glc} L^{-1} 0.25 $g_{MgSO4 \times 7\ H2O}$ L^{-1}

Identification	Bioreactor	Deviation process	Deviation feed
V4	R1	0.06 mg_{KIO3} L^{-1} two Rushton impellers F = 60 – 120 L h^{-1}	450 g_{Glc} L^{-1} 0.25 $g_{MgSO4 \times 7 H2O}$ L^{-1}
	R2	0.06 mg_{KIO3} L^{-1} VN_c two Rushton impellers F = 60 – 120 L h^{-1}	450 g_{Glc} L^{-1} 0.25 $g_{MgSO4 \times 7 H2O}$ L^{-1}
	R3	0.06 mg_{KIO3} L^{-1} VN_c 2 mL_{TCE1} L^{-1} two Rushton impellers F = 60 – 120 L h^{-1}	450 g_{Glc} L^{-1} 0.25 $g_{MgSO4 \times 7 H2O}$ L^{-1}
	R4	*V. natriegens* Succ1 0.06 mg_{KIO3} L^{-1} two Rushton impellers F = 60 – 120 L h^{-1}	450 g_{Glc} L^{-1} 0.25 $g_{MgSO4 \times 7 H2O}$ L^{-1}
V5	R1	/	450 g_{Glc} L^{-1}
	R2	F = 60 – 90 L h^{-1}	450 g_{Glc} L^{-1} 1 mL_{TCE1} L^{-1} 1 mL_{TCE3} L^{-1} 1.7 $g_{Citric\ acid}$ L^{-1}
	R3	TCE3 1.7 $g_{Citric\ acid}$ L^{-1}	450 g_{Glc} L^{-1} 1 mL_{TCE1} L^{-1}
	R4	MM_{HCDC} F = 60 – 90 L h^{-1}	450 g_{Glc} L^{-1} 1 mL_{TCE1} L^{-1} 1 mL_{TCE3} L^{-1} 1.7 $g_{Citric\ acid}$ L^{-1}

Identification	Bioreactor	Deviation process	Deviation feed
V6	R1	F = 60 – 120 L h^{-1}	450 g_{Glc} L^{-1}
	R2	Triple-phase process (2.6.3) *V. natriegens* Succ1 Δ*ackA* F = 12 – 60 L h^{-1}	450 g_{Glc} L^{-1}
	R3	Triple-phase process (2.6.3) *V. natriegens* Succ1 Δ*ackA* F = 6 – 60 L h^{-1}	450 g_{Glc} L^{-1}
	R4	Triple-phase process (2.6.3) *V. natriegens* Succ1 Δ*ackA* F = 12 – 60 L h^{-1}	450 g_{Glc} L^{-1}
V7	R1	F = 60 – 120 L h^{-1}	450 g_{Glc} L^{-1}
	R2	*V. natriegens* Δ*luxS* F = 60 – 120 L h^{-1}	450 g_{Glc} L^{-1}
	R3	*V. natriegens* Δ*cpsR* F = 60 – 120 L h^{-1}	450 g_{Glc} L^{-1}
	R4	*V. natriegens* Δ*sypK* F = 60 – 120 L h^{-1}	450 g_{Glc} L^{-1}
V8	R1	Triple-phase process (2.6.3) *V. natriegens* Succ1	/
	R2	Triple-phase process (2.6.3) *V. natriegens* Succ1	/
	R3	Triple-phase process (2.6.3) *V. natriegens* Succ1	/
	R4	T = 30 °C F = 60 – 120 L h^{-1}	/

Identification	Bioreactor	Deviation process	Deviation feed
V9	R1	*V. natriegens* Δ*wbfF* F = 60 – 120 L h^{-1}	t_{Feed} = 3.6 h
V10	R1	F = 60 – 120 L h^{-1}	/
	R2	*V. natriegens* Δ*cpsR* F = 60 – 120 L h^{-1}	/
	R3	*V. natriegens* Δ*wbfF* F = 60 – 120 L h^{-1}	t_{Feed} = 3.1 h
V11	R1	0.0135 g_{CaCO3} L^{-1} no $CaCl_2$	VN_{mc}
	R2	10 g_{Glc} L^{-1} 0.0135 g_{CaCO3} L^{-1} no $CaCl_2$	t_{Feed} = 3.6 h 600 g_{Glc} L^{-1} VN_{mc} combination of exponential and constant feed
V12	R1	/	/
	R2	*V. natriegens* Δ*cpsR*	/
	R3	*V. natriegens* Δ*cps*	/
	R4	*V. natriegens* Δ*wbfF*	t_{Feed} = 3.1 h
V13	R1	/	/
	R2	*V. natriegens* Δ*cpsR*	/
	R3	*V. natriegens* Δ*cps*	/
	R4	*V. natriegens* Δ*syp* Δ*cps*	/

Identification	Bioreactor	Deviation process	Deviation feed
V14	R1	/	/
	R2	*V. natriegens* Δ*cpsR*	/
	R3	*V. natriegens* Δ*cps*	/
	R4	*V. natriegens* Δ*wbfF*	t_{Feed} = 3.1 h
V15	R1	/	/
	R2	*V. natriegens* Δ*syp* Δ*cps*	/
	R3	*V. natriegens* Δ*syp* Δ*cps*	/
	R4	*V. natriegens* Δ*wbfF*	t_{Feed} = 3.1 h
V16	R1	DO was additionally regulated over the oxygen concentration	/
	R2	/	/
	R3	/	/
	R4	*V. natriegens* Δ*wbfF*	t_{Feed} = 3.1 h
V17	R2	/	/
	R3	/	/
	R4	/	/

2.6. Succinate production

The suitability of *V. natriegens* for succinate production was investigated using various cultivation methods. Small-scale cultures, such as test tubes and shaking flasks, were used to characterize the kinetics of potential producer strains. Zero-growth and triple-phase processes were applied to achieve high productivities.

2.6.1. **Small-scale cultivation**

Aerobic cultivations in shaking flasks were carried out as described in 2.3. Small-scale anaerobic cultivation experiments were conducted in parallel in 15 mL test tubes (adapted from Thoma *et al.* (2021)). For this purpose, 2×YTN shaking flask precultures were generated as described above and incubated for 4 – 5 h to obtain a sufficient amount of cell mass (by centrifugation at 4,000×g at RT for 20 min) to subsequently inoculate 120 mL of VN medium to an OD of 5. Subsequently, 100 mM $KHCO_3$ and 5 g glucose L^{-1} were added to start the cultivation, and a sample was taken immediately (t = 0 h) just before the cell suspension was aliquoted into the airtight tubes. A whole tube was harvested every hour to ensure anaerobic conditions in the remaining parallel cultures.

2.6.2. **Zero-growth anaerobic bioprocess for succinate production**

A two-stage process and the corresponding seed train were established for succinate production (Figure 6). Starting from O/N incubated reaction tubes (2.3), 500 µL of the bacterial suspension was used each time to inoculate a total of nine 2×YTN shaking flask precultures. The precultures were cultivated at 37 °C and 180 rpm. During the exponential growth phase, the cells were harvested by centrifugation (10 min, RT, 4,347×g) and used to inoculate three bioreactors containing 1.5 L of 2×YTN medium. The pH was adjusted to 7.5. To achieve microaerobic conditions, the aeration rate was set to 0.5 vvm and the agitation rate was kept constant at 600 rpm. After 2.5 h, the bioreactor broths were harvested by centrifugation (10 min, RT, 4,347×g) and the cell pellet was resuspended in 0.4 L VN medium initially containing 100 g glucose L^{-1} and 150 mM $KHCO_3$. The resuspension was used to inoculate the main culture at a CDW of approximately 17 – 20 g_X L^{-1}. Anaerobic conditions were achieved by limiting the stirrer rate to a constant 180 rpm and by flushing the headspace of the bioreactor with 12 L CO_2 h^{-1} for about 5 min to displace residual oxygen. No submerged aeration was applied during the cultivation. The temperature was set at 37 °C and the pH was adjusted to 7.5. A constant feed of 100 mM $KHCO_3$ h^{-1} was started immediately after inoculation. All process parameters were regulated as described in 2.4, unless otherwise stated.

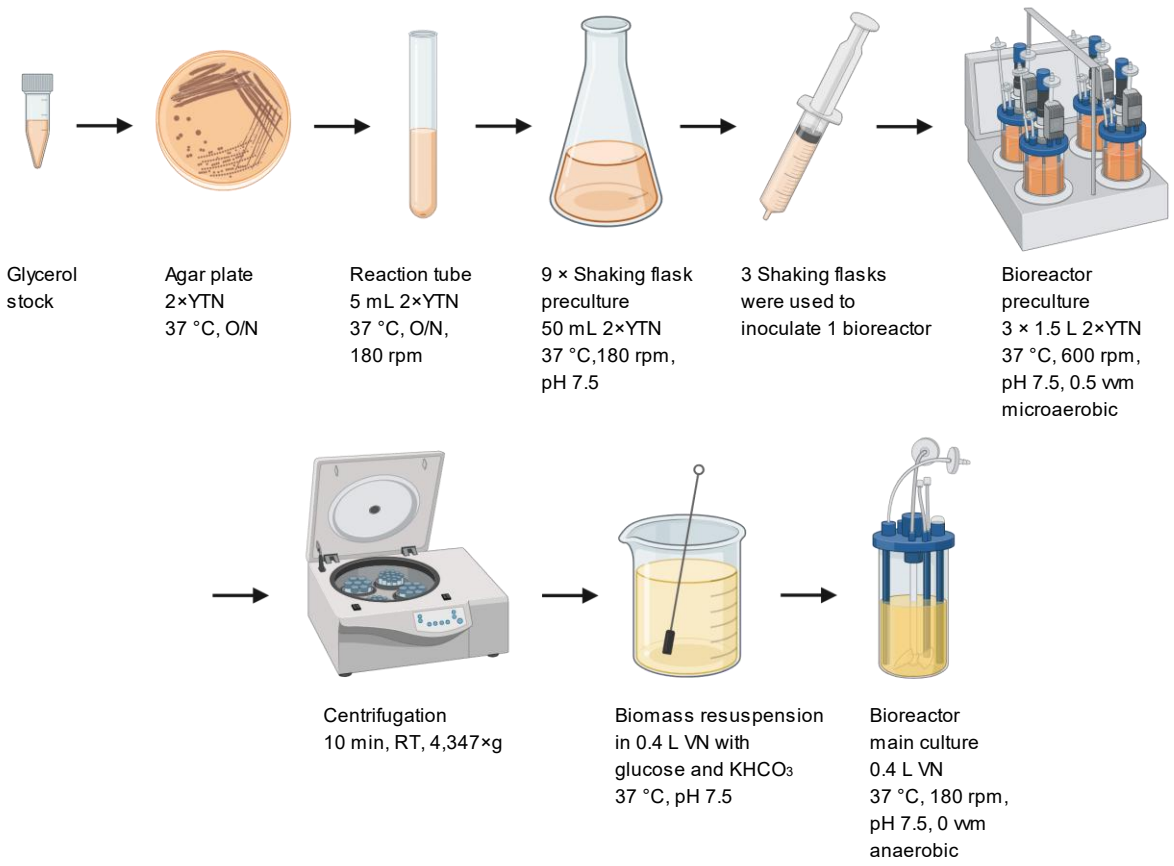

Figure 6: Seed train for succinate processes.

An overview of all succinate fermentations is given in Table 11. During the process development, various strategies have been investigated and the previous description does not apply to all succinate processes. The differences mainly concern the precultures used (shaking flasks and/or bioreactors), the initial glucose and biomass concentrations, and the supply of inorganic carbon. Furthermore, microaerobic and aerobic precultures have been tested as well.

Table 11: Overview of all succinate processes. Only deviations from the reference process are mentioned. Reference: Bioreactor precultures were performed at 37 °C and a pH of 7.5. The agitation rate was set to 600 rpm and the aeration rate to 0.5 vvm of pressurized air to obtain microaerobic conditions. The temperature and pH remained the same for the main culture, but the agitation rate was limited to 180 rpm and no submerged gassing was applied. The headspace of the bioreactor was flushed with 12 L_{CO2} h^{-1} for about 5 min. The complex medium in VA – VG did not contain 50 mM_{MgCl2}. The abbreviation SF stands for shaking flasks. The gassing rate is indicated by F and the agitation rate by N.

ID	Preculture	Main culture	Provision of CO_2/HCO_3^-	Strain	CDW | $g_X\ L^{-1}$	Provision of glucose
VA	3 x 0.2 L 2×YTN SF 3 x 1.0 L 2×YTN Bioreactor (aerobic) pH = 7 N = 400 – 1,500 rpm F = 1 vvm	0.5 L VN no flushing of headspace N = 600 rpm	F_{CO2} = 15 L h^{-1}	Succ1 Δ*ackA*	17.1	225 $g_{Glc}\ L^{-1}$
VB	4 x 0.2 L 2×YTN SF 4 x 1.0 L 2×YTN Bioreactor (aerobic) pH = 7 N = 400 – 1,500 rpm F = 1 vvm	0.5 L VN no flushing of headspace N = 600 rpm	200 mM_{KHCO3} F_{CO2} = 15 L h^{-1}	Succ1 Δ*ackA*	7.8	100 $g_{Glc}\ L^{-1}$
VC	4 x 0.2 L 2×YTN SF 4 x 1.0 L 2×YTN Bioreactor (aerobic) pH = 7 N = 400 – 1,500 rpm F = 1 vvm	0.5 L VN no flushing of headspace pH = 7 N = 300 rpm	100 mM_{KHCO3} F_{CO2} = 15 L h^{-1}	Succ1 Δ*ackA*	13.8	100 $g_{Glc}\ L^{-1}$
Vd	20 x 0.2 L 2×YTN SF	0.5 L VN N = 300 rpm no flushing of headspace	100 mM_{KHCO3} F_{CO2} = 12 L h^{-1}	Succ1 Δ*ackA*	14.4	50 $g_{Glc}\ L^{-1}$
Ve	12 x 0.05 L 2×YTN SF	0.5 L VN headspace flushed with 6 $L_{CO2}\ h^{-1}$	100 mM_{KHCO3}	Succ1 Δ*ackA*	1.5	5 $g_{Glc}\ L^{-1}$

ID	Preculture	Main culture	Provision of CO_2/HCO_3^-	Strain	CDW | $g_X\ L^{-1}$	Provision of glucose
Vf_R1	10 x 0.05 L 2×YTN SF	0.5 L VN headspace flushed with 6 $L_{CO2}\ h^{-1}$	100 mM_{KHCO3}	Succ1 Δ*ackA*	1.4	100 $g_{Glc}\ L^{-1}$
Vf_R2	10 x 0.05 L 2×YTN SF	0.5 L VN no flushing of headspace	100 mM_{KHCO3} F_{CO2} = 6 L h^{-1}	Succ1 Δ*ackA*	1.3	5 $g_{Glc}\ L^{-1}$
VF	2 x 0.05 L 2×YTN SF 1 x 1.0 L 2×YTN Bioreactor F = 1 vvm	0.5 L VN headspace flushed with 6 $L_{CO2}\ h^{-1}$	100 mM_{KHCO3}	Succ1 Δ*ackA*	1.6	5 $g_{Glc}\ L^{-1}$
VG_R3	2 x 0.05 L 2×YTN SF 1 x 1.0 L 2×YTN Bioreactor (aerobic) N = 400 – 1,500 rpm F = 1 vvm	0.5 L VN	100 mM_{KHCO3}	Succ1 Δ*ackA*	1.9	5 $g_{Glc}\ L^{-1}$
VG_R4	2 x 0.05 L 2×YTN SF 1 x 1.0 L 2×YTN Bioreactor N = 450 rpm	0.5 L VN	100 mM_{KHCO3}	Succ1 Δ*ackA*	1.2	5 $g_{Glc}\ L^{-1}$
VH	9 x 0.05 L 2×YTN SF 3 x 1.5 L 2×YTN Bioreactor F = 0.3 vvm	0.5 L VN	100 mM_{KHCO3}	Succ1	12.5	5 $g_{Glc}\ L^{-1}$
VI_R3	3 x 0.05 L 2×YTN SF 1 x 1.5 L 2×YTN Bioreactor	0.5 L VN	400 mM_{KHCO3}	Succ1	1.5	5 $g_{Glc}\ L^{-1}$
VI_R4	3 x 0.05 L 2×YTN SF 1 x 1.5 L 2×YTN Bioreactor	0.5 L VN	20 mM_{KHCO3} 50 $mM_{KHCO3}\ h^{-1}$ feed	Succ1	1.4	50 $g_{Glc}\ L^{-1}$

ID	Preculture	Main culture	Provision of CO_2/HCO_3^-	Strain	CDW | $g_X\ L^{-1}$	Provision of glucose
VJ	9 x 0.05 L 2×YTN SF 3 x 1.5 L 2×YTN Bioreactor	0.5 L VN	400 mM_{KHCO3}	Succ1	13.5	50 $g_{Glc}\ L^{-1}$
VK	9 x 0.05 L 2×YTN SF 3 x 1.5 L 2×YTN Bioreactor	0.4 L 1.5xVN	400 mM_{KHCO3} 400 mM_{KHCO3} puls at t = 2 and 6 h	Succ1	19.5	100 $g_{Glc}\ L^{-1}$ 100 $g_{Glc}\ L^{-1}$ puls at t = 6 h
VL	9 x 0.05 L 2×YTN SF 3 x 1.5 L 2×YTN Bioreactor	0.4 L 1.5xVN	400 mM_{KHCO3} 200 mM_{KHCO3} puls at t = 6 h	Succ1	17.1	100 $g_{Glc}\ L^{-1}$ 50 $g_{Glc}\ L^{-1}$ puls at t = 6h
VM	9 x 0.05 L 2×YTN SF 3 x 1.5 L 2×YTN Bioreactor	0.4 L 1.5xVN	400 mM_{KHCO3}	Succ1	13.2	100 $g_{Glc}\ L^{-1}$
VN	9 x 0.05 L 2×YTN SF 3 x 1.5 L 2×YTN Bioreactor	0.4 L VN	150 mM_{KHCO3} 8 $mM_{KHCO3}\ h^{-1}$ feed	Succ1	18.0	100 $g_{Glc}\ L^{-1}$
VO	9 x 0.05 L 2×YTN SF 3 x 1.5 L 2×YTN Bioreactor	0.4 L 1.5xVN 5 $g_{Yeast\ extract}\ L^{-1}$	200 mM_{KHCO3} applied feed: 0 – 3 h: 100 $mM_{KHCO3}\ h^{-1}$ 3 – 4 h: 75 $mM_{KHCO3}\ h^{-1}$ 4 – 20.75 h: 50 $mM_{KHCO3}\ h^{-1}$	Succ1	21.3	150 $g_{Glc}\ L^{-1}$
VP	9 x 0.05 L 2×YTN SF 3 x 1.5 L 2×YTN Bioreactor	0.4 L VN	150 mM_{KHCO3} 8 $mM_{KHCO3}\ h^{-1}$ feed	Succ1	19.8	100 $g_{Glc}\ L^{-1}$
VQ	9 x 0.05 L 2×YTN SF 3 x 1.5 L 2×YTN Bioreactor	0.4 L VN	150 mM_{KHCO3} 8 $mM_{KHCO3}\ h^{-1}$ feed	Succ1	17.4	100 $g_{Glc}\ L^{-1}$

2.6.3. **Triple-phase process**

Triple-phase processes (V6 and V8, Table 10) were performed, consisting of an aerobic biomass formation phase, a microaerobic transition, and an anaerobic production phase. In order to obtain a sufficient CDW, a glucose-limited fed-batch process was applied as described in chapter 2.5., and some adjustments were made to support succinate production.

Three parallel fermentations were carried out with *V. natriegens* Succ1 Δ*ackA* and different methods to initiate microaerobic conditions after 23 h were tested. In V6_R2, a microaerobic phase was induced by limiting the agitation rate to 1,200 rpm. In V6_R3, the gas flow of the pressurized air was adjusted to 0.1 vvm, and in V6_R4, a 50:50 mixture of CO_2 and pressurized air was used at a flow rate of 0.5 vvm. After approximately 23.5 – 24 h, microaerobic conditions were reached in all bioreactors, and an additional second feed containing 750 g glucose L^{-1}, 15 g NaCl L^{-1}, and 1.2 g $MgSO_4 \times 7\ H_2O$ L^{-1} was pumped into the bioreactors at 40 mL h^{-1}. After 26 h, strict anaerobic conditions were achieved by sparging with 0.2 vvm CO_2 and by reducing the agitation rate to 800 rpm.

In V8, a different approach was chosen to achieve microaerobic conditions. From the beginning, the agitation rate was limited to 1,300 rpm instead of 1,500 rpm to allow the cells to grow into the microaerobic state on their own, as sufficient oxygen supply was no longer guaranteed at higher cell concentrations. After approximately 24 h, *V. natriegens* Succ1 entered the microaerobic phase and a glucose pulse (50 g L^{-1}) was added to provide sufficient carbon for succinate synthesis. After 2 h at a DO of about 0%, the gas flow was stopped and the agitation rate was limited to 600 rpm to achieve anaerobic conditions.

2.7. Pyruvate production

Potential producer strains were first characterized in shaking flasks cultures, as already described in 2.3 and suitable candidates were subsequently tested on a larger scale. For this purpose, a fed-batch process was applied as shown in Figure 7. Starting from a glycerol stock, cells were streaked onto an agar plate, and thereafter, O/N-grown single colonies were used to inoculate 2×YTN reaction tubes (2.3). Shaking flask precultures containing 50 mL of VN supplemented with 7.5 g glucose L^{-1} and 1 g acetate L^{-1} were then inoculated with 500 µL each of the O/N reaction tube cultures. After 4 – 5 h of incubation on a rotary shaker (37 °C, 180 rpm), the cells were harvested by centrifugation (10 min, RT, 4,347×g), resuspended in 1 mL of 0.9% NaCl (w v^{-1}), and an appropriate volume was used to inoculate a bioreactor containing 0.5 L of VN medium supplemented with 100 g glucose L^{-1} and 2 g acetate L^{-1} to an OD_{600} of 0.5. A constant acetate feed (8 mM_{Ace} h^{-1}) was started immediately after inoculation. For pyruvate production, the temperature was set at 37 °C and the pH was maintained at 7.5. A gassing

rate of 1 vvm pressurized air was applied. The regulation of the process parameters was carried out as described in 2.4.

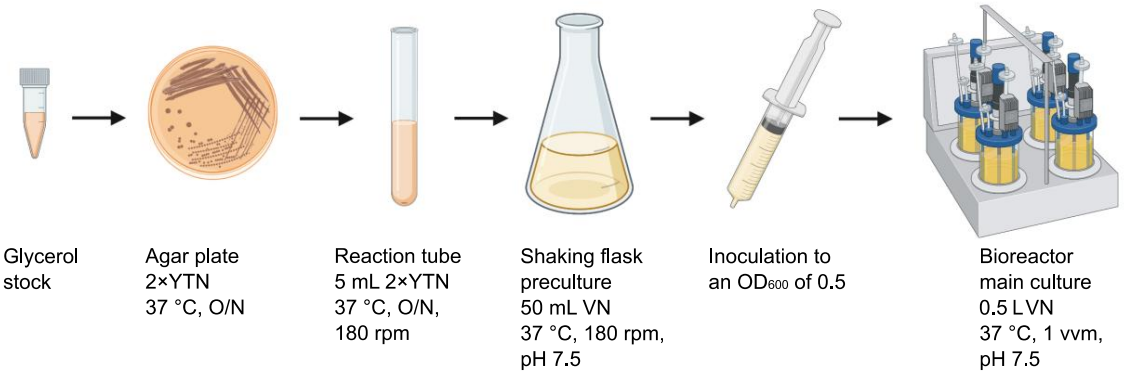

Figure 7: Seed train for pyruvate processes.

During the establishment of a pyruvate process, some process parameters were altered to achieve optimal production conditions. Table 12 summarizes all pyruvate processes and lists possible differences regarding the main culture and the provision of acetate. The generation of the precultures remained the same.

Table 12: Overview of all pyruvate production processes. Only deviations from the reference process are stated. Reference: A bioreactor containing 0.5 L of VN medium supplemented with 100 g glucose L^{-1} and 2 g acetate L^{-1} was inoculated to an OD_{600} of 0.5. The temperature was set at 37 °C and the pH was adjusted to 7.5. The gassing rate was kept constant at 1 vvm of pressurized air. The DO was controlled at 50% via the agitation rate (400 – 1,500 rpm) and one Rushton impeller was installed. A feed of 8 mM acetate h^{-1} was started immediately after the inoculation (t_{Feed} = 0 h). Triplicates are indicated with n = 3.

Identification	Bioreactor	Main culture	Provision of acetate	Strain
PyrA	1	OD = 0.1	No feed	*V. natriegens* Δ*aceE*
PyrB	1 (n = 3)	OD = 0.1	No feed	*V. natriegens* Δ*aceE*
	2 (n = 3)	OD = 0.1	No feed	*V. natriegens* Δ*vnp12* Δ*aceE*::*cat*

PyrC	1	OD = 0.1	No feed	*V. natriegens* Δ*vnp12* Δ*aceE*::*cat*
	2	OD = 0.1	2 mM_{Ace} h^{-1} feed t_{Feed} = 5 h	*V. natriegens* Δ*vnp12* Δ*aceE*::*cat*
PyrD	1	OD = 0.1	No feed	*V. natriegens* Δ*vnp12* Δ*aceE*::*cat*
	2	OD = 0.1	2 mM_{Ace} h^{-1} feed t_{Feed} = 5 h	*V. natriegens* Δ*vnp12* Δ*aceE*::*cat*
	3	OD = 0.1	8 mM_{Ace} h^{-1} feed t_{Feed} = 5 h	*V. natriegens* Δ*vnp12* Δ*aceE*::*cat*
	4	OD = 0.1	16 mM_{Ace} h^{-1} feed t_{Feed} = 5 h	*V. natriegens* Δ*vnp12* Δ*aceE*::*cat*
PyrE	1	/	No feed	*V. natriegens* Δ*vnp12* Δ*aceE*
	2	/	t_{Feed} = 5 h	*V. natriegens* Δ*vnp12* Δ*aceE*
	3	/	/	*V. natriegens* Δ*vnp12* Δ*aceE*
PyrF	1	/	No feed	*V. natriegens* Δ*vnp12* Δ*aceE*
	2	/	/	*V. natriegens* Δ*vnp12* Δ*aceE*
PyrG	1	/	No feed	*V. natriegens* Δ*vnp12* Δ*aceE*
	2	/	/	*V. natriegens* Δ*vnp12* Δ*aceE*
PyrH	2	10% ammonia water for titration	/	*V. natriegens* Δ*vnp12* Δ*aceE*
	3	pH 6.5	/	*V. natriegens* Δ*vnp12* Δ*aceE*

PyrI	2	30 °C	/	*V. natriegens* Δ*vnp12* Δ*aceE*
	3	25 °C	/	*V. natriegens* Δ*vnp12* Δ*aceE*
	4	20 °C	/	*V. natriegens* Δ*vnp12* Δ*aceE*
PyrJ	1	/	/	*V. natriegens* Δ*vnp12* Δ*aceE* Δ*papA*
	4	/	/	*V. natriegens* Δ*vnp12* Δ*aceE* pekEx-*papA*
PyrK	1	/	/	*V. natriegens* Δ*vnp12* Δ*aceE* Δ*papA*
	2	/	/	*V. natriegens* Δ*vnp12* Δ*aceE* pekEx-*papA*
	3	/	/	*V. natriegens* Δ*vnp12* Δ*aceE* Δ*papA*
	4	/	/	*V. natriegens* Δ*vnp12* Δ*aceE* pekEx-*papA*
PyrL	1	/	/	*V. natriegens* Δ*vnp12* Δ*aceE* pekEx-*papA*
	3	/	/	*V. natriegens* Δ*vnp12* Δ*aceE* pekEx-*papA*

2.8. Analytics

The following subchapters provide an overview of sample preparation, measurement methods for the quantification of substrates and (by)products, and the calculation of important KPIs.

2.8.1. **Quantification of sugars and acids**

Samples were prepared by centrifugation (10 min, RT, 4,347×g) and the supernatant was analyzed via a high-performance liquid chromatography (HPLC). For high-viscosity samples, the supernatant was additionally processed through a 0.2 µm filter (Filtropur S plus 0.2, SARSTEDT, Nümbrecht, Germany). An Agilent 1260 infinity II series device (Agilent Technologies, Waldbronn, Germany) equipped with a Hi-Plex H column (7.7 × 300 mm, 8 µm) and protected by a Hi-Plex H guard cartridge (3.0 × 5.0 mm, 8 µm) was used for the quantification of sugars and acids, such as glucose, lactate, succinate, pyruvate, and acetate. The isocratic separation of the analytes was achieved with a 5 mM H_2SO_4 mobile phase (0.4 mL min^{-1} at 50 °C) and a refractive index detector (RID) was used for detection. The concentration of the analytes was calculated by the comparison of the peak areas with a 7-point external standard ranging from 1 to 200 mM (Siebert *et al.*, 2021).

For the quantification of amino acids, an identical device equipped with an AdvanceBio Amino Acid Analysis (AAA) column (4.6 × 100 mm, 2.7 µm) protected by an AdvanceBio AAA guard column (4.6 × 5 mm, 2.7 µm) was used. Amino acids were derivatized online with o-phthaldialdehyde, and the subsequent separation of the analytes was achieved by a gradient of a polar phase, consisting of 10 mM Na_2HPO_4 and 10 mM $Na_2B_4O_7$ at a pH 8.2, versus a non-polar phase, containing 45% (v v^{-1}) acetonitrile, 45% (v v^{-1}) methanol, and 10% (v v^{-1}) H_2O, by linearly increasing the gradient from 2% non-polar fraction to 43% within 10 min and from 43 to 100% within 2.5 min, at a flow rate of 1 mL min^{-1} at 40 °C. A fluorescence detector (FLD, excitation wavelength 340 nm, emission wavelength 450 nm, and photomultiplier tube (PMT) gain 10) was applied for detection. An internal standard (100 µm norvaline) was used to normalize the peak area, and the final concentration of the analytes was calculated by comparing the peak area to a 7-point external standard ranging from 1 to 400 µM (Siebert *et al.*, 2021).

For the quantification of EPS, the samples were centrifuged (15,871×g, 10 min) and the supernatants were stored at -20 °C until measurement. After thawing, the samples were first gel-filtrated (96-well SpinColumn G-25, Harvard Apparatus) to remove monomeric sugars. In a next step, the polymer was hydrolyzed with 4 M trifluoroacetic acid at 121 °C for 1.5 h to release the monomers, which were then analyzed using the high throughput 1-phenyl-3-methyl-5-pyrazolone (HT-PMP) method coupled with an ultra high-performance liquid chromatography with ultraviolet and electrospray ionization ion trap tandem mass spectrometry (UHPLC-UV-ESI-MS/MS). A detailed method description can be found in

Rühmann *et al.* (2014, 2015) and Schulze *et al.* (2023). The limit of detection for the monomeric sugars ranged from 0.2 to 0.6 mg L^{-1}, and the limit of quantification varied from 0.5 to 2 mg L^{-1} (Rühmann *et al.*, 2015).

2.8.2. Determination of growth parameters and key performance indicators

The OD_{600} was determined by using a spectrophotometer (Ultrospec 10 cell density meter, Harvard Biochrom, Holliston, MA, USA). The CDW was then calculated by conversion with a predetermined correlation factor of 0.3. A semi-logarithmic plot of the CDW over the process time was used to determine the growth rate by the slope of a linear regression curve. The biomass yield was obtained by linear regression of the CDW versus the respective glucose concentration for the exponential growth phase. The biomass-specific glucose consumption rate was calculated using Equation 3. However, the terms for m_S and $q_{P,S}$ were neglected for simplification, unless otherwise noted.

The oxygen transfer rate (OTR) was calculated via gas mass balance of the exhaust gas according to Equation 5. Therefore, a gas analyzer GA4 (Eppendorf, Jülich, Germany) equipped with a galvanic measurement cell was connected to the bioreactors and used to detect O_2 and CO_2 in the exhaust gas.

$$OTR = \frac{(F_{in} \times y_{O2,in} - F_{out} \times y_{O2,out})}{V_R \times V_m} \mid mol\ L^{-1}\ h^{-1} \quad (5)$$

F_{in} | L h^{-1}	Gas flow to the bioreactor
F_{out} | L h^{-1}	Gas flow from the bioreactor
$y_{O2,in}$ |	Oxygen content in the gas flow to the bioreactor
$y_{O2,out}$ |	Oxygen content in the gas flow from the bioreactor
V_m | L mol^{-1}	Molar gas volume at standard conditions

Since the inlet and outlet gas flows should be identical, Equation 5 can be simplified as follows (Equation 6):

$$OTR = \frac{F \times (y_{O2,in} - y_{O2,out})}{V_R \times V_m} \mid mol\ L^{-1}\ h^{-1} \quad (6)$$

The quality of a production process is often evaluated using KPIs such as product titer, yield, and volumetric productivity. The titer can be determined by HPLC as described in 2.8.1. The product yield $Y_{P/S}$ is the quotient of the product formed versus the substrate consumed (Equation 7). The value can be given either in $g_P\ g_S^{-1}$ or $mol_P\ mol_S^{-1}$.

$$Y_{P/S} = \frac{\Delta c_P}{\Delta c_S} = \frac{c_{P,end} - c_{P,start}}{c_{S,start} - c_{S,end}} \mid g_P\ g_S^{-1} \quad (7)$$

$c_{P,end}$ | $g_P\ L^{-1}$ Final product concentration

$c_{P,start}$ | $g_P\ L^{-1}$ Initial product concentration

$c_{S,start}$ | $g_S\ L^{-1}$ Initial substrate concentration

$c_{S,end}$ | $g_S\ L^{-1}$ Final substrate concentration

The volumetric productivity is calculated from the amount of product formed per time and volume (Equation 8).

$$Q_P = \frac{m_P}{t \times V_R} \mid g_P\ L^{-1}h^{-1} \quad (8)$$

m_P | g_P Final product mass

2.8.3. Rheological measurements

Samples for rheological measurements were prepared by centrifugation (10 min, RT, 15,871×g) and the supernatant was stored at -20 °C until measurement. The viscosity was determined at 20 °C using a rotational rheometer (MCR302, Anton-Paar, Graz, Austria) which was equipped with a TEK150 chamber and a CP50-1 measuring cell.

2.8.4. Transcriptome analysis

Next generation sequencing was performed by Genewiz Germany GmbH (Leipzig, Germany) for *V. natriegens* wt, *V. natriegens* Δ*cpsR*, and *V. natriegens* Δ*cps*. For this purpose, biological triplicates of shaking flask cultures were performed for the aforementioned strains as described in 2.3. After 2 h, when a CDW of 0.5 $g_X\ L^{-1}$ was reached, samples were removed from the main cultures, centrifuged (1 min, RT, 15,871×g), and subsequently the supernatant was discarded. The cell pellets were immediately shock frozen in liquid nitrogen and stored at -80 °C until shipment to Genewiz. The INVIEW Transcriptome Bacteria package of 2 x 150 base pair reads for a total of 10 million reads was purchased, which covered further sample preparation, library preparation with rRNA depletion, sequencing, and processing of the raw data including mapping of the reads to the available genome of *V. natriegens* ATCC 14048. The reference sequences for chromosome 1 and 2 were NZ_CP016345.1 and NZ_CP016346.1, respectively (Weinstock et al., 2016). The processed data obtained from Genewiz were then filtered using a log2 fold-change of ± 1.5 as well as an adjusted p-value of ≤ 0.05 and finally used to compare the transcriptional changes between the strains.

3. Results

3.1. Characterization of *V. natriegens* wildtype

The following section deals with the cultivation and characterization of *V. natriegens* wt in different culture vessels under various conditions.

3.1.1. **Cultivation in shaking flasks**

In shaking flask cultures in VN minimal medium supplemented with glucose, *V. natriegens* wt showed a lag phase of about half an hour. Thereafter, it grew exponentially with a growth rate μ of 1.56 ± 0.01 h^{-1} and reached a final cell dry weight CDW_{max} of 3.06 ± 0.26 g_X L^{-1} (Figure 8). A biomass yield of 0.47 ± 0.03 g_X g_S^{-1} and a biomass-specific glucose consumption rate of 3.35 ± 0.27 g_S g_X h^{-1} were obtained. At the transition from the exponential to the stationary phase, a strong increase in pyruvate (1.97 ± 0.16 g L^{-1}) was observed. In addition, acetate and lactate accumulated in the medium to maximum concentrations of 1.02 ± 0.03 g L^{-1} and 0.21 ± 0.04 g L^{-1}, respectively. No succinate formation was detected throughout the cultivation. *V. natriegens* stopped glucose consumption after 4 h and 0.90 ± 0.25 g glucose L^{-1} were left. The pH measurements at the end of the cultivation showed a decrease from the initial value of 7.5 to about 5.

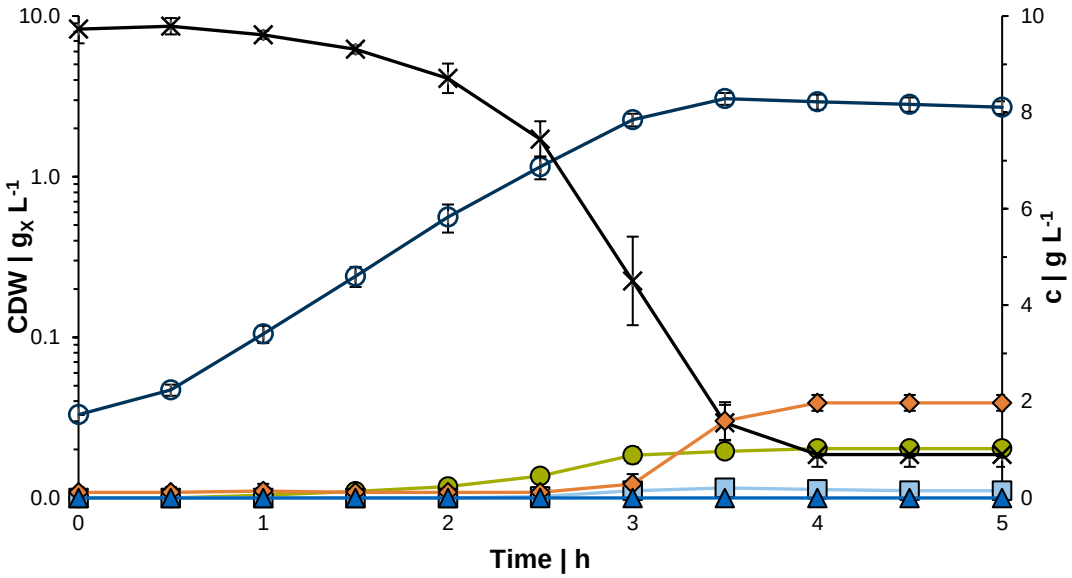

Figure 8: Growth of *V. natriegens* wildtype in shaking flasks with VN minimal medium on glucose. The cell dry weight is depicted with transparent circles and the course of glucose is represented by crosses. Formed products are pictured as follows: acetate (circle), pyruvate (diamond), succinate (triangle), and lactate (square). Results given are means and standard deviations of three independent biological replicates.

3.1.2. **Batch process in minimal medium with and without chloride**

In a bioreactor with VN minimal medium on glucose, *V. natriegens* wt grew exponentially for around 3 h with a μ of 1.68 ± 0.01 h^{-1} during a batch cultivation (Figure 9, left). After 4 h, glucose was depleted and a q_S of 3.66 ± 0.02 g_S g_X h^{-1} and a $Y_{X/S}$ of 0.46 ± 0.01 g_X g_S^{-1} were obtained. The experiment was repeated with a modified medium (VN_{V2}) to determine whether it is possible to replace NaCl with Na_2SO_4. No significant change was found for the $Y_{X/S}$ (0.49 ± 0.04 g_X g_S^{-1}). A reduction of the μ (1.39 ± 0.02 h^{-1}) and consequently of the q_S (2.88 ± 0.21 g_S g_X h^{-1}) was observed (Figure 9, right). Furthermore, the lag-phase was extended when only traces of chloride were present. Final CDWs of approximately 4 g_X L^{-1} were achieved in both cultivations.

Regardless of the medium, neither succinate nor lactate was produced, and only small amounts of pyruvate (≤ 0.5 g L^{-1}) were detected. In the standard VN medium, a maximum concentration of 1.89 ± 0.01 g acetate L^{-1} was determined, which is about 25% less compared to the cultivation in chloride-free medium.

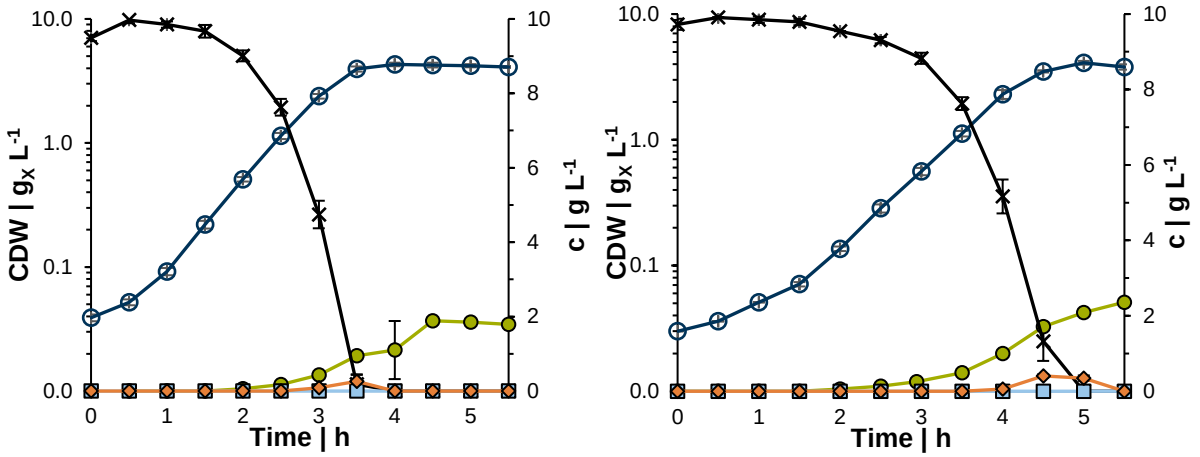

Figure 9: Growth of *V. natriegens* wildtype during a batch process in VN (left) and VN_{V2} (right) minimal medium. The cell dry weight is depicted with transparent circles and the course of glucose is represented by crosses. Formed products are pictured as follows: acetate (circle), pyruvate (diamond), succinate (triangle), and lactate (square). Results given are means and standard deviations of three independent biological replicates.

3.2. Development of a fed-batch process for *V. natriegens* wildtype

A glucose-limited fed-batch process was established to achieve high space-time yields as a basis for further production processes. Therefore, different growth rates, media, and feed compositions as well as the adjustment of process parameters were investigated to obtain the optimal process for *V. natriegens* wt.

3.2.1. **Growth rates**

V. natriegens wt exhibits an acetate overflow metabolism. A first fermentation (V1) was conducted to overcome acetate production in order to channel all the carbon towards biomass formation. To achieve this, different growth rates between 0.1 and 0.7 h^{-1} were tested during the fed-batch phase, starting at 2.9 h, to observe the impact on byproduct formation (Figure 10).

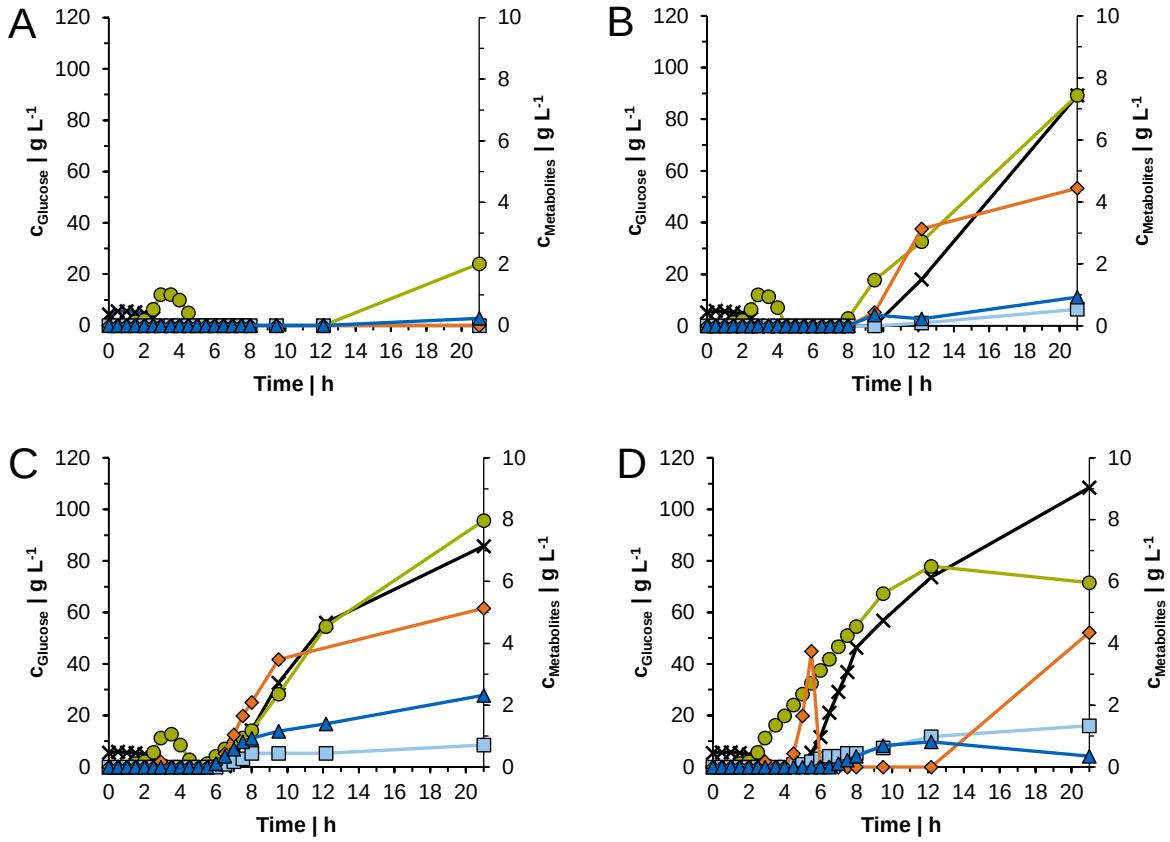

Figure 10: Growth of *V. natriegens* wildtype during a fed-batch process with the following growth rates: 0.1 h^{-1} (A), 0.3 h^{-1} (B), 0.5 h^{-1} (C), and 0.7 h^{-1} (D). Glucose and metabolites are shown as follows: glucose (cross), acetate (circle), pyruvate (diamond), succinate (triangle), and lactate (square).

Significant differences were observed regarding glucose accumulation and byproduct formation. At a μ_{set} of 0.1 h^{-1}, only 2 g acetate L^{-1} and 0.23 g succinate L^{-1} were secreted into the medium after 21 h, and the supplied glucose was completely consumed. In the remaining bioreactors, glucose accumulation started already between 5 and 9.5 h, and a maximum concentration of 108 g glucose L^{-1} was found for *V. natriegens* growing at a μ_{set} of 0.7 h^{-1}. In the other cultivations, approximately 90 g glucose L^{-1} were detected together with 4 – 5 g pyruvate L^{-1}, 1 g lactate L^{-1}, and 6 – 8 g acetate L^{-1}. The carbon balance (C-balance) of the batch phase was closed to 95 – 102% for all bioreactors. However, this changed drastically in the fed-batch phase. While the C-balance was still closed to 83% after 21 h for the bioreactor with the lowest μ_{set}, only 66, 55, and 63% of the carbon was recovered from glucose for the processes with a μ_{set} of 0.3, 0.5, and 0.7 h^{-1}, respectively. No other carbon sinks were detected, indicating the formation of unknown products. Further, it was observed that the measured µ deviated from the μ_{set} in all bioreactors and the actual values varied between 0.06 and 0.40 h^{-1}. In addition, only small amounts of biomass were obtained, ranging from 5 g_X L^{-1} for the lowest growth rate to 10 – 14 g_X L^{-1} for the remaining bioreactors. Possible reasons for this were investigated in the following fed-batch processes.

3.2.2. **Medium and process optimization**

In the previously conducted fed-batch process, the application of a μ_{set} of 0.1 h^{-1} during the feeding phase significantly reduced byproduct formation. However, a discrepancy between the μ_{set} and the actual measured µ was observed and, in addition, the CDW decreased already after 12 h. To further support biomass formation, several adjustments were made to the process conditions of V1 in terms of medium composition and regulation of the process parameters, as listed in Table 13 below.

Table 13: Overview of the process development for a fed-batch process. Only deviations from the first process (V1) are mentioned. Reference V1: Fed-batch process with *V. natriegens* wt in 1 L of VN medium supplemented with 6 g glucose L^{-1}. After 2.9 h, a feed containing 450 g glucose L^{-1}, 0.25 g $MgSO_4 \times 7\ H_2O$ L^{-1}, and 15 g NaCl L^{-1} was started to adjust the growth rate μ_{set} to 0.1 h^{-1}. The glucose uptake for cell maintenance m_S was not considered in the calculation of the feed for V1, but it was included for all other fermentations and is not mentioned again under deviations in this table. The temperature was set to 37 °C and the pH was adjusted to 7. The gassing rate F was kept constant at 1 vvm (≙ 60 L h^{-1}). The dissolved oxygen was controlled at 50% via the agitation rate (400 – 1,500 rpm), and two Rushton impellers were installed. A slash indicates that there were no deviations from V1. The start of the feed is displayed with t_{Feed}.

Identification	Bioreactor	Deviation process	Deviation feed	CDW_{max} | g_X L^{-1}
V2	R1	/	/	9.5
	R2	0.4 mg_{TCE2} L^{-1}	/	9.8
	R3	2.5 $g_{Yeast\ extract}$ L^{-1}	/	13.2
	R4	0.06 mg_{KIO3} L^{-1} 1.2 $g_{MgSO4 \times 7\ H2O}$ L^{-1} 0.1 $g_{Fe(III)\ citrate \times H2O}$ L^{-1}	/	18.0
V3	R1	0.06 mg_{KIO3} L^{-1} 1.2 $g_{MgSO4 \times 7\ H2O}$ L^{-1} 0.1 $g_{Fe(III)\ citrate \times H2O}$ L^{-1} F = 60 – 90 L_{Air} h^{-1}	t_{Feed} = 2.6 h	30.0
	R2	0.06 mg_{KIO3} L^{-1}	t_{Feed} = 2.6 h	6.6
	R3	1.2 $g_{MgSO4 \times 7\ H2O}$ L^{-1} F = 60 – 90 L_{Air} h^{-1}	t_{Feed} = 2.6 h	21.0
	R4	0.1 $g_{Fe(III)\ citrate \times H2O}$ L^{-1} F = 60 – 90 L_{Air} h^{-1}	t_{Feed} = 2.6 h	12.6

Identification	Bioreactor	Deviation process	Deviation feed	CDW_{max} | g_X L^{-1}
V4	R1	0.06 mg_{KIO3} L^{-1} 1.2 $g_{MgSO4 \times 7\ H2O}$ L^{-1} 0.1 $g_{Fe(III)\ citrate \times H2O}$ L^{-1} F = 60 – 120 L_{Air} h^{-1}	t_{Feed} = 2.6 h	21.6
	R2	0.06 mg_{KIO3} L^{-1} 0.1 $g_{Fe(III)\ citrate \times H2O}$ L^{-1} VN_c F = 60 – 120 L_{Air} h^{-1}	t_{Feed} = 2.6 h	18.0
	R3	0.06 mg_{KIO3} L^{-1} 0.1 $g_{Fe(III)\ citrate \times H2O}$ L^{-1} VN_c 2 mL_{TCE1} L^{-1} F = 60 – 120 L_{Air} h^{-1}	t_{Feed} = 2.6 h	19.8
V5	R1	1.2 $g_{MgSO4 \times 7\ H2O}$ L^{-1} 0.1 $g_{Fe(III)\ citrate \times H2O}$ L^{-1} three Rushton impellers	1.2 $g_{MgSO4 \times 7\ H2O}$ L^{-1} t_{Feed} = 2.6 h	25.2
	R2	1.2 $g_{MgSO4 \times 7\ H2O}$ L^{-1} 0.1 $g_{Fe(III)\ citrate \times H2O}$ L^{-1} three Rushton impellers F = 60 – 120 L_{Air} h^{-1}	1.2 $g_{MgSO4 \times 7\ H2O}$ L^{-1} 1 mL_{TCE1} L^{-1} 1 mL_{TCE3} L^{-1} 1.7 $g_{Citric\ acid}$ L^{-1} t_{Feed} = 2.6 h	22.8
	R3	1.2 $g_{MgSO4 \times 7\ H2O}$ L^{-1} 0.1 $g_{Fe(III)\ citrate \times H2O}$ L^{-1} 1 mL_{TCE3} L^{-1} 1.7 $g_{Citric\ acid}$ L^{-1} three Rushton impellers	1.2 $g_{MgSO4 \times 7\ H2O}$ L^{-1} 1 mL_{TCE1} L^{-1} t_{Feed} = 2.6 h	12.0

Identification	Bioreactor	Deviation process	Deviation feed	CDW_{max} | g_X L^{-1}
	R4	1.2 $g_{MgSO4 \times 7\ H2O}$ L^{-1} 0.1 $g_{Fe(III)\ citrate \times H2O}$ L^{-1} MM_{HCDC} 1 mL_{TCE3} L^{-1} three Rushton impellers F = 60 – 120 L_{Air} h^{-1}	1.2 $g_{MgSO4 \times 7\ H2O}$ L^{-1} 1 mL_{TCE1} L^{-1} 1 mL_{TCE3} L^{-1} 1.7 $g_{Citric\ acid}$ L^{-1} t_{Feed} = 2.6 h	14.4
V8	R4	1.2 $g_{MgSO4 \times 7\ H2O}$ L^{-1} 0.1 $g_{Fe(III)\ citrate \times H2O}$ L^{-1} three Rushton impellers T = 30 °C F = 60 – 120 L_{Air} h^{-1}	1.2 $g_{MgSO4 \times 7\ H2O}$ L^{-1} 550 $g_{Glucose}$ L^{-1} t_{Feed} = 2.6 h	31.2
V11	R1	1.2 $g_{MgSO4 \times 7\ H2O}$ L^{-1} 0.1 $g_{Fe(III)\ citrate \times H2O}$ L^{-1} three Rushton impellers 0.0135 g_{CaCO3} L^{-1} instead of 0.01 g_{CaCl2} L^{-1}	VN_{mc} 550 $g_{Glucose}$ L^{-1} t_{Feed} = 2.6 h	12.9
	R2	10 $g_{Glucose}$ L^{-1} instead of 6 g L^{-1} 1.2 $g_{MgSO4 \times 7\ H2O}$ L^{-1} 0.1 $g_{Fe(III)\ citrate \times H2O}$ L^{-1} three Rushton impellers 0.0135 g_{CaCO3} L^{-1} instead of 0.01 g_{CaCl2} L^{-1}	VN_{mc} 600 $g_{Glucose}$ L^{-1} combination of exponential and constant feed t_{Feed} = 2.6 h	23.4

In V2, in addition to the commonly used TCE1 solution, different TCE were provided, which were selected based on studies by Erian *et al.* (2018) and Nimbalkar *et al.* (2018). Further, yeast extract and a combination of KIO_3, $MgSO_4 \times 7\ H_2O$, and Fe(III) citrate × H_2O were added to overcome possible limitations. The provision of TCE2 solution had no clear advantage for the formation of biomass. A higher CDW of 13.2 $g_X\ L^{-1}$ was obtained with yeast extract. The most beneficial effect was observed for the addition of KIO_3, $MgSO_4 \times 7\ H_2O$, and Fe(III) citrate × H_2O. A maximum CDW of 18.0 $g_X\ L^{-1}$ was achieved, which was about twice as high compared to the control group (bioreactor 1, R1) (Figure 11).

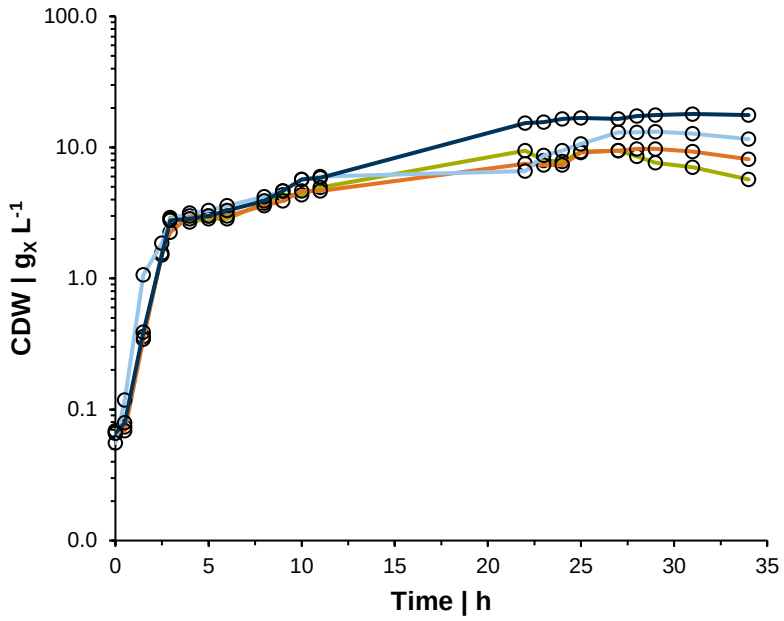

Figure 11: Effect of different supplements on the cell dry weight for the fed-batch process V2. The bioreactors are depicted as follows: bioreactor 1 in green, bioreactor 2 (supplemented with TCE2) in orange, bioreactor 3 (supplemented with yeast extract) in light blue, and bioreactor 4 (supplemented with KIO_3, Fe(III) citrate × H_2O, and $MgSO_4 \times 7\ H_2O$) in dark blue.

Following up, a next fermentation set (V3) was conducted to analyze which of the three supplements was responsible for the improved growth. The results indicate that there seems to be a synergistic effect, since the highest CDW of 30 $g_X\ L^{-1}$ was achieved in the control group (V3_R1, Table 13), in which KIO_3, $MgSO_4 \times 7\ H_2O$, and Fe(III) citrate × H_2O were provided. Hence, the supplements were also added in the following fermentations. In addition, the CDW_{max} was raised by 67% compared to V2_R4, possibly caused by increasing the gassing rate from 60 to 90 $L_{Air}\ h^{-1}$ when the DO fell below 10%, thus preventing a drop to 0% (Figure 12). However, even before the gassing rate was adjusted, the DO remained stable for a longer period of time.

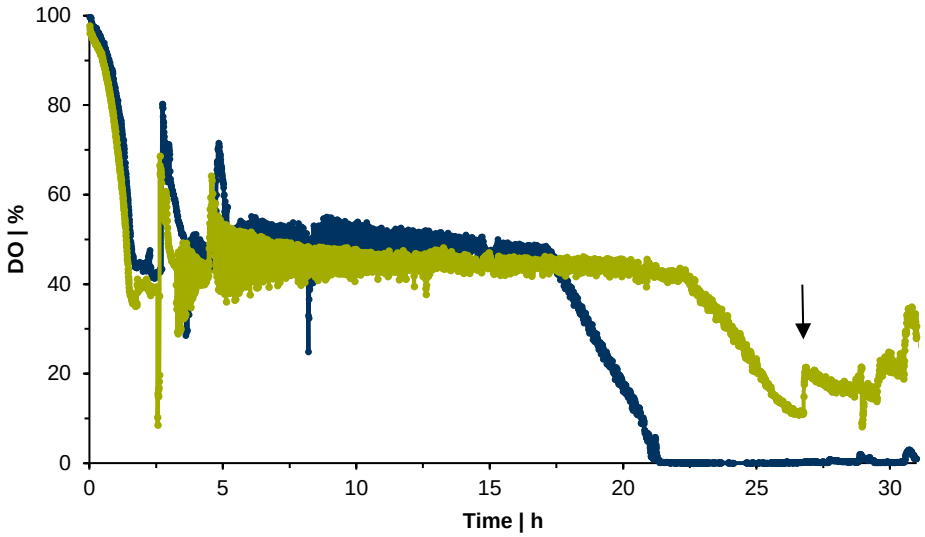

Figure 12: Influence of the gassing rate on the dissolved oxygen. The course of the dissolved oxygen is depicted in dark blue for V2_R4 and in green for V3_R1. Both media in the bioreactors were supplemented with KIO_3 and Fe(III) citrate × H_2O, and had an elevated $MgSO_4$ × 7 H_2O concentration. An arrow indicates the increase of the gassing rate from 60 to 90 L_{Air} h^{-1}.

Next, a higher concentration of the VN minimal medium (VN_c) and twice the amount of TCE1 were tested, but no improvement was observed (V4, Table 13). Furthermore, based on media from a high cell density cultivation (HCDC) with *E. coli* and a fed-batch process with *V. natriegens* (Riesenberg *et al.*, 1991; Erian *et al.*, 2020), the medium MM_{HCDC}, the trace element solution TCE3, and the addition of citric acid were tried. A variation of different feeds containing TCE solutions and citric acid was tested as well, but none of the supplements resulted in a higher CDW compared to the reference (V5, Table 13). It was speculated that KIO_3, in contrast to $MgSO_4$ × 7 H_2O and Fe(III) citrate × H_2O, did not contribute to an improved biomass formation and was therefore no longer provided. This is also indicated by the results of V3_R2, in which KIO_3 was added, but less CDW was formed compared to a process without the additional supplementation (V2_R1, Table 13). None of the aforementioned compounds could further improve the growth phase and the CDW_{max}. However, the addition of a third Rushton impeller (V5, Table 13) resulted in an 18% increase of the OTR (Figure 13) and a 17% increase of the CDW_{max}. Hence, all subsequent fermentations were conducted with a third Rushton impeller.

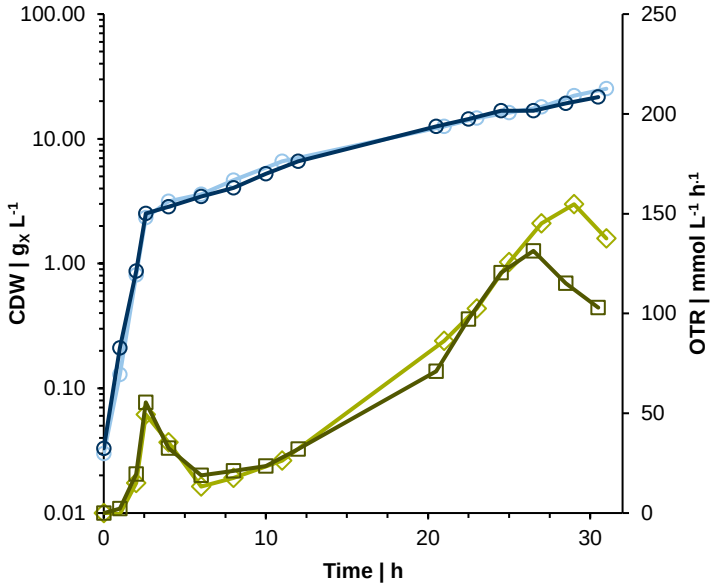

Figure 13: Impact of a third Rushton impeller on cell dry weight and oxygen transfer rate. The course over time is depicted for bioreactor 1 of V4 (dark blue) and V5 (light blue). Both bioreactors were supplemented with Fe(III) citrate × H_2O and $MgSO_4$ × 7 H_2O. In V4, KIO_3 was added as well. A third Rushton impeller was installed in V5. The OTR is depicted in dark green for V4 and light green for V5.

In addition to the changes of the medium and feed, the effect of reducing the cultivation temperature to 30 °C was investigated as well (V8_R4, Table 13 and Figure 14).

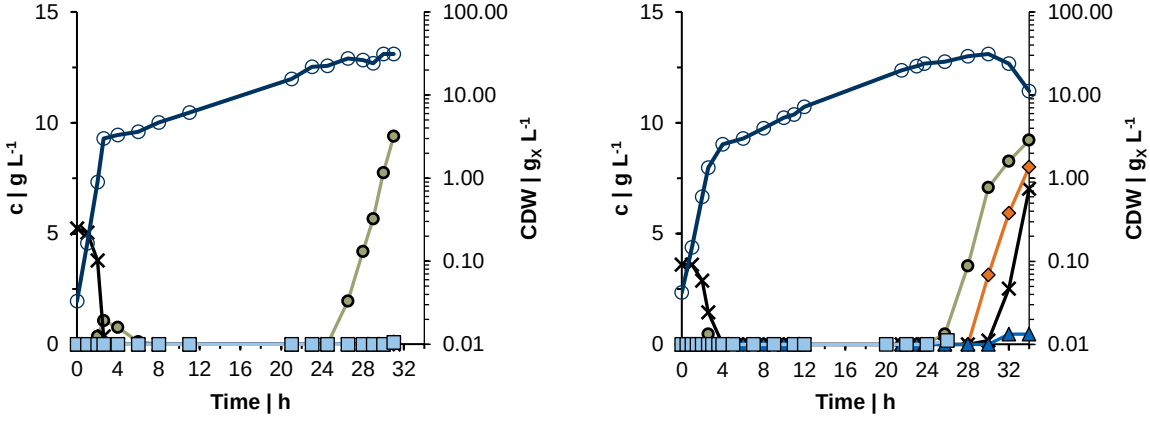

Figure 14: Growth of *V. natriegens* wildtype during a fed-batch process at different temperatures. On the left, the control group cultivated at 37 °C (V7_R1) is depicted and on the right, a cultivation with a reduced temperature of 30 °C (V8_R4) is shown. The cell dry weight is indicated by transparent circles and the concentration of the metabolites are presented as follows: glucose (cross), acetate (circle), pyruvate (diamond), succinate (triangle), and lactate (square).

During the exponential growth phase, the culture grown at a temperature of 30 °C exhibited a reduced μ of 1.38 h^{-1}. Subsequently, a μ of 0.12 h^{-1} was obtained and a CDW_{max} of 31.2 g_X L^{-1} was reached within 30 h. Around 26 h, acetate formation occurred and the concentration in the medium increased to a total of 9.2 g L^{-1}. Subsequently, glucose accumulated to 7.0 g L^{-1}, and 8 g pyruvate L^{-1} was secreted along with about 0.5 g succinate and lactate L^{-1}. The most recently performed fermentation V7 was used as a control (Table 10 and Figure 14, left). At an optimal growth temperature of 37 °C, the μ was significantly increased by 30% (μ = 1.8 h^{-1}). During the fed-batch phase, the μ_{set} of 0.1 h^{-1} was reached and an identical CDW_{max} of 31.2 g_X L^{-1} was observed. Acetate began to accumulate as well at about 26 h to a final concentration of 9.4 g L^{-1}. Although no differences were found for acetate formation, a significant reduction was measured for the other byproducts. No pyruvate formation occurred during the entire cultivation and only during the last hour of the process low concentrations of about 0.1 g succinate and lactate L^{-1} were measured. As no positive effect of a reduced cultivation temperature was observed, all subsequent fermentations were carried out at 37 °C unless otherwise indicated.

Based on a publication by Thiele *et al.* (2021), a final fermentation series (V11, Table 13) was performed (Figure 15). Therefore, $CaCl_2$ was substituted with $CaCO_3$ and, in addition, the medium VN_{mc} was fed (V11_R1). In V11_R2, a combination of different feed profiles was tested. First, the feeding rate was increased exponentially for 4 h to reach a μ_{set} of 0.5 h^{-1}, and then it was kept constant for the remainder of the process.

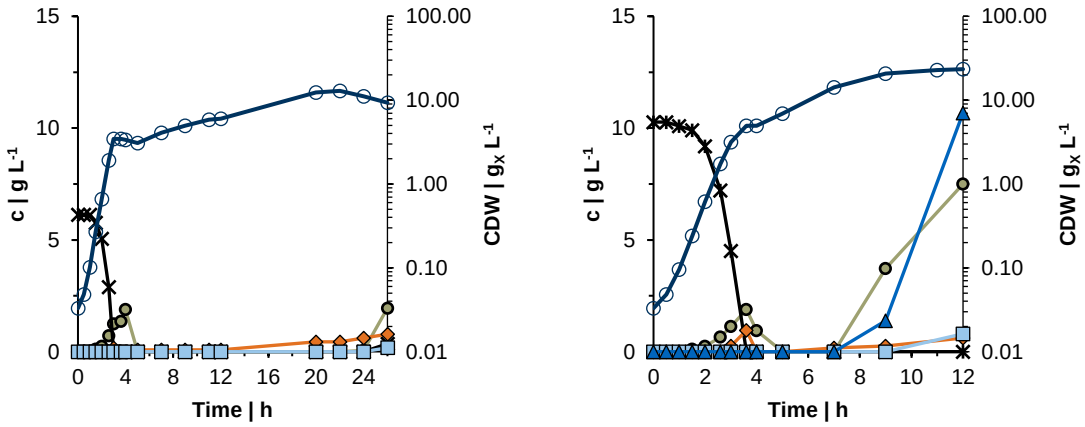

Figure 15: Growth of *V. natriegens* wildtype during a fed-batch process with a combined exponential and constant feeding strategy. On the left, the VN medium was slightly modified ($CaCO_3$ was used) and a multi-concentrated VN medium was fed. On the right, the initial glucose concentration was raised to 10 g glucose L^{-1} and the feeding was delayed for 1 h. After 4 h, the exponential feed was changed to a constant feed. The cell dry weight is indicated by transparent circles and the concentrations of the metabolites are presented as follows: glucose (cross), acetate (circle), pyruvate (diamond), succinate (triangle), and lactate (square).

No significant differences were observed during the exponential growth phase. In both bioreactors, *V. natriegens* grew with a μ of 1.74 – 1.78 h^{-1}, yielded 0.55 – 0.56 g_X g_S^{-1}, and showed a q_S of 3.16 g_S g_X^{-1} h^{-1}. However, the alteration of the medium and its feeding resulted in a higher CDW. In bioreactor 1, the cells grew with a μ of 0.09 h^{-1} to a CDW of 12.9 g_X L^{-1} during the fed-batch phase. At the end of the fermentation, about 2 g acetate L^{-1}, 1 g pyruvate L^{-1}, and 0.2 g lactate L^{-1} were detected. After 26 h, glucose accumulated to 0.4 g L^{-1} (Figure 15, left). The combination of exponential and constant feeding resulted in 23.4 g_X L^{-1} within only 12 h (Figure 15, right). However, around 7 h, the DO dropped drastically to 1 – 2% and remained there until the end of the fermentation. At this time, byproduct formation increased sharply and high concentrations of succinate (10.7 g L^{-1}) and acetate (7.5 g L^{-1}) were measured. Lactate and pyruvate were secreted as well, but in smaller amounts (between 0.6 and 0.8 g L^{-1}). The μ_{set} of 0.5 h^{-1} was not reached and only a μ of 0.37 h^{-1} was obtained.

Hitherto, the best approach to achieve a high CDW while reducing byproduct formation for *V. natriegens* wt has been a reduction of the growth rate during the fed-batch phase to 0.1 h^{-1} and the addition of a third Rushton impeller to enable higher OTRs. Furthermore, the supplementation of 0.1 g Fe(III) citrate × H_2O together with 1.2 g $MgSO_4$ × 7 H_2O L^{-1} promoted biomass formation, and thus these changes were adopted for all subsequent processes (V11 – V17).

3.2.3. Characterization of *V. natriegens* wildtype in a fed-batch process

V. natriegens wt grew with a growth rate of 1.67 ± 0.01 h^{-1} and exhibited a $Y_{X/S}$ of 0.49 ± 0.01 g_X g_S^{-1} and a q_S of 3.44 ± 0.10 g_S g_X^{-1} h^{-1} during the exponential growth phase of a fed-batch process. Acetate rapidly accumulated to 1.2 g L^{-1} in the medium, but it was quickly reutilized after 2.6 h when glucose-limited conditions were introduced (Figure 16B). During the fed-batch phase, the growth rate was limited to 0.10 ± 0.01 h^{-1}. A $Y_{X/S}$ and a q_S of 0.36 ± 0.01 g_X g_S^{-1} and 0.27 ± 0.01 g_S g_X^{-1} h^{-1}, respectively, were observed. After 24 h, the DO dropped below 5% (Figure 16A) and acetate secretion resumed. Thereafter, pyruvate accumulated as well, and after 28 h, a decline of the growth rate and subsequently of the CDW was measurable. In total, 13.78 ± 0.62 g acetate L^{-1} and 10.77 ± 1.06 g pyruvate L^{-1} were formed. A maximum CDW of 28.40 ± 0.75 g_X L^{-1} was achieved (Figure 16A and B).

During the process, an increased viscosity was observed and later confirmed via rotational rheometer measurements. At the end of the process, the highest viscosity η of 3,344 ± 903 mPa s (at a shear rate of 0.1 s^{-1}) was detected, which corresponds to an increase by a factor of 800 compared to the beginning of the process (Figure 16B).

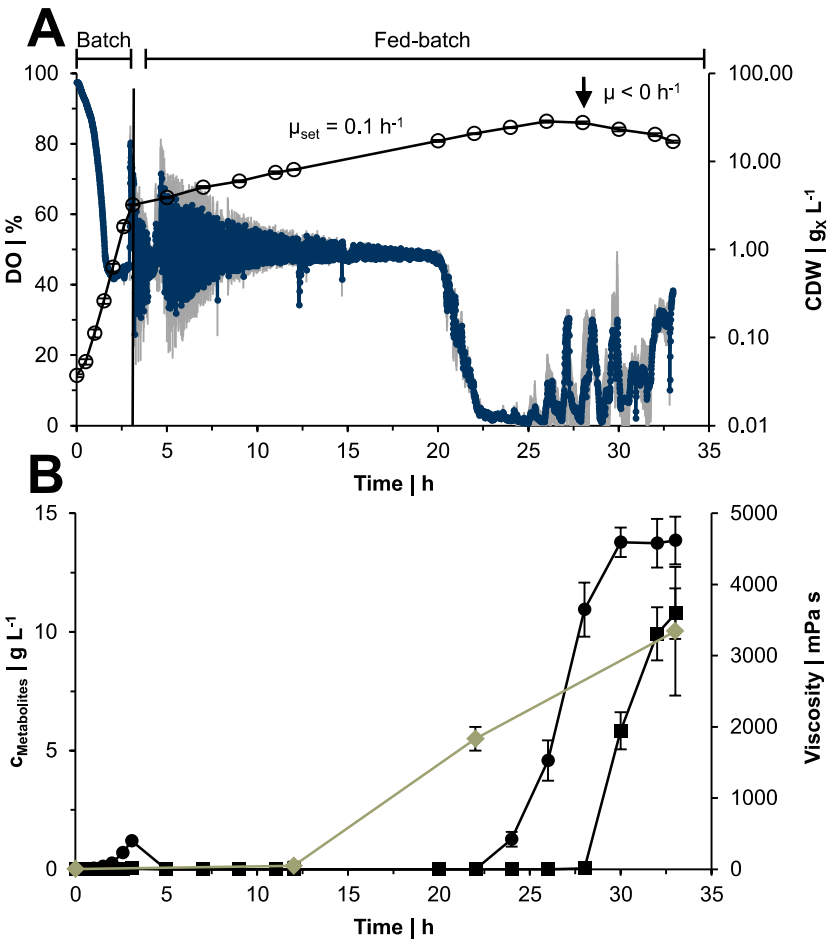

Figure 16: Final glucose-limited fed-batch process with *V. natriegens* wildtype. The courses of the cell dry weight (hollow circle) and dissolved oxygen (dark blue) are shown in (A). The concentrations of acetate (circle), pyruvate (square), and viscosity (green line) measured at a shear rate of 0.1 s^{-1} are depicted in (B). Results shown are means and standard deviations (error bars for cell dry weight and metabolites; gray line for dissolved oxygen) of three independent experiments. The arrow indicates a deviation from the growth rate μ_{set}. (Schulze *et al.*, 2023)

3.3. Exopolysaccharides

In glucose-limited fed-batch processes with *V. natriegens* wt, an 800-fold increase in viscosity was observed. It was speculated that the formation of EPS was the cause for this. Therefore, genes and gene clusters that might be involved in EPS formation were deleted in order to find potential targets to affect EPS formation in *V. natriegens.* This resulted in the following EPS mutant strains: *V. natriegens* Δ*cpsR*, *V. natriegens* Δ*wbfF*, *V. natriegens* Δ*cps*, *V. natriegens* Δ*syp* Δ*cps*, *V. natriegens* Δ*luxS*, and *V. natriegens* Δ*sypK*. CpsR was chosen as it is already described as a positive transcriptional regulator for EPS formation. Two EPS gene clusters, *syp* and *cps*, were identified and subsequently removed. Within the genomic region of the *syp* cluster is the gene *sypK* located. The deletion of this gene could significantly reduce EPS formation in *V. diabolicus*, and was therefore removed as well. Further, the gene *wbfF* was targeted as it is associated with the formation of CPS. Finally, the gene *luxS,* which encodes for an AI-synthase, was selected. These strains were thereupon characterized for their ability to produce EPS, first in shaking flask cultures and then in glucose-limited fed-batch fermentations.

3.3.1. **EPS mutant strains in shaking flasks**

Shaking flasks cultivations in VN minimal medium on glucose were conducted with *V. natriegens* wt and the EPS mutant strains. A wt-like growth was observed for all stains except for *V. natriegens* Δ*wbfF*, which had a prolonged lag phase and subsequently grew with a reduced μ of 1.46 ± 0.04 h^{-1} (Figure 17).

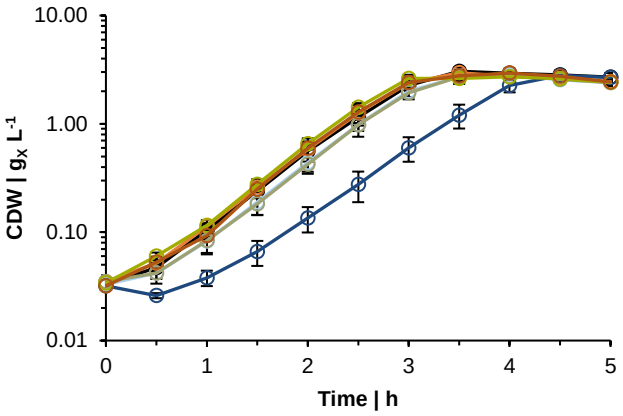

Figure 17: Course of the cell dry weight of the EPS mutant strains in shaking flasks. The strains are depicted as follows: *V. natriegens* wildtype (black), *V. natriegens* Δ*cpsR* (orange), *V. natriegens* Δ*wbfF* (dark blue), *V. natriegens* Δ*cps* (light blue), *V. natriegens* Δ*syp* Δ*cps* (olive green), *V. natriegens* Δ*luxS* (light green), and *V. natriegens* Δ*sypK* (dark orange). Results given are means and standard deviations of biological triplicates.

The wt yielded 0.47 ± 0.03 g_X g_S^{-1} and showed a q_S of 3.35 ± 0.27 g_S g_X^{-1} h^{-1}. Besides biomass, 1.02 ± 0.03 g acetate L^{-1}, 1.97 ± 0.16 g pyruvate L^{-1}, and 0.21 ± 0.04 g lactate L^{-1} were produced. No succinate was detected. Glucose was not depleted and 0.90 ± 0.25 g L^{-1} remained at the end of the cultivation. After 3.5 h, a maximum CDW of 3.06 ± 0.26 g_X L^{-1} was reached. All EPS mutant strains showed similar characteristics as the wt. The only noteworthy difference was a slightly increased acetate concentration (1.24 ± 0.05 g L^{-1}) for *V. natriegens* Δ*wbfF*. A detailed overview of the growth kinetics, CDW, and byproduct formation is given in the following Table 14.

Table 14: Growth parameters for *V. natriegens* wildtype and the EPS mutant strains. Results given are means and standard deviations of three independent biological replicates.

	V. natriegens						
Growth parameters	**wt**	**Δ*cpsR***	**Δ*wbfF***	**Δ*cps***	**Δ*syp* Δ*cps***	**Δ*luxS***	**Δ*sypK***
μ | h^{-1}	1.56 ± 0.01	1.55 ± 0.02	1.46 ± 0.04	1.58 ± 0.03	1.60 ± 0.08	1.56 ± 0.03	1.59 ± 0.05
$Y_{X/S}$ | g_X g_S^{-1}	0.47 ± 0.03	0.44 ± 0.04	0.46 ± 0.04	0.48 ± 0.02	0.51 ± 0.10	0.46 ± 0.04	0.47 ± 0.02
q_S | g_S g_X^{-1} h^{-1}	3.35 ± 0.27	3.52 ± 0.30	3.22 ± 0.20	3.33 ± 0.11	3.24 ± 0.46	3.45 ± 0.35	3.42 ± 0.29
$c_{Acetate,max}$ | g L^{-1}	1.02 ± 0.03	1.00 ± 0.01	1.24 ± 0.05	1.02 ± 0.03	1.00 ± 0.01	1.10 ± 0.03	1.12 ± 0.05
$c_{Pyruvate,max}$ | g L^{-1}	1.97 ± 0.16	2.06 ± 0.04	1.89 ± 0.04	2.06 ± 0.04	2.09 ± 0.01	2.00 ± 0.14	1.97 ± 0.15
$c_{Lactate,max}$ | g L^{-1}	0.21 ± 0.04	0.27 ± 0.01	0.24 ± 0.04	0.24 ± 0.04	0.24 ± 0.04	0.21 ± 0.04	0.18 ± 0.01
$c_{Glucose,left}$ | g L^{-1}	0.90 ± 0.25	1.08 ± 0.15	1.14 ± 0.31	1.02 ± 0.22	0.96 ± 0.31	0.90 ± 0.15	0.78 ± 0.31
CDW_{max} | g_X L^{-1}	3.06 ± 0.26	2.96 ± 0.06	2.80 ± 0.07	2.83 ± 0.09	2.93 ± 0.16	2.72 ± 0.19	2.94 ± 0.05

3.3.2. Pre-characterization of EPS mutant strains in a fed-batch process

A first fed-batch series (V7) was conducted with the EPS mutant strains *V. natriegens* Δ*luxS*, *V. natriegens* Δ*cpsR*, and *V. natriegens* Δ*sypK* and a comparison was made to the wt.

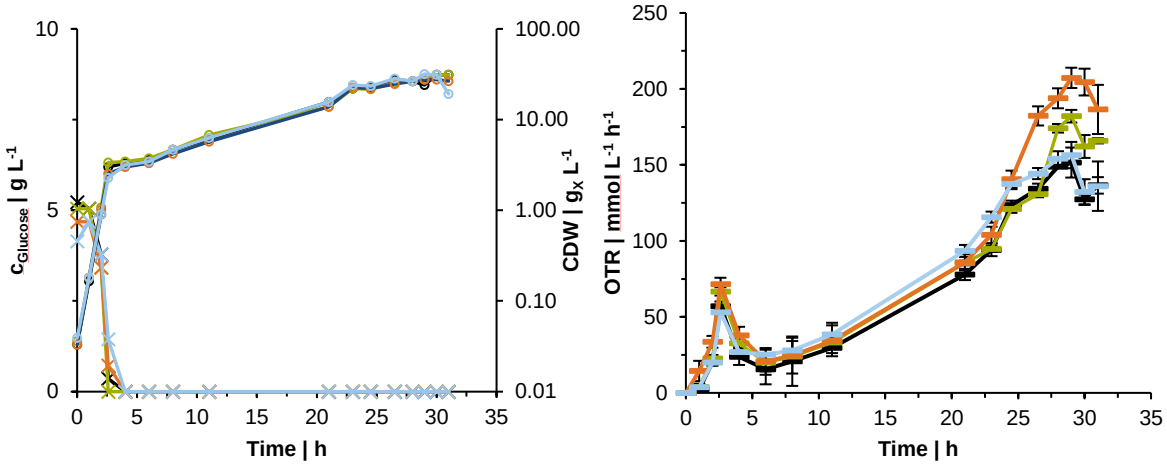

Figure 18: The course of the oxygen transfer rate as well as the concentration of glucose and cell dry weight for *V. natriegens* wildtype (black), *V. natriegens* Δ*cpsR* (orange), *V. natriegens* Δ*luxS* (green), and *V. natriegens* Δ*sypK* (blue). On the left, the cell dry weight (hollow circle) and glucose concentration (cross) are shown over time. The oxygen transfer rates over time are depicted on the right.

The course of the CDW over time was similar for all strains (Figure 18, left), and CDWs between 31 and 32 g_X L^{-1} were achieved, with the exception of *V. natriegens* Δ*cpsR*, which reached only 28 g_X L^{-1}. Glucose was depleted shortly after the fed-batch phase was initiated, and no further accumulation occurred during the process for all strains (Figure 18, left). Furthermore, almost no byproduct formation was detected after 31 h ($c_{byproducts\ excluding\ acetate} \leq 0.4$ g L^{-1}), apart from acetate, which accumulated between 5 and 9 g L^{-1} in the medium. The highest concentration was found for the wt and the lowest for *V. natriegens* Δ*sypK*.

The EPS concentration was determined for the 31 h samples. The wt produced 367 mg EPS L^{-1}. A higher value of 405 mg EPS L^{-1} was obtained for *V. natriegens* Δ*luxS*. By far the highest concentration was measured for *V. natriegens* Δ*sypK*, which produced 2.5 times more EPS (925 mg EPS L^{-1}) than the wt. The only gene deletion that actually reduced the formation of EPS was *cpsR*. This strain produced 292 mg EPS L^{-1}, which corresponds to a reduction of 20% compared to the wt. It was assumed that the reduction of EPS formation had a positive impact on the OTR in the bioreactors (Figure 18, right). For *V. natriegens* Δ*cpsR*, which secreted the least EPS, the highest OTR_{max} of 207 mM^{-1} h^{-1} was observed. However, although *V. natriegens* Δ*sypK* secreted far more EPS, the course of the OTR was similar to that of the wt, and an OTR_{max} of around 150 mM^{-1} h^{-1} was obtained for both strains. The OTR during the cultivation with *V. natriegens* Δ*luxS* was about 20% higher compared to the wt.

In addition to the EPS concentration, the composition was analyzed as well (Table 15). The EPS produced by *V. natriegens* Δ*luxS* was very similar to *V. natriegens* wt and no significant deviations were found. For *V. natriegens* Δ*sypK*, the same was true for glucose, galacturonic acid, and rhamnose. However, about 30% more galactose and reduced values for the remaining carbohydrates were found (3% fucose, 1% glucosamine, and 6% ribose). The EPS of *V. natriegens* Δ*cpsR* differed the most from the EPS produced by the wt and the other mutant strains. The EPS is characterized by a reduced glucose content of 42% and a remarkably higher rhamnose content of 24%. Furthermore, the galactose content was significantly reduced to 9%. The values for galacturonic acid, fucose, glucosamine, and ribose were slightly higher compared to the EPS produced by the other strains.

Table 15: Carbohydrate content of the exopolysaccharides produced by different *V. natriegens* strains in fed-batch processes. Results given are mean values of technical triplicates of the 31 h samples for the wildtype and the EPS mutant strains.

Carbohydrate content | mass % (31 h)	***V. natriegens***			
	wt	**Δ*luxS***	**Δ*cpsR***	**Δ*sypK***
Glucose	51	53	42	52
Galactose	17	16	9	22
Galacturonic acid	2	3	5	2
Rhamnose	14	13	24	13
Fucose	6	6	8	3
Glucosamine	2	2	3	1
Ribose	8	8	9	6

Since the deletions of *luxS* and *sypK* did not result in a reduced EPS formation, no further experiments were conducted with these strains. Instead, new EPS mutant strains (*V. natriegens* Δ*wbfF*, *V. natriegens* Δ*cps*, and *V. natriegens* Δ*syp* Δ*cps*) were characterized in subsequent fed-batch processes, which are described in the following subchapter.

3.3.3. Characterization of EPS mutant strains in a fed-batch process

The strains *V. natriegens* Δ*wbfF*, *V. natriegens* Δ*cps*, and *V. natriegens* Δ*syp* Δ*cps* were characterized in addition to *V. natriegens* Δ*cpsR* and to the wt with respect to their growth parameters, substrate consumption, and product formation. During the processes, samples were taken for rheological measurements to investigate a possible correlation between EPS formation, viscosity and the OTR. In addition, the course of EPS formation was analyzed and the composition over the 22 – 28 h period was considered rather than just the endpoint determinations.

During the unlimited growth phase, all strains carrying single gene deletions grew wt-like (μ_{WT} = 1.67 h^{-1}), whereas *V. natriegens* Δ*syp* Δ*cps* showed a slightly reduced μ of 1.52 ± 0.08 h^{-1}. During the feeding phase, maximal CDWs between 24 and 28 g_X L^{-1} were reached and the μ_{set} of 0.1 h^{-1} remained stable until around 26 h. Subsequently, the CDW decreased and glucose accumulated in the medium (Figure 19A). The formation of the most abundant byproducts, acetate and pyruvate, started already after 24 h. The concentration for both metabolites was significantly reduced for the deletion strains compared to the wt strain, which produced 13.78 ± 0.62 g acetate L^{-1} and 10.77 ± 1.06 g pyruvate L^{-1}. Among the mutant strains, *V. natriegens* Δ*wbfF* secreted the most pyruvate (2.67 ± 0.46 g L^{-1}), whereas *V. natriegens* Δ*syp* Δ*cps* produced the least (0.06 ± 0.04 g L^{-1}). The highest acetate concentration was detected for *V. natriegens* Δ*cps* (7.54 ± 0.90 g L^{-1}) and the lowest one for *V. natriegens* Δ*wbfF* (5.18 ± 1.61 g L^{-1}). At the end of the process, small amounts of succinate (≤ 0.5 g L^{-1}) were present in all cultivations and the deletion strains additionally formed lactate (≤ 0.7 g L^{-1}).

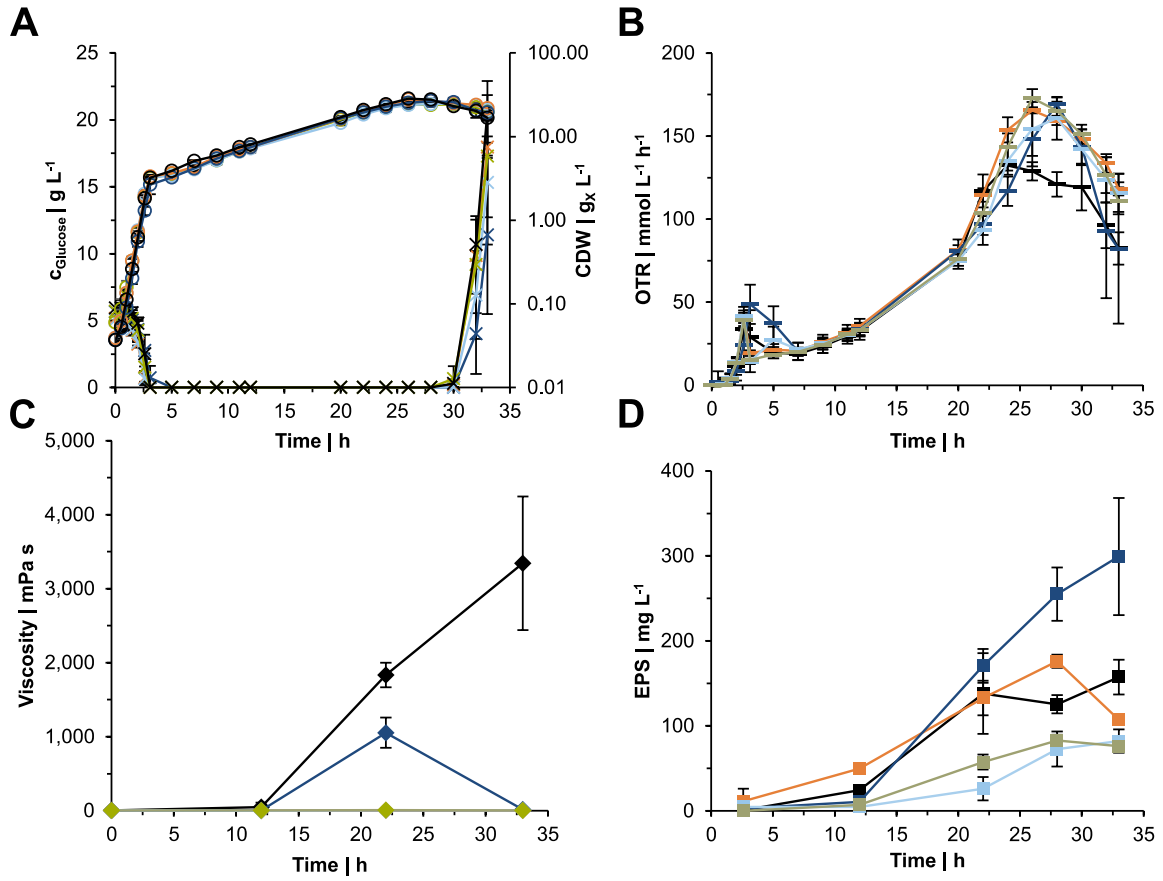

Figure 19: Glucose-limited fed-batch processes with *V. natriegens* wildtype (black), *V. natriegens* Δ*cpsR* (orange), *V. natriegens* Δ*wbfF* (dark blue), *V. natriegens* Δ*cps* (light blue), and *V. natriegens* Δ*syp* Δ*cps* (green). The courses of cell dry weight (hollow circle) and glucose concentration (cross) are shown in (A). In (B), the oxygen transfer rate (bar) is depicted over time. The course of the viscosity (diamond) measured at a shear rate of 0.1 s^{-1} is shown in (C) and the EPS concentrations are pictured in (D). Results given are means and standard deviations of three independent biological replicates. (Schulze *et al.*, 2023)

The OTR in the bioreactor with the wt increased steadily, peaked at the end of the batch phase, and thereafter continued to rise to a maximum OTR of 132 ± 3 mM^{-1} h^{-1} at 24 h. The course over time was similar for the bioreactors with the EPS mutant strains. However, the OTR further increased up to 26 – 28 h and an OTR_{max} of around 170 mM h^{-1} was observed (Figure 19B). During the cultivation, the wt produced 157 ± 20 mg EPS L^{-1} and a steady increase of the viscosity up to 3,344 ± 903 mPa s was measured (Figure 19C). For *V. natriegens* Δ*wbfF*, a continuously increasing EPS concentration was found as well, and the highest concentration of 299 ± 69 mg EPS L^{-1} was observed. However, although the EPS concentration increased throughout the process, the viscosity peaked at 22 h with 1,054 ± 203 mPa s and subsequently declined to 15 ± 5 mPa s at the end of the fermentation. The bioreactor broths for both strains exhibited a shear thinning behavior (Figure A1 and Figure A2). The cultivations with the remaining deletion strains showed no alterations of the viscosity and remained

constantly low between 3 ± 1 mPa s and 7 ± 1 mPa s (Figure 19C). Nevertheless, all three strains still secreted EPS into the medium (Figure 19D). *V. natriegens* Δ*cpsR* produced 176 ± 8 mg EPS L^{-1} and both strains carrying the EPS cluster deletions formed about 80 mg EPS L^{-1}. The aforementioned KPIs are summarized in Table 16.

Table 16: Growth parameters, substrate and metabolite concentrations, as well as the viscosity for fed-batch processes with *V. natriegens* wildtype and the given deletion mutants. Results given are means and standard deviations of three independent biological replicates. (Schulze *et al.*, 2023)

	KPI	*V. natriegens* wt	Δ*cpsR*	Δ*wbfF*	Δ*cps*	Δ*syp* Δ*cps*
Batch phase	μ | h^{-1}	1.67 ± 0.01	1.63 ± 0.03	1.57 ± 0.09	1.66 ± 0.05	1.52 ± 0.08
	$Y_{X/S}$ | g_X g_S^{-1}	0.49 ± 0.01	0.45 ± 0.01	0.36 ± 0.01	0.46 ± 0.05	0.42 ± 0.03
	q_S | g_S g_X^{-1} h^{-1}	3.44 ± 0.10	3.66 ± 0.05	4.41 ± 0.33	3.66 ± 0.27	3.61 ± 0.09
Fed-batch phase	μ | h^{-1}	0.10 ± 0.01	0.10 ± 0.01	0.11 ± 0.01	0.10 ± 0.01	0.10 ± 0.01
	$Y_{X/S}$ | g_X g_S^{-1}	0.36 ± 0.01	0.37 ± 0.03	0.40 ± 0.01	0.32 ± 0.02	0.36 ± 0.03
	q_S | g_S g_X^{-1} h^{-1}	0.27 ± 0.01	0.28 ± 0.01	0.27 ± 0.01	0.31 ± 0.02	0.28 ± 0.01
	CDW_{max} | g_X L^{-1}	28.4 ± 0.75	27.6 ± 1.70	26.6 ± 2.04	24.8 ± 0.75	24.2 ± 0.75
	η_{max} | mPa s	3,344 ± 903	3 ± 1	1,054 ± 203	5 ± 1	7 ± 1
	OTR_{max} | mmol L^{-1} h^{-1}	132 ± 3	165 ± 2	169 ± 4	161 ± 13	173 ± 6
	$c_{Acetat,max}$ | g L^{-1}	13.78 ± 0.62	6.97 ± 0.21	5.18 ± 1.61	7.54 ± 0.90	5.41 ± 0.50
	$c_{Pyruvate,max}$ | g L^{-1}	10.77 ± 1.06	0.38 ± 0.53	2.67 ± 0.46	0.87 ± 1.17	0.06 ± 0.04
	$c_{EPS,max}$ | mg L^{-1}	157 ± 20	176 ± 8	299 ± 69	82 ± 14	83 ± 7

Next, the composition of EPS was analyzed (Table 17) and the same seven carbohydrates were found for all strains as in the previous measurements (3.3.2). The EPS of the strains *V. natriegens* Δ*cpsR*, *V. natriegens* Δ*cps,* and *V. natriegens* Δ*syp* Δ*cps* had a reduced glucose content of around 35% compared to the wt and *V. natriegens* Δ*wbfF*. High similarities were observed for the strains with the EPS gene cluster deletions. Both strains had a higher galacturonic acid, glucosamine, and ribose content by a factor of around 2 to 3 in comparison to the wt. The same increased ribose content was observed for *V. natriegens* Δ*cpsR*. In addition, rhamnose was increased by a factor of 2.5, but only about one third of galactose was detected. In contrast, the EPS produced by *V. natriegens* Δ*wbfF* had

the highest galactose (22%) and lowest rhamnose (3%) content. No fucose was detected for this strain or for *V. natriegens* Δ*cps* and *V. natriegens* Δ*syp* Δ*cps*.

Table 17: Carbohydrate content of exopolysaccharides secreted between 22 and 28 h during fed-batch processes. Results given are means and standard deviations of three independent biological replicates. For fucose, "trace" indicates a lower value than the limit of quantification (< 2 mg L^{-1}). (Schulze *et al.*, 2023)

Carbohydrate Content | mass % (22 – 28 h)	***V. natriegens***				
	wt	**Δ*cpsR***	**Δ*wbfF***	**Δ*cps***	**Δ*syp* Δ*cps***
Glucose	53 ± 6	36 ± 2	64 ± 4	34 ± 10	36 ± 3
Galactose	14 ± 4	5 ± 1	22 ± 2	13 ± 2	14 ± 2
Galacturonic acid	7 ± 2	6 ± 1	5 ± 1	15 ± 3	15 ± 2
Rhamnose	12 ± 4	30 ± 2	3 ± 2	18 ± 8	16 ± 2
Fucose	4 ± 1	6 ± 1	trace	0 ± 1	0 ± 1
Glucosamine	5 ± 1	5 ± 1	3 ± 1	18 ± 11	11 ± 2
Ribose	6 ± 2	12 ± 1	4 ± 1	12 ± 5	8 ± 1

3.3.4. **Analysis of transcriptomic data**

Whole transcriptome analysis was performed on samples collected during the mid-exponential growth phase of shaking flask cultures in VN medium containing glucose to identify changes at the transcriptional level of *V. natriegens* Δ*cpsR* and *V. natriegens* Δ*cps* compared to *V. natriegens* wt. Cultivations were performed as biological triplicates and the cells were harvested at a CDW of 0.5 g_X L^{-1}. Table 18 provides an overview of the significantly up- or downregulated genes, to which a clear function could be assigned.

Table 18: Log2 fold-change of genes from *V. natriegens* Δ*cpsR* and *V. natriegens* Δ*cps* compared to *V. natriegens* wt. Annotations were adopted from kegg.jp. Data obtained from Genewiz were filtered using a log2 fold-change of ± 1.5 and an adjusted p-value of ≤ 0.05. A slash indicates that no significant change was observed.

			Log2 fold-change for *V. natriegens*	
Description	**Genes**	**Annotation**	**Δ*cps***	**Δ*cpsR***
Mannose-sensitive hemagglutinin (MSHA) pilus biogenesis protein	PN96_00320	Protein MshK	/	-1.6
	PN96_00325	Protein MshL	/	-1.8
	PN96_00330	Protein MshM	/	-1.8
	PN96_00335	Protein MshN	/	-1.8
	PN96_00340	Protein MshE	/	-1.9
	PN96_00345	Protein MshG	/	-1.9
Flagellar synthesis	PN96_02585	Histidine kinase	/	-2.4
	PN96_02590	Regulator FlrC	/	-2.4
	PN96_02595	Flagellar hook-basal body protein FliE	/	-2.1
	PN96_02600	Flagellar M-ring protein FliF	/	-2.6
	PN96_02605	Flagellar motor switch protein FliG	/	-2.3
	PN96_02610	Flagellar assembly protein FliH	/	-2.1
	PN96_02615	Flagellum-specific ATP synthase	/	-2.1
	PN96_02620	Flagellar protein FliJ	/	-2.1
	PN96_02625	Flagellar hook-length control protein FliK	/	-2.3
	PN96_02630	Flagellar protein FliL	/	-2.4
	PN96_02635	Flagellar motor switch protein FliM	/	-2.1
	PN96_02640	Flagellar motor switch protein FliN	/	-2.1

	PN96_02645	Flagellar protein FliO	/	-2.0
	PN96_02650	Flagellar protein FliP	/	-2.1
	PN96_02655	Flagellar protein FliQ	/	-1.8
	PN96_02660	Flagellar protein FliR	/	-1.8
	PN96_02665	Flagellar protein FlhB	/	-1.5
	PN96_02670	Flagellar protein FlhA	/	-2.4
	PN96_02675	Flagellar biosynthesis regulator FlhF	/	-2.5
	PN96_02680	Flagellar protein FlhG	/	-1.8
CpsR regulator	PN96_10960	Positive regulator of biofilm formation	/	-7.8
cps cluster	PN96_14985	Polysaccharide biosynthesis protein VpsM	/	/
	PN96_14990	Polysaccharide biosynthesis/export protein VpsN	/	/
	PN96_14995	Polysaccharide biosynthesis transport protein	-8.0	/
	PN96_15000	Capsular biosynthesis protein	-7.3	/
	PN96_15005	Capsular biosynthesis protein	-7.6	/
	PN96_15010	Ligase	-8.0	/
	PN96_15015	Capsular biosynthesis protein	-7.8	/
	PN96_15020	Capsular biosynthesis protein	-8.1	/
	PN96_15025	Capsular biosynthesis protein	-7.7	/
	PN96_15030	Polysaccharide biosynthesis protein VpsQ	-7.2	/
	PN96_15035	N4-acetylcytidine amidohydrolase	-10.3	/

	PN96_15040	TetR family transcriptional regulator	-10.7	/
	PN96_15045	NADP-dependent oxidoreductase	-10.8	/
	PN96_15050	Glutathione S-transferase	-4.7	/
Pilus synthesis	PN96_01805	Pilus assembly protein Flp/PilA	/	-2.0

For the transcriptomic data of *V. natriegens* Δ*cps*, hardly any significant changes were observed compared to *V. natriegens* wt. Besides the downregulation of the *cps* cluster, five other genes were affected. Genes presumably belonging to a peptidase (PN96_04095), a chromosome condensation regulator (PN96_10180), and a maltoporin (PN96_06530) had a log2 fold-change of -1.6 and an ABC transporter ATPase of -3.5 (PN96_10160). The transcription of a gene (PN96_15600) encoding a 4-α-glucanotransferase was increased by a factor of 3. For *V. natriegens* Δ*cpsR*, no alterations in the gene expression of the *cps* cluster were detected (Table 18). In addition to the downregulation of the *cpsR* gene, the transcription of several other genes involved in the synthesis of pili and flagella was decreased (Table 18). Furthermore, Log2 fold-changes of -1.6 and -2.5 were measured for genes presumably encoding for aquaporin (PN96_02980) and ATPase (PN96_07805), respectively.

3.4. Succinate production

V. natriegens wt was engineered to produce succinate under anaerobic conditions while preventing byproduct formation. Shaking flask experiments, batch and fed-batch fermentations were performed to characterize the resulting strains *V. natriegens* Succ1 and *V. natriegens* Succ1 Δ*ackA*. The additional deletion of the *ackA* gene, which encodes for an acetate kinase, was performed to reduce the formation of acetate, as it is a major byproduct of succinate production (Figure 3).

3.4.1. **Strain characterization in aerobic shaking flasks**

Aerobic growth experiments were conducted in baffled shaking flasks to characterize the growth, glucose consumption, and product formation. *V. natriegens* Succ1 grew with 1.38 ± 0.02 h^{-1}, had a $Y_{X/S}$ of 0.47 ± 0.07 g_X g_S^{-1}, and showed a q_S of 3.01 ± 0.56 g_S g_X^{-1} h^{-1}. *V. natriegens* Succ1 Δ*ackA* exhibited a μ of 1.36 ± 0.05 h^{-1}, a $Y_{X/S}$ of 0.53 ± 0.07 g_X g_S^{-1}, and a q_S of 2.61 ± 0.34 g_S g_X^{-1} h^{-1}. The performance

of both strains was quite similar (Figure 20). The strains grew exponentially for about 3 h. Glucose was not depleted and around 1 g L^{-1} remained. The most abundant product was pyruvate (3 g L^{-1}), and small amounts of acetate (< 0.75 g L^{-1}), succinate (≤ 0.15 g L^{-1}), and ethanol (≤ 0.11 g L^{-1}) were found for both strains. No formate or lactate formation occurred during cultivation.

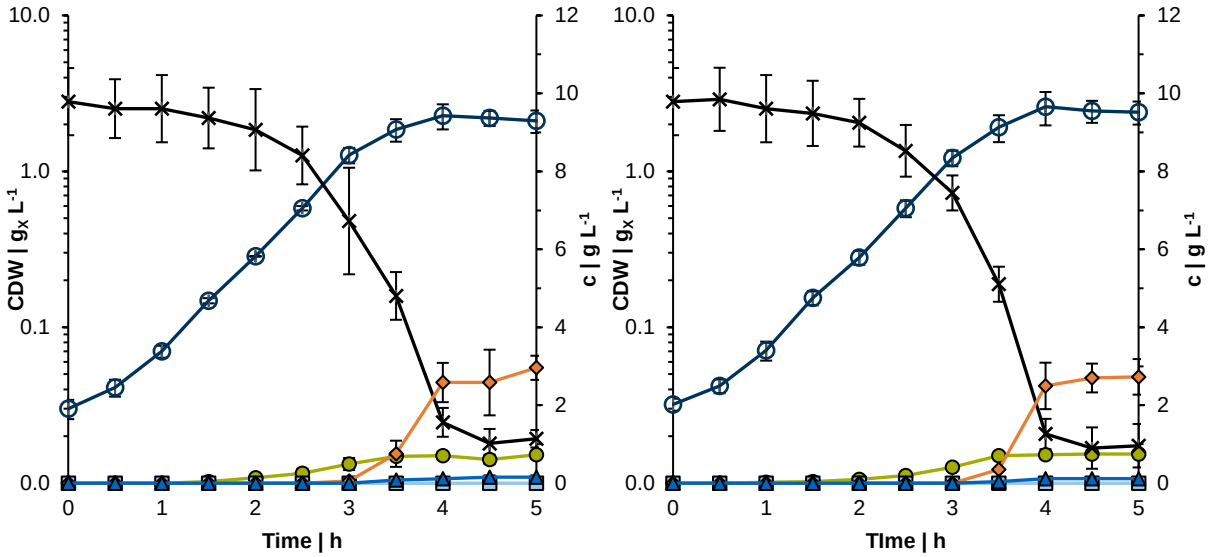

Figure 20: Growth of *V. natriegens* Succ1 (left) and *V. natriegens* Succ1 Δ*ackA* (right) in shaking flasks with VN minimal medium. The cell dry weight is represented by transparent circles and the course of glucose by crosses. Formed products are pictured as follows: acetate (circle), pyruvate (diamond), succinate (triangle), and lactate (square). Results shown are means and standard deviations of three independent biological replicates.

3.4.2. Strain characterization in anaerobic falcons

The ability of the mutants to form succinate was tested under anaerobic conditions in falcon tubes and compared to the wt (Figure 21). The wt depleted glucose within 3 h and formed the least amount of succinate (1.55 ± 0.05 g L^{-1}). Both engineered strains produced more than twice as much succinate and consumed the glucose completely. However, in contrast to the others, *V. natriegens* Succ1 needed about 5 h for glucose depletion. It produced 4.29 ± 0.19 g succinate L^{-1} and showed a $Y_{P/S}$ of 1.34 ± 0.07 mol_{Suc} mol_{Glc}^{-1}. *V. natriegens* Succ1 Δ*ackA* secreted 4.72 ± 0.20 g_{Suc} L^{-1} and yielded 1.48 ± 0.06 mol_{Suc} mol_{Glc}^{-1}, which corresponds to 87% of the theoretical maximum. Small amounts below 0.1 g pyruvate L^{-1} were detected and higher concentrations were observed for acetate. The wt formed the most with 1.02 ± 0.07 g acetate L^{-1} and *V. natriegens* Succ1 Δ*ackA* produced the least with 0.45 ± 0.06 g acetate L^{-1}. The CDW remained stable at about 1.5 g_X L^{-1} for all strains during the cultivation.

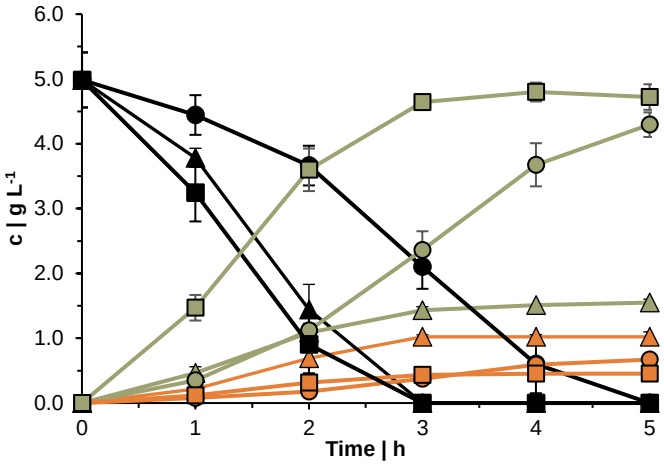

Figure 21: Glucose consumption and (by)product formation of *V. natriegens* wildtype (triangle), *V. natriegens* Succ1 (circle), and *V. natriegens* Succ1 Δ*ackA* (square) under anaerobic conditions in falcon tubes. The time course of glucose is shown with black lines. Acetate is represented by orange lines and succinate formation by green lines. Results given are means and standard deviations of three independent biological replicates.

3.4.3. **Process development for anaerobic succinate production**

Several fermentations were carried out to establish and optimize a succinate production process with engineered *V. natriegens*. An overview is given in Table 19. A first attempt (VA) was made to develop a process. Therefore, three 1 L shaking flasks containing 0.2 L 2×YTN medium were inoculated with *V. natriegens* Succ1 Δ*ackA*. The cells were harvested during the exponential growth phase and used to inoculate three bioreactor precultures with 1 L 2×YTN medium, which were then used to inoculate a VN minimal medium bioreactor culture (V = 0.5 L). In this resting cell approach, high biomass and glucose concentrations were used (17.1 g_X L^{-1} and 225 g glucose L^{-1}), and CO_2 gassing was applied to achieve anaerobic conditions and to provide additional carbon for the synthesis of succinate. However, almost no succinate (0.9 g L^{-1}) was produced. Further fermentations (VB and VC) with *V. natriegens* Succ1 Δ*ackA* were conducted at lower CDW, 100 g glucose L^{-1}, and with the additional supplementation of $KHCO_3$ for anaplerotic carboxylation reactions, but the succinate titer was not improved.

Another series of fermentations (Vd – Vf_R2) was carried out in which the bioreactor precultures were eliminated. The final concentration of succinate remained low. However, two fermentations (Ve, Vf_R1) were conducted with *V. natriegens* Succ1 Δ*ackA*, which achieved succinate titers in a low gram range. In both processes, CO_2 gassing was omitted and instead only the headspace of the bioreactor was flushed with CO_2 for 5 min to displace the oxygen. The highest concentration so far of 14.2 g succinate L^{-1} was obtained from 100 g glucose L^{-1} with a low CDW of 1.4 g_X L^{-1} (Vf_R1). In comparison, a parallel bioreactor with the same preculture but with CO_2 gassing achieved only

0.5 g succinate L^{-1} (Vf_R2). These results indicated a strong negative effect of submerged CO_2 gassing. Therefore, it was no longer used.

Next, the bioreactor preculture was reintroduced and furthermore, microaerobic conditions were established. A titer of 4.3 g succinate L^{-1} was achieved in VF with *V. natriegens* Succ1 Δ*ackA*. A Q_P of 2.1 g_{Suc} L^{-1} h^{-1} and a $Y_{P/S}$ of 0.89 mol_{Suc} mol_{Glc}^{-1} were obtained. To investigate whether the microaerobic conditions in the bioreactor preculture were responsible for the increased titer, another fermentation with *V. natriegens* Succ1 Δ*ackA* was performed with two parallel bioreactors, one inoculated with an aerobic (VG_R3) and the other with a microaerobic bioreactor preculture (VG_R4). Only 0.1 g succinate L^{-1} were produced in the first mentioned process, whereas 3.4 g succinate L^{-1} were formed from 5 g glucose L^{-1} when a microaerobic preculture was used. Based on these results, all subsequent processes were performed using microaerobic bioreactor precultures. VG_R4 was repeated with *V. natriegens* Succ1, using a higher CDW of 12.5 g_X L^{-1} instead of 1.2 g_X L^{-1}. In this process, VH, a titer of 4.3 g succinate L^{-1} was reached within 1 h, and thus for the first time a productivity was achieved that meets the requirements of industrial production, although the titer has to be increased considerably. All further processes were carried out with *V. natriegens* Succ1.

In the next fermentations, more $KHCO_3$ (VI_R3) and glucose (VI_R4) were supplied. However, the Q_P was low in both cases with about 1.6 g_{Suc} L^{-1} h^{-1}. Only a combination of high concentrations of CDW, glucose, and $KHCO_3$ (VJ) achieved good results. A total of 34.4 g succinate L^{-1} was produced with an excellent Q_P of 11.5 g_{Suc} L^{-1} h^{-1}. A $Y_{P/S}$ of 1.10 mol_{Suc} mol_{Glc}^{-1} was obtained. Although the process duration of 3 h was short, the Q_P already decreased by 12% after 2 h. Further improvement attempts were made to keep the productivity high and to prolong the production phase. The addition of two $KHCO_3$ pulses and one glucose pulse in VK had no beneficial effect. The number and the concentration of the pulses were reduced in VL to one pulse with 400 mM $KHCO_3$ and one with 50 g glucose L^{-1} after 6 h. Prior to the addition of the pulses, *V. natriegens* Succ1 produced a high titer of 61.5 g succinate L^{-1}. However, no extended succinate production was observed thereafter, and thus the process was repeated (VM) without additional pulses. This process achieved the highest titer so far (69.6 g_{Suc} L^{-1}). However, a decreased Q_P (7.0 g_{Suc} L^{-1} h^{-1}) was observed.

The most promising results were obtained with the process VN. The main culture contained 0.4 L of VN medium with 100 g glucose L^{-1} and 150 mM $KHCO_3$. A feed with 100 mM $KHCO_3$ h^{-1} was applied immediately after inoculation. Within 7 h, *V. natriegens* Succ1 produced 60.2 g succinate L^{-1} and reached a $Y_{P/S}$ of 1.17 mol_{Suc} mol_{Glc}^{-1}. Moreover, a remarkable maximum Q_P of 21.5 g_{Suc} L^{-1} h^{-1} was achieved with an overall Q_P of 8.6 g_{Suc} L^{-1} h^{-1}. Although the Q_P decreased over time, as already observed, the value was still higher after 3 h (15.2 g_{Suc} L^{-1} h^{-1}) compared to VJ. To avoid possible overfeeding, a final fermentation was conducted in which the feed was successively reduced to 75 and finally to 50 mM $KHCO_3$ h^{-1}. However, after 7 h, the titer and Q_P were reduced (50.5 g succinate L^{-1} and 7.2 g_{Suc} L^{-1} h^{-1}) and the $Y_{P/S}$ was the same as in VN. Hence, the best performing process was VN, which

was then reproduced twice (VP and VQ) to obtain a triplicate. The final results are presented in the following subchapter.

Table 19: Development of an anaerobic process for the production of succinate. From VK onwards, the main cultures were conducted in 0.4 L VN medium instead of the previous 0.5 L. The complex medium in VA – VG did not contain 50 mM_{MgCl2}. The pH was adjusted to 7.5 and the temperature to 37 °C. n.d. stands for not determined.

ID	Preculture	Provision of CO_2/HCO_3^-	Strain	CDW | $g_X\ L^{-1}$	Provision of glucose	Titer | $g\ L^{-1}$	Q_P | $g\ L^{-1}\ h^{-1}$	$Y_{P/S}$ | $mol_{Suc}\ mol_{Glc}^{-1}$
VA	3 x 0.2 L 2×YTN SF 3 x 1.0 L 2×YTN Bioreactor (aerobic)	F_{CO2} = 15 L h^{-1}	Succ1 Δ*ackA*	17.1	225 $g_{Glc}\ L^{-1}$	0.9	0.4	n.d.
VB	4 x 0.2 L 2×YTN SF 4 x 1.0 L 2×YTN Bioreactor (aerobic)	200 mM_{KHCO3} F_{CO2} = 15 L h^{-1}	Succ1 Δ*ackA*	7.8	100 $g_{Glc}\ L^{-1}$	0.4	0.2	n.d.
VC	4 x 0.2 L 2×YTN SF 4 x 1.0 L 2×YTN Bioreactor (aerobic)	100 mM_{KHCO3} F_{CO2} = 15 L h^{-1}	Succ1 Δ*ackA*	13.8	100 $g_{Glc}\ L^{-1}$	0.4	0.4	n.d.
Vd	20 x 0.2 L 2×YTN SF	100 mM_{KHCO3} F_{CO2} = 12 L h^{-1}	Succ1 Δ*ackA*	14.4	50 $g_{Glc}\ L^{-1}$	0.6	0.2	n.d.
Ve	12 x 0.05 L 2×YTN SF	100 mM_{KHCO3}	Succ1 Δ*ackA*	1.5	5 $g_{Glc}\ L^{-1}$	4.1	1.4	0.88
Vf_R1	10 x 0.05 L 2×YTN SF	100 mM_{KHCO3}	Succ1 Δ*ackA*	1.4	100 $g_{Glc}\ L^{-1}$	14.2	0.7	n.d.
Vf_R2	10 x 0.05 L 2×YTN SF	100 mM_{KHCO3} F_{CO2} = 6 L h^{-1}	Succ1 Δ*ackA*	1.3	5 $g_{Glc}\ L^{-1}$	0.5	0.1	0.52

ID	Preculture	Provision of CO_2/HCO_3^-	Strain	CDW | $g_X\ L^{-1}$	Provision of glucose	Titer | $g\ L^{-1}$	Q_P | $g\ L^{-1}\ h^{-1}$	$Y_{P/S}$ | $mol_{Suc}\ mol_{Glc}^{-1}$
VF	2 x 0.05 L 2×YTN SF 1 x 1.0 L 2×YTN Bioreactor (microaerobic)	100 mM_{KHCO3}	Succ1 Δ*ackA*	1.6	5 $g_{Glc}\ L^{-1}$	4.3	2.1	0.89
VG_R3	2 x 0.05 L 2×YTN SF 1 x 1.0 L 2×YTN Bioreactor (aerobic)	100 mM_{KHCO3}	Succ1 Δ*ackA*	1.9	5 $g_{Glc}\ L^{-1}$	0.1	0.1	0.20
VG_R4	2 x 0.05 L 2×YTN SF 1 x 1.0 L 2×YTN Bioreactor (microaerobic)	100 mM_{KHCO3}	Succ1 Δ*ackA*	1.2	5 $g_{Glc}\ L^{-1}$	3.4	1.6	1.04
VH	9 x 0.05 L 2×YTN SF 3 x 1.5 L 2×YTN Bioreactor (microaerobic)	100 mM_{KHCO3}	Succ1	12.5	5 $g_{Glc}\ L^{-1}$	4.3	4.3	1.33
VI_R3	3 x 0.05 L 2×YTN SF 1 x 1.5 L 2×YTN Bioreactor (microaerobic)	400 mM_{KHCO3}	Succ1	1.5	5 $g_{Glc}\ L^{-1}$	4.6	1.6	1.38
VI_R4	3 x 0.05 L 2×YTN SF 1 x 1.5 L 2×YTN Bioreactor (microaerobic)	20 mM_{KHCO3} feed with 50 $mM_{KHCO3}\ h^{-1}$ at t = 0 h	Succ1	1.4	50 $g_{Glc}\ L^{-1}$	13.0	1.6	1.15
VJ	9 x 0.05 L 2×YTN SF 3 x 1.5 L 2×YTN Bioreactor (microaerobic)	400 mM_{KHCO3}	Succ1	13.5	50 $g_{Glc}\ L^{-1}$	34.4	11.5	1.10

ID	Preculture	Provision of CO_2/HCO_3^-	Strain	CDW | $g_X\ L^{-1}$	Provision of glucose	Titer | $g\ L^{-1}$	Q_P | $g\ L^{-1}\ h^{-1}$	$Y_{P/S}$ | $mol_{Suc}\ mol_{Glc}^{-1}$
VK	9 x 0.05 L 2×YTN SF 3 x 1.5 L 2×YTN Bioreactor (microaerobic)	400 mM_{KHCO3} puls with 400 mM_{KHCO3} at t = 2 and 6 h	Succ1	19.5	100 $g_{Glc}\ L^{-1}$ puls with 100 $g_{Glc}\ L^{-1}$ at t = 6 h	35.4	5.9	0.93
VL	9 x 0.05 L 2×YTN SF 3 x 1.5 L 2×YTN Bioreactor (microaerobic)	400 mM_{KHCO3} puls with 200 mM_{KHCO3} at t = 6 h	Succ1	17.1	100 $g_{Glc}\ L^{-1}$ puls with 50 $g_{Glc}\ L^{-1}$ at t = 6h	61.5	3.4	0.64
VM	9 x 0.05 L 2×YTN SF 3 x 1.5 L 2×YTN Bioreactor (microaerobic)	400 mM_{KHCO3}	Succ1	13.2	100 $g_{Glc}\ L^{-1}$	69.6	7.0	1.30
VN	9 x 0.05 L 2×YTN SF 3 x 1.5 L 2×YTN Bioreactor (microaerobic)	150 mM_{KHCO3} feed with 100 $mM_{KHCO3}\ h^{-1}$ at t = 0 h	Succ1	18.0	100 $g_{Glc}\ L^{-1}$	60.2	8.6	1.17
VO	9 x 0.05 L 2×YTN SF 3 x 1.5 L 2×YTN Bioreactor (microaerobic)	200 mM_{KHCO3} applied feed: 0 – 3 h: 100 $mM_{KHCO3}\ h^{-1}$ 3 – 4 h: 75 $mM_{KHCO3}\ h^{-1}$ 4 – 20.75 h: 50 $mM_{KHCO3}\ h^{-1}$	Succ1	21.3	150 $g_{Glc}\ L^{-1}$	50.5	7.2	1.17
VP	9 x 0.05 L 2×YTN SF 3 x 1.5 L 2×YTN Bioreactor (microaerobic)	150 mM_{KHCO3} feed with 100 $mM_{KHCO3}\ h^{-1}$ at t = 0 h	Succ1	19.8	100 $g_{Glc}\ L^{-1}$	60.8	8.7	1.15

ID	Preculture	Provision of CO_2/HCO_3^-	Strain	CDW | $g_X\ L^{-1}$	Provision of glucose	Titer | $g\ L^{-1}$	Q_P | $g\ L^{-1}\ h^{-1}$	$Y_{P/S}$ | $mol_{Suc}\ mol_{Glc}^{-1}$
VQ	9 x 0.05 L 2×YTN SF 3 x 1.5 L 2×YTN Bioreactor (microaerobic)	150 mM_{KHCO3} feed with 100 $mM_{KHCO3}\ h^{-1}$ at t = 0 h	Succ1	17.4	100 $g_{Glc}\ L^{-1}$	61.8	8.8	1.11

3.4.4. Final succinate production process

A final succinate process was performed as a triplicate using *V. natriegens* Succ1, which consisted of the processes VN, VP, and VQ (Table 19, and Figure 22). The main culture was inoculated with 18.40 ± 1.02 $g_X\ L^{-1}$ from cells grown under microaerobic conditions, and the VN medium used was supplemented with 100 g glucose L^{-1} and 150 mM $KHCO_3$. Immediately after inoculation, feeding with 100 mM $KHCO_3\ h^{-1}$ was started. Glucose was almost depleted within 7 h (1.20 ± 1.22 g L^{-1} remained) and 60.44 ± 0.90 g succinate L^{-1} were produced. Acetate and alanine were measured as well with final concentrations of 4.82 ± 0.70 g L^{-1} and 0.95 ± 0.14 g L^{-1}, respectively. No other products were detected. However, the C-balance was only closed to 62 ± 1%. The process yielded 1.14 ± 0.02 $mol_{Suc}\ mol_{Glc}^{-1}$, which corresponds to 67% of the theoretical maximum, and a total Q_P of 8.63 ± 0.13 $g_{Suc}\ L^{-1}\ h^{-1}$ was achieved. At the beginning of the process, the Q_P was highest with 20.82 ± 0.22 $g_{Suc}\ L^{-1}\ h^{-1}$.

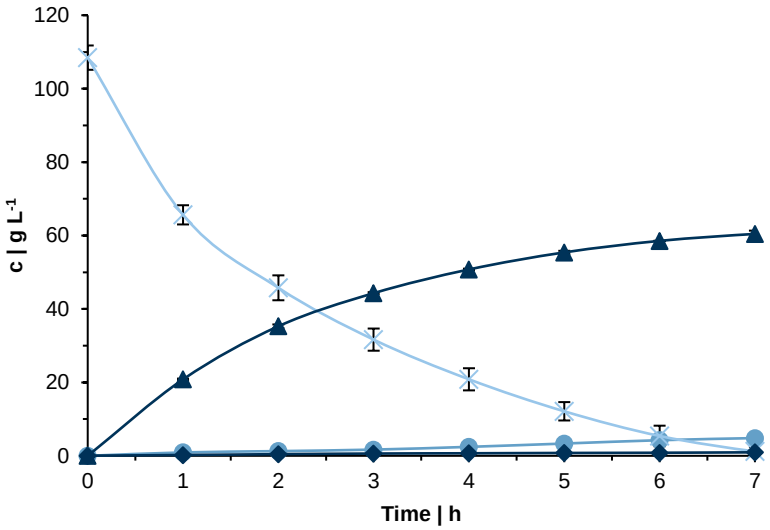

Figure 22: Anaerobic zero-growth process for succinate production with *V. natriegens* Succ1 (Δ*lldh* Δ*dldh* Δ*pfl* Δ*ald* Δ*dns*::*pyc*$_{Cg}$). The course of glucose is represented by crosses, and the products formed

are shown as follows: acetate (circle), alanine (diamond), and succinate (triangle). Results given are means and standard deviations of three independent biological replicates.

3.4.5. **Triple-phase process**

So far, succinate fermentation requires aerobic bioreactor precultures for high biomass concentrations, a microaerobic transition phase, and a separate bioreactor is needed for the anaerobic succinate production. To simplify the production of succinate, a process should be developed that combines all three phases. This triple-phase process is based on previously conducted glucose-limited fed-batch processes, and thus the growth of the producer strain *V. natriegens* Succ1 was first tested in such a process (V4_R4, Table 10). The strain grew with a µ of 1.64 h^{-1} during the unlimited growth phase and thereafter had a stable µ of 0.09 h^{-1}. No growth impairment was observed. After 26 h, the CDW decreased. In total, a CDW_{max} of 16.2 g_X L^{-1} was obtained.

Next, different approaches to achieve microaerobic conditions were tested in three parallel bioreactors (V6, Table 10). After about 24 h, when the DO dropped below 1%, 50 g glucose L^{-1} were pulsed and a feed was added to provide sufficient carbon for succinate production. Microaerobic conditions were introduced in bioreactor 2 (V6_R2) by reducing the agitation rate from 1,500 to 1,200 rpm. However, only a low concentration of 2.6 g succinate L^{-1} was reached after 32 h. Approximately 5 g succinate L^{-1} were formed when a limited aeration rate (V6_R3) or a gas mixture containing CO_2 (V6_R4) was applied to achieve microaerobic conditions. Accumulation of glucose was observed in all bioreactors and the CDW started to decrease after the transition to microaerobiosis. Moreover, pyruvate accumulated in all bioreactors until the onset of CO_2 gassing at 26 h. However, its formation was reduced by about 25% when a CO_2 gas mixture was supplied.

Due to the low titers and productivities of the previous performed fermentations, a different approach was chosen for the next process (V8_R123, Table 10 and Figure 23). This time, the agitation rate was set to a maximum of 1,300 rpm from the beginning to limit the oxygen supply, and thus automatically achieve microaerobic conditions once a certain CDW was reached. After about 2 h of a microaerobic phase, the gassing was stopped to achieve anaerobic conditions. *V. natriegens* Succ1 grew with 1.53 ± 0.11 h^{-1} during the exponential growth phase and thereafter maintained a µ of 0.12 ± 0.01 h^{-1} during the glucose-limited phase. At about 18 h, the set DO cascade set up was not sufficient anymore to maintain the DO at 50%, and the value dropped to almost 0% at around 24 h. At this time, the CDW reached a maximum concentration of 20.00 ± 0.75 g_X L^{-1}. A glucose pulse (50 g L^{-1}) was given to provide sufficient carbon for the synthesis of succinate. During the 2 h of microaerobiosis, 6.81 ± 1.44 g succinate L^{-1} were secreted, corresponding to a Q_P of 3.40 ± 0.72 g_{Suc} L^{-1} h^{-1}. At 26 h, the anaerobic phase was initiated by switching off the gas supply. However, the succinate production rate

decreased over time from 0.19 ± 0.04 g_{Suc} g_X^{-1} h^{-1} to 0.13 ± 0.06 g_{Suc} g_X^{-1} h^{-1} after 30 h, and a total titer of 9.98 ± 3.63 g succinate L^{-1} was obtained. As before, pyruvate was the most abundant byproduct, accumulating to 7.72 ± 0.36 g pyruvate L^{-1} in the bioreactor broth. Smaller amounts of acetate and lactate were found (2.28 ± 0.40 g L^{-1} and 0.36 ± 0.29 g L^{-1}, respectively).

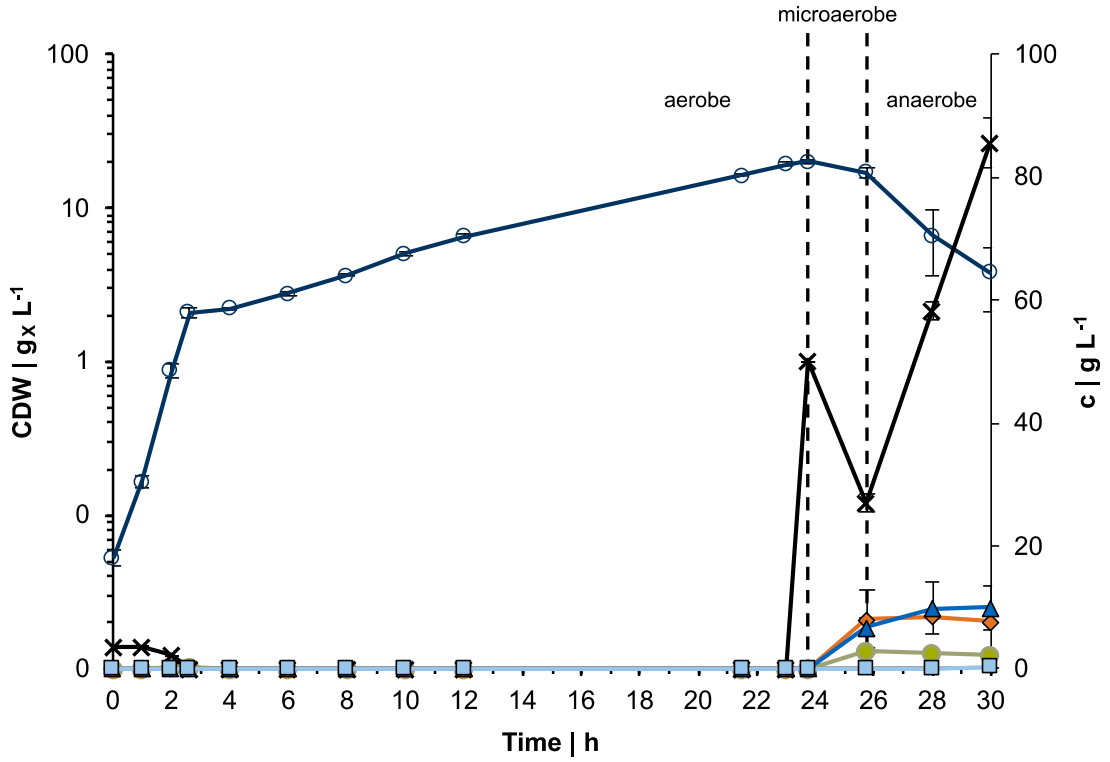

Figure 23: Triple-phase process (V8) with *V. natriegens* Succ1 for succinate production. The cell dry weight is represented by transparent circles and the course of glucose by crosses. The products formed are depicted as follows: acetate (circle), pyruvate (diamond), succinate (triangle), and lactate (square). Dashed lines indicate the transition from aerobic to microaerobic or from microaerobic to anaerobic conditions. Results given are means and standard deviations of three independent biological replicates.

3.4.6. **Impact of exopolysaccharides on succinate production**

During succinate production (3.4.4), an increased viscosity was observed, which made it extremely difficult to separate the biomass from the bioreactor broth by centrifugation at the end of the process. To investigate the effect of EPS, *cpsR* and *cps* were deleted in *V. natriegens* Succ1 and the zero-growth process was repeated as described in 2.6.2. *V. natriegens* Succ1 produced 45 g succinate L^{-1}, exhibited a $Y_{P/S}$ of 1.10 mol_{Suc} mol_{Glc}^{-1} and achieved a Q_P of 7.5 g_{Suc} L^{-1} h^{-1}. During cultivation, the viscosity increased from 7 to 36 mPa s (Figure 24). No viscosity changes were observed for the strains with the additional EPS deletions. *V. natriegens* Succ1 Δ*cpsR* and *V. natriegens* Succ1 Δ*cps* secreted 51.1 and

46.4 g succinate L^{-1}, respectively. Both strains achieved high Q_P of 8.5 g_{Suc} L^{-1} h^{-1} and 7.7 g_{Suc} L^{-1} h^{-1}, respectively. The $Y_{P/S}$ was increased by 27% for both strains to a $Y_{P/S}$ of 1.4 mol_{Suc} mol_{Glc}^{-1}. This corresponds to 81% of the theoretical maximum (Figure 24). Furthermore, the C-balance was closed to about 80%, whereas only 64% of the carbon could be recovered for *V. natriegens* Succ1.

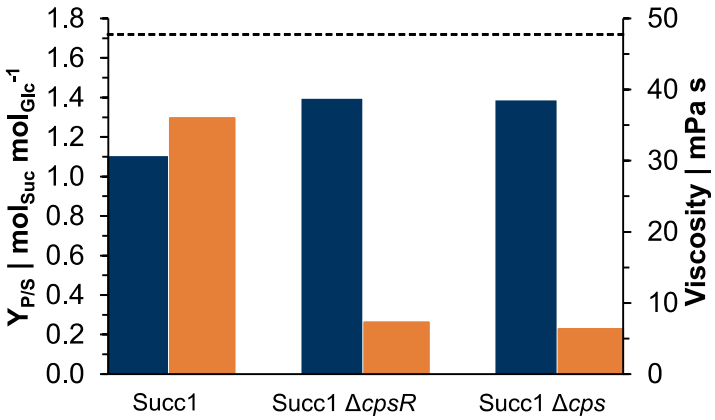

Figure 24: Product yield (dark blue) and final viscosity (orange) of an anaerobic resting cell approach for succinate production. Fermentations were performed with *V. natriegens* Succ1, *V. natriegens* Succ1 Δ*cpsR*, and *V. natriegens* Succ1 Δ*cps* (n = 1). The black dashed line represents the maximum theoretical yield on glucose (1.71 mol_{Suc} mol_{Glc}^{-1}). The viscosity was measured in a technical triplicate at a shear rate of 0.1 s^{-1}.

3.5. Pyruvate production

The development of a pyruvate production process started with the characterization of potential pyruvate-producing strains. Two prophage regions, VNP1 and VNP2, were deleted to improve cell robustness and to increase pyruvate production, as previously described by Pfeifer et al. (2019). Furthermore, the gene *aceE*, which encodes for the E1 subunit of the PDHC, was removed to block the carbon flux from glycolysis to TCA. The resulting strains *V. natriegens* Δ*aceE* and *V. natriegens* Δ*vnp12* Δ*aceE* were transferred into bioreactor cultures and different options for supplying acetate to the acetate auxotrophic strains were tested. In addition, strain and process engineering approaches were carried out to limit the formation of an unwanted byproduct, later identified as parapyruvate.

3.5.1. **Strain characterization in shaking flasks**

Aerobic growth experiments were performed in baffled shaking flasks with two potential pyruvate producer strains (Figure 25). *V. natriegens* Δ*aceE* grew exponentially with 1.22 ± 0.02 h^{-1} up to 4 h and depleted both substrates (7.5 g glucose L^{-1} and 1 g acetate L^{-1}) within 4.5 h. At this time, the maximum titer of 4.02 ± 0.15 g pyruvate L^{-1} was reached. The second strain, carrying an additional *vnp12* deletion, grew slightly slower (μ = 1.15 ± 0.01 h^{-1}) and the exponential growth phase was prolonged to 4.5 h. This strain depleted both substrates as well and secreted 4.17 ± 0.42 g pyruvate L^{-1}.

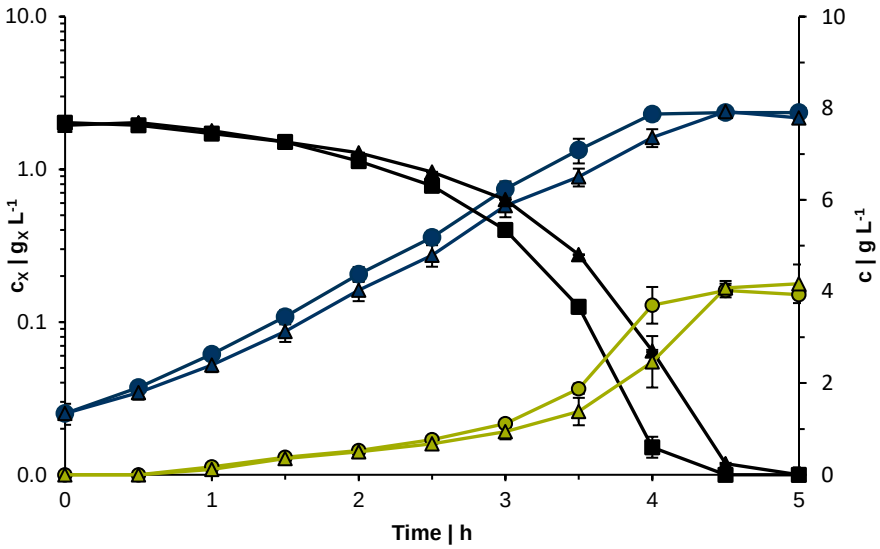

Figure 25: Characterization of *V. natriegens* Δ*aceE* (circle) and *V. natriegens* Δ*vnp12* Δ*aceE* (triangle) in shaking flasks containing VN minimal medium. The cell dry weight is depicted in blue and the course

of glucose in black. Formed pyruvate is pictured in green. Results given are means and standard deviations of three independent biological replicates.

3.5.2. **Bioreactor processes**

Various processes were conducted to achieve optimal conditions for pyruvate production and an overview of all processes is given in the following Table 20.

Table 20: Process development for pyruvate production. The bioreactor contained 0.5 L of VN medium. The temperature was set to 37 °C and the pH was adjusted to 7.5. The gassing rate was kept constant at 1 vvm. The DO was controlled at 50% via the agitation rate (400 – 1,500 rpm), and one Rushton impeller was installed. A slash indicates that there were no deviations from the aforementioned process parameters. ID stands for Identification. Triplicates are marked with n = 3 and the means and standard deviations are given. The start of an acetate feed is indicated with t_{Feed}.

ID	Bioreactor	Main culture	Provision of acetate	Strain	CDW_{max} | $g_X\ L^{-1}$	c_{Glc} | g L^{-1}	Titer | g L^{-1}	Q_P | g L^{-1}	$Y_{P/S}$ | mol_{Pyr} mol_{Glc}^{-1}
PyrA	R1	/	2 $g_{Ace}\ L^{-1}$	*V. natriegens* Δ*aceE*	2.9	50	20.4	0.95	0.99
PyrB	1 (n = 3)	/	2 $g_{Ace}\ L^{-1}$	*V. natriegens* Δ*aceE*	2.7 ± 0.2	100	22.5 ± 2.0	2.05 ± 0.15	1.50 ± 0.26
	2 (n = 3)	/	2 $g_{Ace}\ L^{-1}$	*V. natriegens* Δ*vnp12* Δ*aceE*	2.6 ± 0.2	100	23.3 ± 2.4	1.79 ± 0.15	1.48 ± 0.31
PyrC	R1	/	2 $g_{Ace}\ L^{-1}$	*V. natriegens* Δ*vnp12* Δ*aceE*	3.4	75	16.5	1.37	n.d.
	R2	/	2 $g_{Ace}\ L^{-1}$ Feed 2 $mM_{Ace}\ h^{-1}$ (t_{Feed} = 5 h)	*V. natriegens* Δ*vnp12* Δ*aceE*	3.6	75	24.3	2.02	n.d.

ID	Bioreactor	Main culture	Provision of acetate	Strain	CDW_{max} | $g_X\ L^{-1}$	c_{Glc} | g L^{-1}	Titer | g L^{-1}	Q_P | g L^{-1}	$Y_{P/S}$ | mol_{Pyr} mol_{Glc}^{-1}
PyrD	R1	/	2 $g_{Ace}\ L^{-1}$	*V. natriegens* Δ*vnp12* Δ*aceE*	5.6	75	17.8	1.48	0.83
	R2	/	2 $g_{Ace}\ L^{-1}$ Feed 2 $mM_{Ace}\ h^{-1}$ (t_{Feed} = 5 h)	*V. natriegens* Δ*vnp12* Δ*aceE*	5.5	75	21.2	1.77	0.98
	R3	/	2 $g_{Ace}\ L^{-1}$ Feed 8 $mM_{Ace}\ h^{-1}$ (t_{Feed} = 5 h)	*V. natriegens* Δ*vnp12* Δ*aceE*	5.3	75	26.1	2.61	0.91
	R4	/	2 $g_{Ace}\ L^{-1}$ Feed 16 $mM_{Ace}\ h^{-1}$ (t_{Feed} = 5 h)	*V. natriegens* Δ*vnp12* Δ*aceE*	6.8	75	24.7	3.09	0.88
PyrE	R1	/	2 $g_{Ace}\ L^{-1}$	*V. natriegens* Δ*vnp12* Δ*aceE*	3.4	100	20.9	2.09	1.13
	R2	/	2 $g_{Ace}\ L^{-1}$ Feed 8 $mM_{Ace}\ h^{-1}$ (t_{Feed} = 5 h)	*V. natriegens* Δ*vnp12* Δ*aceE*	4.1	100	34.8	3.48	1.15
	R3	/	2 $g_{Ace}\ L^{-1}$ Feed 8 $mM_{Ace}\ h^{-1}$ (t_{Feed} = 0 h)	*V. natriegens* Δ*vnp12* Δ*aceE*	6.0	100	39.4	3.93	1.11

In a first approach (PyrA), *V. natriegens* Δ*aceE* secreted 20.4 g pyruvate L^{-1} within 21.5 h (≙ 0.95 g_{Pyr} L^{-1} h^{-1}) and yielded 0.99 mol_{Pyr} mol_{Glc}^{-1} during a batch fermentation with VN minimal medium. The process was repeated as a triplicate (PyrB_1) and compared to another engineered strain *V. natriegens* Δ*vnp12* Δ*aceE* (PyrB_2). No significant differences were observed between these strains. Both obtained a Q_P of about 2 g_{Pyr} L^{-1} h^{-1}, a titer of 23 g pyruvate L^{-1}, and a $Y_{P/S}$ of 1.5 mol_{Pyr} mol_{Glc}^{-1}. However, the CDW of *V. natriegens* Δ*vnp12* Δ*aceE* remained more stable at the end of the process and was therefore used in all further pyruvate production processes unless otherwise stated (Figure 26).

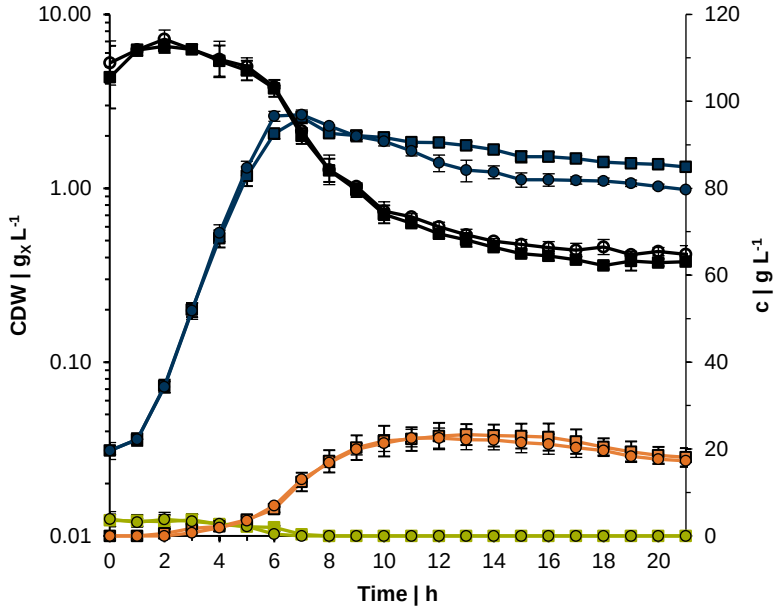

Figure 26: Pyruvate production with *V. natriegens* Δ*aceE* (circles) and *V. natriegens* Δ*vnp12* Δ*aceE* (squares) in a batch process with VN minimal medium. The cell dry weight is represented by dark blue lines and the course of glucose by black lines. The formation of acetate is shown with green lines and that of pyruvate with orange lines. Results given are means and standard deviations of three independent biological replicates.

To further improve the supply of acetate, a feed of 2 mM_{Ace} h^{-1} was started after 5 h (PyrC_R2), shortly before acetate depletion. The titer was increased by almost 50% from 16.5 g pyruvate L^{-1} to 24.3 g pyruvate L^{-1} compared to a control group without feed (PyrC_R1). A range between 2 and 16 mM_{Ace} h^{-1} was tested to determine the ideal feed concentration (Figure 27).

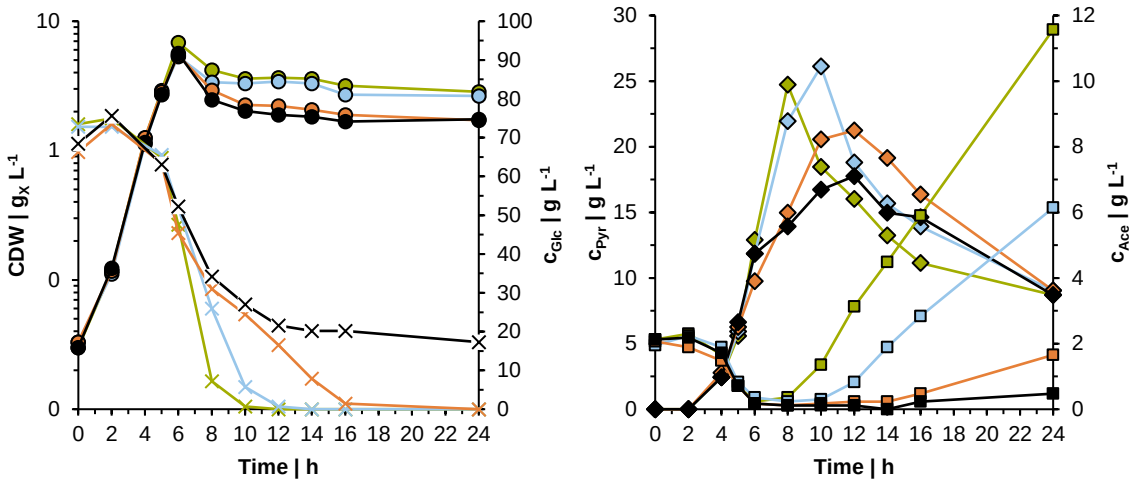

Figure 27: Pyruvate production with *V. natriegens* Δ*vnp12* Δ*aceE* in a fed-batch process with the following acetate feeds: 2 mM_{Ace} h^{-1} (orange), 8 mM_{Ace} h^{-1} (blue), and 16 mM_{Ace} h^{-1} (green). A control group without feed is depicted in black. The cell dry weight is shown with circles, glucose with crosses, acetate with squares, and pyruvate with diamonds.

In all cultivations (PyrD, Table 20), *V. natriegens* Δ*vnp12* Δ*aceE* grew with a growth rate around 0.9 h^{-1} and exhibited a $Y_{X/S}$ between 0.2 and 0.3 g_X g_{Glc}^{-1}. The CDW_{max} was reached after 6 h and about 5.5 g_X L^{-1} were obtained in all bioreactors, except in the one with the highest feed rate, which showed an increased value of 6.8 g_X L^{-1}. Thereafter, the biomass decreased and this effect was most pronounced for the control group and the bioreactor with the lowest feed concentration. Glucose was depleted when an acetate feed was applied, and consumption was faster at higher feed concentrations. The strongest decrease of glucose occurred between 5 and 8 h. During this time, the q_S of the control group was 2.6 g_{Glc} g_X^{-1} h^{-1}. This value increased with higher feed concentrations. In R4, 3.9 g_{Glc} g_X^{-1} h^{-1} were obtained when 16 mM_{Ace} h^{-1} were fed. In addition, differences were observed in terms of final product titer and acetate accumulation. At a concentration of 8 mM_{Ace} h^{-1}, 6 g acetate L^{-1} were detected. This amount was even doubled at the next higher feed concentration, whereas only 1.7 g acetate L^{-1} and 0.5 g acetate L^{-1} were obtained at the lowest feed concentration as well as in the control group, respectively. However, pyruvate was not produced as fast or as much in the latter, and maximum titers of 18 to 21 g pyruvate L^{-1} were measured after 12 h. In the bioreactor with the 16 mM_{Ace} h^{-1} feed, 24.7 g pyruvate L^{-1} were obtained within 8 h, and the highest titer of 26.1 g pyruvate L^{-1} was achieved after 10 h in R3.

Next, two fed-batch fermentations were carried out, one with a feed of 8 mM_{Ace} h^{-1} starting immediately after inoculation (PyrE_R3) and the other with a delayed start after 5 h of process time (PyrE_R2), as in the previous processes. Due to the earlier start of feeding and the resulting higher amount of available acetate, the CDW_{max} was increased to 6 g_X L^{-1}. In both processes, approximately 100 g glucose L^{-1} were consumed and 5 g acetate L^{-1} accumulated in the bioreactor broths. The highest titer of 39.4 g pyruvate L^{-1} was reached after 10 h when the feed was started directly at the beginning of the

process. A Q_P of 3.9 g_{Pyr} L^{-1} h^{-1} and a $Y_{P/S}$ of 1.1 mol_{Pyr} mol_{Glc}^{-1} were obtained. The process with the delayed feed performed slightly worse. The $Y_{P/S}$ was identical, but the Q_P and titer were lowered to 3.5 g_{Pyr} L^{-1} h^{-1} and 34.8 g pyruvate L^{-1}, respectively, thus 8 mM_{Ace} h^{-1} were provided in the final process from the start.

3.5.3. **Final pyruvate production process**

For pyruvate production, a fed-batch process was applied using VN minimal medium supplemented initially with 100 g glucose L^{-1} and 2 g acetate L^{-1} (Figure 28). During the previous process development, it was shown that a feed of 8 mM_{Ace} h^{-1}, started at the beginning of the process, could improve the production of pyruvate in terms of rate and titer. The most suitable strain was found to be *V. natriegens* Δ*vnp12* Δ*aceE*. A triplicate (PyrE_R3, PyrF_R2, and PyrG_R2) was conducted and compared to a control group (PyrE – PyrG, R1) without feed. All bioreactors were inoculated with a CDW of approximately 0.15 g_X L^{-1}. A µ of 0.88 ± 0.02 h^{-1} and a CDW_{max} of 3.42 ± 0.08 g_X L^{-1} were reached after 5 h in the absence of a feed. Furthermore, a $Y_{X/S}$ of 0.28 ± 0.03 g_X g_{Glc}^{-1} and a q_S of 3.15 ± 0.26 g_{Glc} g_X^{-1} h^{-1} were obtained. During the stationary phase of cell growth, glucose was still consumed at a high rate of 1.93 ± 0.12 g_{Glc} g_X^{-1} h^{-1}. However, about 60 g glucose L^{-1} were still left at the end of the process. A maximum pyruvate concentration of 22.17 ± 0.91 g L^{-1} was reached within 10 h, which corresponds to a Q_P of 2.22 ± 0.09 g_{Pyr} L^{-1} h^{-1}. A $Y_{P/S}$ of 1.21 ± 0.06 mol_{Pyr} mol_{Glc}^{-1} was obtained. During the biomass formation phase, no significant differences regarding the µ (0.80 ± 0.03 h^{-1}), $Y_{X/S}$ (0.25 ± 0.02 g_X g_{Glc}^{-1}), and q_S (3.15 ± 0.18 g_{Glc} g_X^{-1} h^{-1}) were observed when an acetate feed was applied. However, the exponential growth phase was extended to 6.5 h and a CDW_{max} of 6.58 ± 0.42 g_X L^{-1} was obtained. After 10 h, an increased pyruvate titer (40.97 ± 1.83 g_{Pyr} L^{-1}) by 85% was achieved compared to the control group and an elevated Q_P of 4.10 ± 0.18 g_{Pyr} L^{-1} h^{-1} was reached. The q_S remained high during the stationary phase with 3.46 ± 0.16 g_{Glc} g_X^{-1} h^{-1}. However, a reduced $Y_{P/S}$ of 1.05 ± 0.04 mol_{Pyr} mol_{Glc}^{-1} was obtained and 14.05 ± 7.07 g glucose L^{-1} were still left.

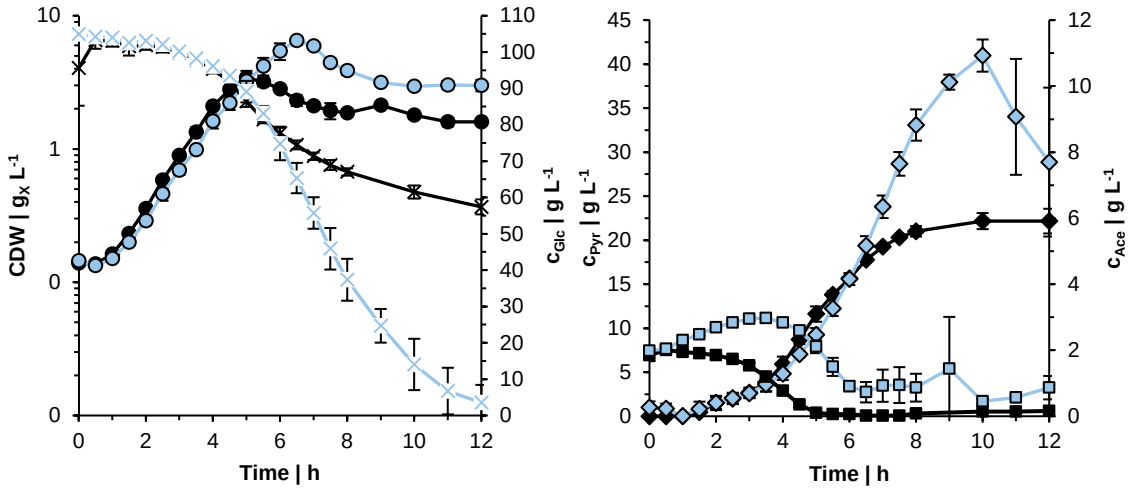

Figure 28: Final pyruvate production with *V. natriegens* Δ*vnp12* Δ*aceE* in a fed-batch process with a feed of 8 mM_{Ace} h^{-1} (blue). The control group without feed is depicted in black. The cell dry weight is shown with circles, glucose with crosses, acetate with squares, and pyruvate with diamonds. Results given are means and standard deviations of three independent biological replicates.

For both processes, byproduct formation was analyzed, but only small amounts (< 1 g L^{-1}) of acetate, lactate, and succinate were measured. After 10 h, when pyruvate formation peaked, the C-balance was closed to 87 ± 1% without feed, but only 74 ± 5% carbon were recovered when a feed was applied. This value decreased drastically to 40 ± 11% at the end of the process. Investigation of the RI signal measured by HPLC showed an emerging peak that increased with decreasing pyruvate concentrations. This peak was later identified as parapyruvate and was found to be responsible for the carbon sink (Figure A3).

3.5.4. **Investigation of parapyruvate formation**

It was assumed that the carbon sink during pyruvate production was caused by the chemical and/or enzymatical formation of parapyruvate, and thus process parameters were adjusted to shift the chemical equilibrium towards pyruvate. In addition, two strains were engineered and tested in the bioreactor to gain more insight into parapyruvate metabolism.

3.5.4.1. Process engineering

Parapyruvate formation is favored at high temperatures and pH values. Two fermentation series were conducted to test different conditions under which parapyruvate is less likely to form. In the first round, the pH was addressed. In one bioreactor the pH was lowered to pH 6.5 (PyrH_R3) and in the other

(PyrH_R2) the base used for titration had a lower ammonia concentration (10 instead of 25%) to avoid local pH peaks. The results are shown in Figure 29.

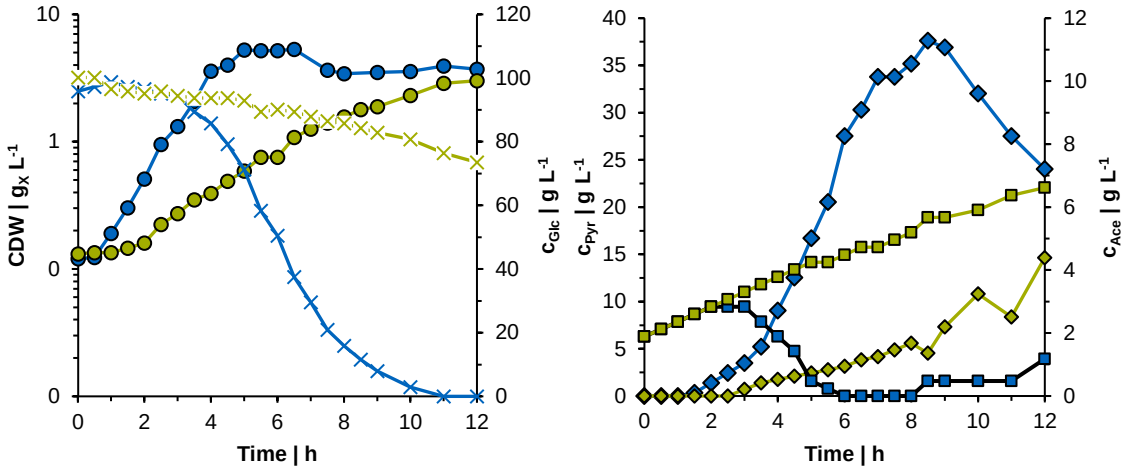

Figure 29: Pyruvate production with *V. natriegens* Δ*vnp12* Δ*aceE* in a fed-batch process with a feed of 8 mM_{Ace} h^{-1} with either a reduced pH value of 6.5 (green) or a decreased concentration of the base (10% ammonia water) (blue). The cell dry weight is shown as circles, glucose as crosses, acetate as squares, and pyruvate as diamonds.

The pH of 6.5 significantly inhibited the growth of *V. natriegens* Δ*vnp12* Δ*aceE* (μ = 0.37 h^{-1}) and acetate accumulated throughout the process. After 12 h, 6.6 g acetate L^{-1} were detected. A final product titer of 14.6 g pyruvate L^{-1} was measured, corresponding to a Q_P of 1.22 g_{Pyr} L^{-1} h^{-1}. However, the $Y_{P/S}$ was increased to 1.40 mol_{Pyr} mol_{Glc}^{-1} and 98% of the carbon could be recovered.

No growth impairment was observed when 10% ammonia water was used for the pH regulation. The cells grew with a μ of 0.87 h^{-1} to a CDW_{max} of 5.3 g_X L^{-1}. Compared to previous processes carried out under the same conditions, a slightly increased $Y_{P/S}$ of 1.21 mol_{Pyr} mol_{Glc}^{-1} and a higher Q_P of 4.83 g_{Pyr} L^{-1} h^{-1} were obtained (3.5.3. and PyrE_R3, PyrF_R2, and PyrG_R2, Table 10). However, the titer was reduced to 34 g pyruvate L^{-1}, and the C-balance was only closed to 53% when pyruvate peaked and this value decreased to 43% at the end of the process.

A second fed-batch series was conducted to test temperatures between 20 and 30 °C (PyrI) (Figure 30). The results were compared to a fed-batch process with a feed of 8 mM_{Ace} h^{-1} at 37 °C (3.5.3. and PyrE_R3, PyrF_R2, and PyrG_R2, Table 20).

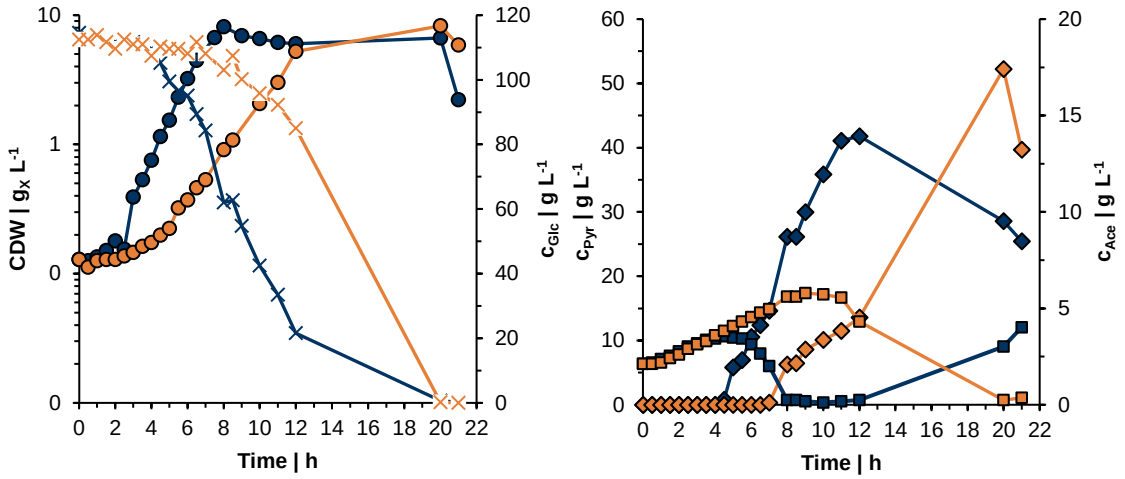

Figure 30: Pyruvate production with *V. natriegens* Δ*vnp12* Δ*aceE* in a fed-batch process with a feed of 8 mM_{Ace} h^{-1} at 25 °C (orange) or at 30 °C (dark blue). The cell dry weight is shown with circles, glucose with crosses, acetate with squares, and pyruvate with diamonds.

Lower cultivation temperatures resulted in an inhibited growth, and no growth was observed at 20 °C (data not shown). At 25 °C, *V. natriegens* Δ*vnp12* Δ*aceE* grew with 0.44 h^{-1} and reached its CDW_{max} of 8.26 g_X L^{-1} after 20 h. At 30 °C, a similar CDW_{max} (8.12 g_X L^{-1}) was reached after 8 h and the cells grew with a reduced growth rate (0.64 h^{-1}) by 20% compared to cultivations at 37 °C. No significant differences were observed for the titer (41.1 g pyruvate L^{-1}) or the carbon recovery (78%). The Q_P was reduced by 15% to 3.74 g_{Pyr} L^{-1} h^{-1}. However, the $Y_{P/S}$ of 1.18 mol_{Pyr} mol_{Glc}^{-1} was increased compared to cultivations at 37 °C. At 25 °C, the highest pyruvate titer so far of 52.2 g pyruvate L^{-1} was achieved after 20 h, when glucose was almost depleted (0.2 g L^{-1} remained). At that time, 71% carbon were recovered, but within 1 h the value decreased to 57%. Although the titer obtained was higher than usual, the $Y_{P/S}$ was not significantly changed (1.11 mol_{Pyr} mol_{Glc}^{-1}) and the Q_P (2.61 g_{Pyr} L^{-1} h^{-1}) decreased to about 40% compared to the 37 °C process.

3.5.4.2. Strain engineering

To obtain more information about the circumstances of parapyruvate formation, the gene *papA*, which encodes for a parapyruvate aldolase, was knocked out as well as overexpressed in the pyruvate strain background. The two resulting strains *V. natriegens* Δ*vnp12* Δ*aceE* Δ*papA* and *V. natriegens* Δ*vnp12* Δ*aceE* pekEx-*papA* were then tested in fed-batch processes as described in 3.5.3 (PyrJ – PyrL) (Figure 31).

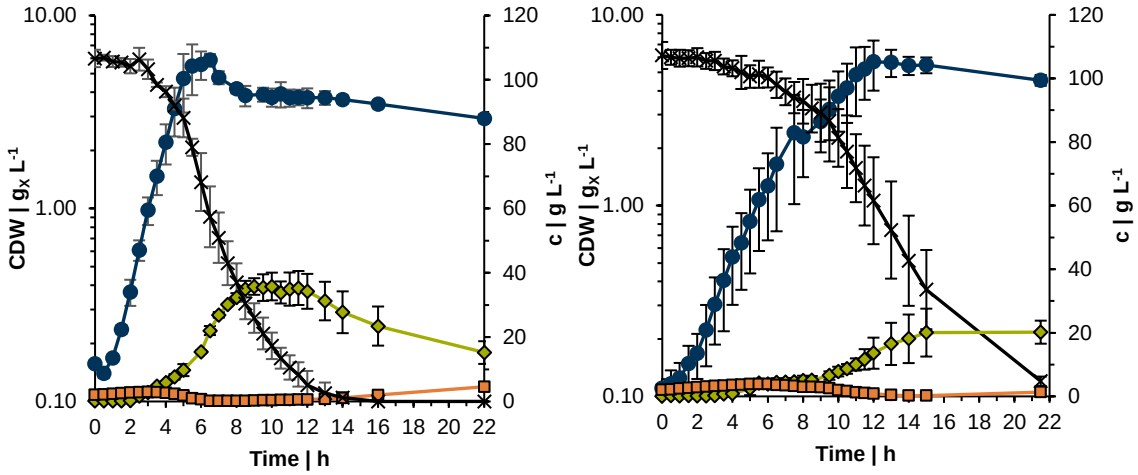

Figure 31: Pyruvate production with *V. natriegens* Δ*vnp12* Δ*aceE* Δ*papA* (left) and *V. natriegens* Δ*vnp12* Δ*aceE* pekEx-*papA* (right). The cell dry weight is represented by dark blue lines, and the course of glucose by black lines. The formation of acetate is shown with orange lines and pyruvate with green lines. Results given are means and standard deviations of three independent biological replicates for *V. natriegens* Δ*vnp12* Δ*aceE* Δ*papA* and five independent biological replicates for *V. natriegens* Δ*vnp12* Δ*aceE* pekEx-*papA*.

V. natriegens Δ*vnp12* Δ*aceE* Δ*papA* behaved very similarly to *V. natriegens* Δ*vnp12* Δ*aceE* and no significant differences were observed. The strain grew with 0.87 ± 0.08 h^{-1} to a CDW_{max} of 5.90 ± 0.42 g_X L^{-1}. During the exponential growth phase, a $Y_{X/S}$ of 0.28 ± 0.08 g_X g_{Glc}^{-1} and a q_S of 3.34 ± 0.83 g_{Glc} g_X^{-1} h^{-1} were obtained. A maximal titer of 35.75 ± 4.31 g pyruvate L^{-1} was reached with a Q_P of 3.58 ± 0.43 g_{Pyr} L^{-1} h^{-1}, and a $Y_{P/S}$ of 0.97 ± 0.19 mol_{Pyr} mol_{Glc}^{-1} was observed. After 12 h, the C-balance was closed to 54 ± 9%. Evaluation of the HPLC peak areas of parapyruvate showed comparable results for *V. natriegens* Δ*vnp12* Δ*aceE* and *V. natriegens* Δ*vnp12* Δ*aceE* Δ*papA* (data not shown).

The growth of *V. natriegens* Δ*vnp12* Δ*aceE* pekEx-*papA* was not as reproducible or as fast as it was observed for all other pyruvate producer strains. It grew with a reduced μ of 0.46 ± 0.06 h^{-1} to a CDW_{max} of 5.67 ± 1.66 g_X L^{-1}. The q_S was significantly reduced to 2.06 ± 0.22 g_{Glc} g_X^{-1} h^{-1}, but a similar $Y_{X/S}$ of 0.23 ± 0.06 g_X g_{Glc}^{-1} was obtained compared to *V. natriegens* Δ*vnp12* Δ*aceE* Δ*papA*. After 15 h, the titer was reduced by 43% to 20.06 ± 7.53 g pyruvate L^{-1}. Furthermore, a decreased Q_P of 1.34 ± 0.55 g_{Pyr} L^{-1} h^{-1} and a $Y_{P/S}$ of 0.64 ± 0.16 mol_{Pyr} mol_{Glc}^{-1} were measured. Only 52 ± 9% of the carbon could be recovered and larger peak areas for parapyruvate were observed in comparison to the other two producer strains.

4. Discussion

4.1. Characterization of *V. natriegens* wildtype

4.1.1. **Batch process**

During batch cultivations in bioreactors containing minimal medium, *V. natriegens* achieved a remarkably high growth rate of $1.68 \pm 0.01\ h^{-1}$ together with a high glucose consumption rate of $3.66 \pm 0.02\ g_S\ g_X\ h^{-1}$ and yielded $0.46 \pm 0.01\ g_X\ g_S^{-1}$. These results are consistent with previously published data (Hoffart *et al.*, 2017; Long *et al.*, 2017). A CDW_{max} of $4.30 \pm 0.14\ g_X\ L^{-1}$ was achieved, which is about 40% higher than in shaking flask cultures. In contrast to the latter, glucose was depleted, lactate formation was absent, and pyruvate formation was significantly reduced from 1.97 ± 0.16 g L^{-1} to 0.26 ± 0.19 g L^{-1}. These byproducts indicate an insufficient oxygen supply, which could be the case for higher CDW in shaking flasks. *V. natriegens* performs a mixed acid fermentation, resulting in a decrease of the pH. Due to its intolerance of low pH, it is likely that this caused the cessation of biomass formation and glucose consumption (Payne *et al.*, 1961; Hoffart *et al.*, 2017). During the batch process, *V. natriegens* exhibited an acetate overflow and secreted 1.89 ± 0.01 g acetate L^{-1} from 10 g glucose L^{-1} into the medium. This is in the same range as reported for *E. coli*, which secretes 10 – 30% acetate from glucose (Farmer and Liao, 1997).

The minimal medium used for the cultivation of *V. natriegens* contains sodium chloride, as sodium is required for proliferation. The usage of sodium chloride might be disadvantageous due to its ability to cause corrosion on metal surfaces in bioreactors and its possible negative effect on product-broth separation with ion exchange approaches during downstream processing (Junker, 2009; Hoffart *et al.*, 2017). Thus, a minimal medium was developed, in which sodium chloride was substituted with sodium sulfate. Byproduct formation and biomass yield were not affected by the medium change. The growth rate was reduced by 17%, and a corresponding decrease of the glucose uptake rate was observed as well. The reduction in growth is slightly enhanced compared to a value reported by Hoffart *et al.* (2017), who were able to maintain 91% of the original growth rate in a medium containing only trace amounts of chloride. However, despite this reduction, the growth rate of *V. natriegens* still outperforms other industrially relevant organisms such as *E. coli*, *C. glutamicum*, *B. subtilis*, and *S. cerevisiae* (Sauer et al., 1996; Gombert et al., 2001; Blombach et al., 2013; Gonzalez et al., 2017; Hoffart et al., 2017; Long et al., 2017). No significant differences were observed regarding byproduct spectrum and concentration except for acetate. Approximately 20% less acetate was detected in the VN minimal medium. This could also be due to the effect that acetate was taken up again when glucose was depleted after 4 h, which occurred one hour earlier than in the chloride-free cultivation.

4.1.2. **Development of a fed-batch process**

High productivities are crucial for microbial processes to be cost-efficient and competitive. To achieve sufficient space-time yields, high cell densities are usually required and fed-batch processes are therefore commonly used (Riesenberg *et al.*, 1991; Riesenberg and Guthke, 1999). In addition, this mode of operation has the advantage that the growth rate can be regulated below a critical value to prevent the formation of byproducts such as acetate (Lee *et al.*, 1999). Since acetate secretion has been observed in batch cultures with *V. natriegens*, a glucose-limited fed-batch process was performed to determine the critical growth rate at which no acetate formation occurs. At a set growth rate of 0.1 h^{-1}, only 2 g acetate L^{-1} were observed after 21 h and no glucose was detected in the supernatant of the bioreactor broth, whereas glucose accumulation started between 5 and 9.5 h at set growth rates between 0.3 and 0.7 h^{-1}. Furthermore, the secretion of byproducts increased sharply at higher growth rates and acetate began to accumulate, which has also been reported for glucose-limited continuous cultures with *E. coli* growing with critical growth rates between 0.3 and 0.7 h^{-1} (Meyer et al., 1984; Holms, 1996; Valgepea et al., 2010; Basan et al., 2015). However, pyruvate has also been detected together with small amounts of succinate and lactate. The formation of lactate and succinate mainly occurs as a result of a mixed acid fermentation under oxygen limitation, although it has also been reported for aerobic HCDC with *V. natriegens* (Hoffart et al., 2017, Thiele *et al.*, 2021). Since only small amounts were detected, this may also be caused by oxygen-poor regions within the bioreactor. At a growth rate of 0.1 h^{-1}, the C-balance was closed to 83%. However, this value decreased to 55 – 66% at higher growth rates. Thus, a large fraction of the carbon derived from glucose is not utilized for the intended formation of biomass, but for unknown byproducts. Later on, it was found that *V. natriegens* is an EPS producer, which could explain this observation, as EPS formation is generally promoted by higher carbon availability (Freitas *et al.*, 2011).

In this first fed-batch process, V1, the set growth rate deviated from the actual measured growth rate, but this could be remedied by including the glucose requirement for the cell maintenance in the calculation of the feeding rate (Equation 1 – 3). Subsequently, fed-batch fermentations were performed at a set growth rate of 0.1 h^{-1} and changes of the media and feed were tested to improve biomass formation. Based on the elemental biomass composition of *V. natriegens* ($C_{1.000}H_{1.770}O_{0.607}N_{0.153}P_{0.015}S_{0.003}$, carbon content of 45% (w w^{-1})) (Erian *et al.*, 2020), potential limitations were calculated. The VN minimal medium contained an excess of sulfur and no limitations were expected. The supply of phosphorus should be adequate up to 23 g_X L^{-1}, but the nitrogen provision could be limiting at CDW above 13 g_X L^{-1}. However, ammonia water was used for titration and the influx of base should be sufficient to add enough nitrogen for further growth, thus limitations are unlikely. Nevertheless, concentrated VN minimal medium has been tested, but no significant improvement was observed. The supplementation with yeast extract, different types and concentrations of TCE, and a

combination of iodine, Fe(III) citrate together with an increased magnesium concentration were tested as well. None of these alterations had a significant effect except the combined addition of iodine, magnesium, and Fe(III) citrate, which doubled the CDW_{max} compared to a control process without these supplements. Subsequent fermentations indicated that iodine did not contribute to the increased CDW, but rather the synergy of the other two compounds. A beneficial effect of magnesium supplementation, especially in combination with the chelating agent citrate, has already been reported (Linton *et al.*, 1977; Biener *et al.*, 2023). Moreover, the addition of a third Rushton impeller could enhance the OTR_{max} by 18%.

A positive effect of a lower cultivation temperature has been reported (Thiele *et al.*, 2021) and was therefore tested as well. However, lowering the temperature to 30 °C was not found to be beneficial. No significant differences in biomass formation or acetate secretion were observed, and more lactate, succinate, and especially pyruvate were formed at a reduced temperature. The latter accumulated to 8 g pyruvate L^{-1} at the end of the process, which might indicate that the oxygen supply was not sufficient, although the DO never dropped below 20% (Thoma and Blombach, 2021). Due to the lower temperature, there might be some rate-limiting enzymatic reactions for anaplerotic reactions or for the decarboxylation of pyruvate to acetyl-CoA, leading to the accumulation of pyruvate.

Based on a publication by Thiele *et al.* (2021) in which a CDW of 55 g_X L^{-1} was achieved, the VN medium was slightly modified and a multi-concentrated VN medium was fed. In a separate process, another feeding strategy was tested that combined exponential feeding with a set growth rate of 0.5 h^{-1} followed by constant feeding. Neither approach resulted in a higher CDW. On the contrary, only 12.9 g_X L^{-1} were obtained after 22 h when concentrated medium was fed. Possibly, a compound of the feed had a limiting effect on cell growth, which could be ammonium, as it is already known for its inhibitory effect on growth at higher concentrations (Thompson *et al.*, 1985). The combination of exponential and constant feeding resulted in a higher CDW_{max} of 23.4 g_X L^{-1} within only 12 h. However, the rapid formation of biomass led to a huge oxygen demand that could not be satisfied and the DO dropped sharply to 1 – 2% around 7 h. Therefore, this approach is only suitable when oxygen-enriched air or pure oxygen is used for aeration. In addition, a significant increase in byproducts was measured, particularly for succinate and acetate, and therefore this approach was not pursued further.

Overall, the best approach to obtain a high CDW with nearly eliminated byproduct formation for *V. natriegens* wt was to limit the growth rate to 0.1 h^{-1} and to install a third Rushton impeller to enable higher OTRs. Furthermore, the addition of 0.1 g Fe(III) citrate × H_2O and 1.2 g $MgSO_4$ × 7 H_2O L^{-1} showed an improved biomass formation. The final process yielded 28.40 ± 0.75 g_X L^{-1}. After 24 h, the DO dropped below 5% and first acetate and subsequently pyruvate accumulated to 13.78 ± 0.6 g L^{-1} and 10.77 ± 1.1 g L^{-1}, respectively. During the process, the viscosity of the bioreactor broth increased to 3,344 ± 903 mPa s (at a shear rate of 0.1 s^{-1}), which might limit the OTR, and thus oxygen availability, leading to a decrease in biomass. Although biomass formation was improved, the CDW is still quite low

in comparison with other microorganisms such as *E. coli* or *B. subtilis*, for which biomass concentrations of over 100 g_X L^{-1} have been easily exceeded (Riesenberg and Guthke, 1999), and even a value of 190 g_X L^{-1} has been reported for a HCDC of *E. coli* using a membrane dialysis bioreactor (Nakano *et al.*, 1997). However, in a setup similar to the one used in this work, CDWs around 100 g_X L^{-1} have been reported. Kim et al. (2004) used a combination of an exponential feeding in conjunction with pH measurements to control the growth rate of *E. coli* at 0.1 h^{-1} during a fed-batch process with minimal medium. A final CDW of 101 g_X L^{-1} was achieved. Riesenberg et al. (1991) controlled the growth rate at 0.11 h^{-1} for HCDC with *E. coli* by adjusting the glucose supply as well as the agitation rate and reached 110 g_X L^{-1} using minimal medium.

4.2. EPS formation

A glucose-limited fed-batch process was established for *V. natriegens* wt to achieve high biomass concentrations. However, this was accompanied by an 800-fold increase in viscosity and EPS secretion. The secretion occurred throughout the process, indicating that the formation is initiated by a regulatory mechanism, such as quorum sensing, rather than by an overflow metabolism, since glucose supply was limited. The genome of *V. natriegens* contains essential components of the quorum sensing apparatus, such as regulators, sensor kinases for signalling molecules, and enzymes for the synthesis of AI (Ball *et al.*, 2017; Schulze *et al.*, 2023). Several targets were chosen to overcome EPS formation and the associated increase in viscosity. In shaking flask experiments, all EPS mutant strains showed the same growth phenotype as the wt strain, with the exception of the *wbfF* deletion strain, which grew slower with a growth rate of 1.46 ± 0.04 h^{-1} and exhibited a prolonged lag-phase. Thus, the feeding phase in fed-batch fermentations was initiated half an hour later compared to the start of feeding for the other strains. In subsequent glucose-limited fed-batch processes, the growth kinetics and the EPS production of *V. natriegens* Δ*cpsR*, *V. natriegens* Δ*sypK,* and *V. natriegens* Δ*luxS* were characterized. All strains grew wt-like to CDWs around 30 g_X L^{-1}. After 31 h, the EPS concentration was determined. The wt strain secreted 367 mg L^{-1}, followed by the *luxS* knockout strain, which produced 405 mg EPS L^{-1}. LuxS is the only annotated AI synthase in *V. natriegens*. However, it is unlikely that there are no other AI-synthases present, as quorum sensing systems typically consist of multiple AI-synthases (Waters and Bassler, 2005; Ball *et al.*, 2017). Furthermore, the gene annotation showed a high level of conformity with the quorum sensing system of *V. harveyi*, which includes the enzymes LuxM and CqsA as well. In addition, the corresponding membrane-bound receptors LuxN and CqsS are also annotated in *V. natriegens*. Thus, it is possible that the inactivation of LuxS does not reduce EPS formation, as it is compensated by other synthases.

The second target to abolish EPS formation was *sypK*, which encodes for an oligosaccharide translocase, and it has already been shown in *V. diabolicus* that EPS formation can be significantly reduced by the knockout of this gene (Goudenège *et al.*, 2014). In this work, the deletion resulted in a strong increase in EPS production by a factor of 2.5. In *V. fischeri*, SypK has been shown to contribute to biofilm formation and to interact with the quorum sensing pathway through LuxQ. The overexpression of *sypK* enabled the activation of small regulatory RNA Qrr1, which is required for the quorum sensing signaling-cascade to transduce AI information into a cellular response. This interaction is sufficient to affect cellular behaviors, such as bioluminescence and motility (Miyashiro *et al.*, 2014). Possibly, *sypK* in *V. natriegens* is involved in complex regulatory pathways of the quorum sensing apparatus, as it is the case in *V. fischeri*, leading to this unexpected increase in EPS. *V. natriegens* Δ*cpsR* was the only strain that produced less EPS (292 mg EPS L^{-1}) than the wt strain, which was reflected by a 36% higher OTR.

The monomeric composition of the EPS secreted by *V. natriegens* Δ*cpsR* showed a reduced glucose and galactose content but an elevated rhamnose content compared to the wt. No significant differences were found for *V. natriegens* Δ*luxS*. The EPS of *V. natriegens* Δ*sypK* exhibited an increased galactose percentage but a decrease in fucose, glucosamine, and ribose. These changed could be due to the production of different EPS or the simultaneous formation of multiple EPS by one or more strains, which cannot be distinguished by the HT-PMP method. Since the deletion of the transcriptional biofilm regulator CpsR was the only successful target showing a reduced EPS formation, it was further investigated in subsequent fermentations along with additional EPS mutant strains.

During the exponential growth phase in fed-batch processes, the strains *V. natriegens* Δ*wbfF*, *V. natriegens* Δ*cps*, *V. natriegens* Δ*syp* Δ*cps*, and *V. natriegens* Δ*cpsR* grew wt-like with a growth rate of about 1.60 h^{-1}, whereas *V. natriegens* Δ*syp* Δ*cps* exhibited a slightly reduced growth rate of 1.52 ± 0.08 h^{-1}. At the end of the process, the CDW started to decrease, while glucose and byproducts accumulated. The wt strain secreted 2 – 3 times more acetate and at least 4 times more pyruvate. Small amounts of succinate (≤ 0.5 g L^{-1}) were detected in all cultivations and the EPS strains additionally secreted lactate (≤ 0.7 g L^{-1}).

The deletion of the EPS gene cluster *cps* resulted in a significantly reduced EPS concentration, but still 82 ± 14 mg EPS L^{-1} were formed. The additional deletion of the second EPS gene cluster *syp* neither reduced EPS production nor changed the composition. As before, inactivation of *cpsR* did not abolish EPS formation and 176 ± 8 mg EPS L^{-1} were still secreted. The composition of the EPS was altered compared to the wt strain, indicating that CpsR is involved in the EPS biosynthesis. Nevertheless, a 1000-fold decrease of the viscosity was measured. The deletion of *wbfF* even doubled the amount of EPS. These results suggest that other pathways also contribute to the EPS synthesis, which is likely since genomic analysis revealed that 0.7% of the genome are genes associated with EPS formation (Schulze *et al.*, 2023).

The monomeric composition of the EPS formed by *V. natriegens* differs from previously published EPS produced by other *Vibrio* species (Casillo *et al.*, 2018). *Vibrio furnissii* VB0S3 (Bramhachari *et al.*, 2007) and *V. harveyi* VB23 (Bramhachari and Dubey, 2006) produce an acidic EPS with emulsifying properties consisting of galactose, glucose, rhamnose, fucose, mannose, ribose, arabinose, and xylose. *V. diabolicus* secretes the hyaluronic acid-like EPS HE800, which consists of equal parts of uronic acids and amino sugars as repeating units (Rougeaux *et al.*, 1999; Zanchetta *et al.*, 2003). Another valuable EPS formed by *V. alginolyticus* (CNCM I-4994) consists of a tetrasaccharide repetition unit, composing of D-galacturonic acid and N-acetyl-D-glucosamine, and is decorated with alanine and serine, which are likely responsible for the biological properties (Drouillard et al., 2015, 2018). In the case of *V. natriegens*, the monomeric backbone of the EPS consisted of glucose, galactose, galacturonic acid, rhamnose, fucose, glucosamine, and ribose. Furthermore, the composition of the EPS, built from these monomers, differed not only from other *Vibrio* species, but also among the individual EPS mutant strains.

Due to their great chemical diversity, EPS have a huge potential for industrial applications in many different sectors, and the variability of EPS produced by *Vibrio* species sparks interest for new properties and applications (Martin-Pastor *et al.*, 2019). Therefore, it is crucial to analyze the physicochemical and biological properties to evaluate their potential. However, industrial production is challenged by low titers and high production costs, and only single to double digit titers in the gram range have been achieved (Finore *et al.*, 2014; García *et al.*, 2022). Titers of 28 mg L^{-1} and 137 mg L^{-1} have been reported for the EPS of *V. harveyi* VB23 and *V. furnissii* VB0S3, respectively (Bramhachari and Dubey, 2006; Bramhachari *et al.*, 2007). Higher concentrations around 1 g L^{-1} were obtained for HE800 produced by *V. diabolicus* CNCM I-1629 (Delbarre-Ladrat *et al.*, 2022) and the EPS secreted by *V. alginolyticus* (Muralidharan and Jayachandran, 2003), while a titer of around 3 g L^{-1} was obtained for MO245 produced by *Vibrio* species from Moorea Island (Martin-Pastor *et al.*, 2019). In this work, *V. natriegens* Δ*sypK* secreted 925 mg EPS L^{-1}, which renders this bacterium a promising host for targeted EPS production in future studies.

Rheological measurements were conducted during fed-batch fermentations to monitor viscosity changes of the bioreactor broth. No clear correlation was found between EPS formation and viscosity. For *V. natriegens* wt, the viscosity increased with rising EPS concentration. However, for *V. natriegens* Δ*wbfF*, the viscosity peaked at 22 h and decreased again although the EPS concentration was still increasing, indicating a dynamic change of the EPS composition or the secretion of polysaccharide-degrading enzymes. No viscosity changes occurred in the bioreactors with *V. natriegens* Δ*cpsR, V. natriegens* Δ*cps,* and *V. natriegens* Δ*syp* Δ*cps*, although all strains still secreted EPS. Besides EPS, other high molecular weight molecules such as proteins, nucleic acids and lipids, which are common parts of biofilms (Wingender *et al.*, 1999), can affect the rheology of the bioreactor broth. Dong *et al.* (2016) have already identified these extracellular polymeric substances for *V. natriegens* in a biofilm formed on steel in seawater. However, no significant amounts of proteins could

be detected in the planktonic cultures of *V. natriegens* using a Bradford assay with bovine serum albumin as standard. The presence of nucleic acids was tested via photometric analysis, but no clear signal was obtained (data not shown). The consistently low viscosity during cultivations with *V. natriegens* Δ*cpsR* and *V. natriegens* Δ*cps* was reflected by a 22 – 25% higher OTR compared to cultivation with the wt strain. However, the improved OTR did not result in further biomass formation, indicating other limitations besides oxygen.

Analysis of the transcriptomic data revealed that the deletion of the *cps* cluster had minimal effect on the expression of the other genes. Therefore, the deletion of a single gene cluster was already sufficient to overcome alterations of the viscosity during fed-batch processes without further interfering with the bacterial metabolism, and thus *cps* is an excellent target to facilitate bioprocesses with *V. natriegens*. On the contrary, the deletion of *cpsR* resulted in the downregulation of a variety of genes. In particular, genes associated with flagellar and pilus synthesis, which are required during the initial stage of biofilm formation (Moorthy and Watnick, 2004), were affected. For *V. natriegens* Δ*cpsR*, MSHA proteins that belong to type IV pili were particularly affected. Type IV pili bind to abiotic and biotic surfaces, such as bacterial and host cells (Souza Santos et al., 2015). For *V. cholerae*, flagella and MSHA pili have been shown to be used synergistically to facilitate surface selection and attachment (Utada et al., 2014), and initial attachment of *V. parahaemolyticus* to surfaces is enabled by MSHA pili as well (Shime-Hattori et al., 2006). MSHA pili appear to be especially important for the attachment of *V. cholerae* to abiotic surfaces, as MSHA-deficient strains of *V. cholerae* E1 Tor have lost their ability to form biofilms on such surfaces (Watnick et al., 1999). The absence of flagella in mutants of *E. coli* and *V. vulnificus* also resulted in a reduced bacterial adhesion (Lee et al., 2004; Friedlander et al., 2013). In conclusion, CpsR appears to be an important regulator responsible for cell motility and attachment and might reduce the ability of *V. natriegens* to form biofilms.

4.3. Succinate production

In shaking flask cultivations, both succinate producers showed a 12 – 13% reduced growth rate compared to the wt. For *V. natriegens* Succ1, no significant differences were measured for the glucose consumption rate or the biomass yield. A reduced glucose uptake rate of 2.61 ± 0.34 $g_S\ g_X^{-1}\ h^{-1}$ was observed for *V. natriegens* Succ1 Δ*ackA*. Only minor differences in the spectrum and concentrations of byproducts were found for both strains compared to the wt. The succinate producers also formed low amounts of ethanol (≤ 0.11 g L^{-1}) and secreted about 1.5 times more pyruvate.

Subsequently, the strains were tested under anaerobic conditions in a small scale of 50 mL. Both strains performed similarly and produced 4 – 5 g succinate L^{-1}, which was more than twice the amount compared to the wt. The highest yield of 1.48 ± 0.06 $mol_{Suc}\ mol_{Glc}^{-1}$ was achieved by

V. natriegens Succ1 Δ*ackA.* This value already corresponds to 87% of the theoretical maximum. The additional deletion of *ackA* reduced acetate formation by about half. Thoma *et al.* (2021) reported that the deletion of *ackA* had no effect on acetate production, therefore more data needs to be collected to determine the most suitable strain.

First attempts were made to upscale the process in a bioreactor. However, no noteworthy amount of succinate was produced. Succinate production was only possible when the carbon supply for the carboxylation of PEP and pyruvate was changed from CO_2 gassing to the supplementation with HCO_3^-. CO_2 gassing is a common approach to provide carbon for anaplerotic carboxylation reactions (Table 1), and it is not clear why *V. natriegens* did not tolerate it. Valley (1928) reviewed that acid-sensitive microorganisms, such as *V. cholerae* are easily inhibited or eliminated by CO_2 gassing. This may be the case for *V. natriegens*, and possibly, CO_2-induced acidification of the medium creates microenvironments with an unfavorable pH for growth and production. In addition, CO_2 can diffuse unhindered through the cell membrane and accumulate there, leading to an increased permeability and fluidity with potentially lethal consequences for the bacterial cell (Blombach and Takors, 2015).

In subsequent fermentations, it was observed that the implementation of a microaerobic preculture could significantly enhance succinate production, and its importance for cell viability and productivity in succinate production processes has already been reported for *E. coli* (Martínez *et al.*, 2010; Zhu *et al.*, 2011). In the final succinate process, *V. natriegens* Succ1 produced 60.4 ± 0.90 g succinate L^{-1}. A high overall volumetric productivity of 8.63 ± 0.13 g_{Suc} L^{-1} h^{-1} was obtained, and a maximum productivity of 20.82 ± 0.22 g_{Suc} L^{-1} h^{-1} was measured at the beginning of the process, which places this strain among the best performing succinate producers to date. In addition, the process was performed using VN minimal medium and did not rely on expensive complex media, vitamins, or amino acids, in contrast to many other studies (Ahn *et al.*, 2016; Lee *et al.*, 2019; Ahn *et al.*, 2020; Dai *et al.*, 2020; Yang *et al.*, 2020, Table 1). However, higher titers have been reported for various organisms, and hence this remains to be addressed for *V. natriegens* Succ1. Furthermore, the succinate yield was reduced by 15% in comparison with the small-scale production in falcon tubes, and only 62% of the carbon were recovered at the end of the process. One possibility could be a re-channeling of carbon caused by quorum sensing, since the bioreactors were inoculated with high cell densities in contrast to the falcon tubes. Thus, future studies are needed that address the physiological response of *V. natriegens* in a bioreactor environment, especially at higher cell concentrations.

Finally, a triple-phase fermentation was performed to combine aerobic growth, microaerobic transition and anaerobic production phase in a single vessel. The transition is challenging, since enzymes responsible for the biotransformation during the production phase are often expressed during the growth phase and remain active throughout the process. Thus, the productivity of the cells is highly dependent on the physiological state at the time of transition (Vemuri *et al.*, 2002). As intended, *V. natriegens* Succ1 started to form succinate when microaerobic conditions were reached. However, the titer remained low.

During the microaerobic phase, 6.81 ± 1.44 g succinate L^{-1}, but also 8.13 ± 4.84 g pyruvate L^{-1} were formed. Thereafter, during the anaerobic phase, the succinate production rate decreased and only a final titer of 9.98 ± 3.63 g succinate L^{-1} was obtained after 30 h of process. Pyruvate frequently accumulates when the oxygen supply is insufficient (Thoma and Blombach, 2021), indicating that the cells have not adapted well enough to the microaerobic conditions within the given time. Furthermore, the aeration rate, and therefore, the oxygen level in the bioreactor during the aerobic growth phase can influence the metabolic flux, and thus the performance during the anaerobic production rate. Martínez *et al.* (2010) investigated the metabolic impact of different aeration rates on anaerobic succinate production using *E. coli* SB550MG (pHL413) and discovered that pyruvate accumulated, while the succinate yield and the productivity decreased during the anaerobic production phase when a higher aeration rate was applied during the biomass formation phase. Hence, the process parameters have to be adjusted to allow the cells to adapt to anaerobic conditions and to avoid the formation of byproducts and impaired succinate production.

During the cultivation of *V. natriegens* Succ1, the viscosity increased under anaerobic resting cell conditions. Consequently, *cpsR* and *cps* were deleted and no viscosity changes occurred anymore. Furthermore, the $Y_{P/S}$ was increased to 1.4 mol_{Suc} mol_{Glc}^{-1}, which corresponds to 81% of the theoretical maximum. In addition, more carbon could be recovered at the end of the process (about 80%). This increase cannot be explained solely by the excess carbon that is no longer channeled towards EPS. Since EPS synthesis requires a considerable amount of energy (Jarman and Pace, 1984; Wolfaardt *et al.*, 1999), the reduction of EPS might improve ATP availability. Possibly, the deletion of *cpsR* and *cps* in *V. natriegens* Succ1 might lead to a beneficial rerouting of the metabolic flux distribution, and thus resulted in an improved carboxylation towards oxaloacetate.

When the succinate process was repeated with *V. natriegens* Succ1, only 45 g succinate L^{-1} were obtained instead of 60 g succinate L^{-1}, and in both cases a $Y_{P/S}$ of 1.1 mol_{Suc} mol_{Glc}^{-1} was obtained. It is not clear why the production of succinate stopped. However, this indicates a change in cellular metabolism. Possibly, the cells entered the VBNC state. Cells were streaked on agar plates and incubated O/N, but no colonies were formed, showing the loss of culturability. The genetic regulation of *Vibrio* species entering the VBNC state is not well understood yet, but VBNC is often mediated by quorum sensing (Li and Zhao, 2020), and a connection between the two has already been observed for *V. vulnificus* and *V. cholerae* (Ayrapetyan *et al.*, 2014; Wu *et al.*, 2020). Potentially, the VBNC state mediated by quorum sensing is the cause for the loss of production and culturability, and future work needs to investigate the relationships between quorum sensing, biofilm formation, and productivity in *V. natriegens*. Microscopic observations of *V. natriegens* showed a decrease in cell size at the end of the succinate production process, which has also been reported to be a characteristic of cells in the VBNC state (Oliver, 2005; Du *et al.*, 2007). However, this phenomenon could also be an indicator of cellular stress and not necessarily of a VBNC state, and more suitable methods, such as live-dead

staining, need to be applied. In addition, stress itself could be a possible cause for cells to enter the dormant state. It has been shown that oxidative stress, especially hydrogen peroxide, as well as the accumulation of reactive oxygen species (ROS) in liquid media led to a cold-induced loss of culturability (CILC) in *V. natriegens* (Weinstock et al., 2016; Wang et al., 2023).

4.4. Pyruvate production

V. natriegens has been engineered for the production of pyruvate. Pyruvate is the end product of glycolysis, and to accumulate the desired product, catabolic pathways must be eliminated. Therefore, the gene *aceE*, which encodes for the E1 subunit of the PDHC, was deleted to prevent further conversion to acetyl-CoA. However, this leads to a disruption of the link between glycolysis and TCA, and thus biomass formation is no longer possible. The addition of acetate can provide an alternative pathway for the production of acetyl-CoA, as it can be converted to acetyl-CoA both directly by AcS and via acetylphosphate by the enzymes AckA and Pta (Figure 3). *V. natriegens* Δ*aceE* secreted 22.52 ± 2.01 g pyruvate L^{-1} during a batch process in minimal medium supplemented with glucose and acetate. A volumetric productivity of 2.05 ± 0.15 g_{Pyr} L^{-1} h^{-1} together with a product yield of 1.50 ± 0.26 mol_{Pyr} mol_{Glc}^{-1} were obtained.

An increase of pyruvate was reported for *V. natriegens*, which lacks the prophage-regions VNP1 and VNP2 (Pfeifer *et al.*, 2019), and consequently these gene clusters were removed as well. However, no significant improvement in pyruvate production was observed for *V. natriegens* Δ*aceE* Δ*vnp12* compared to *V. natriegens* Δ*aceE* for both shaking flasks and bioreactor cultivation. Wu *et al.* (2023) did not observe any increase in pyruvate secretion using a prophage region deficient strain either, and argued that this could be due to differences in media composition or cultivation conditions. Pfeifer *et al.* (2019) cultivated the strains at a lower temperature (30 °C) and shaking frequency (120 rpm) in shaking flasks, and both parameters are known to affect pyruvate formation. In particular, the oxygen content, which is affected by the shaking frequency, has been reported as a major factor to be considered for pyruvate production (Maleki and Eiteman, 2017; Yuan *et al.*, 2022). Nevertheless, the following processes were conducted with *V. natriegens* Δ*aceE* Δ*vnp12*, as the CDW did not decline as much at the end of a batch process compared to *V. natriegens* Δ*aceE*.

In batch processes, the initially provided acetate was depleted within 6 – 7 h. To further improve the supply, fed-batch processes were carried out with an acetate feed at different concentrations between 2 and 16 mM_{Ace} h^{-1}, which were started shortly before acetate depletion. A feed was beneficial even at a low concentration of 2 mM_{Ace} h^{-1} and the pyruvate titer was increased by around 20%. A positive correlation between increasing feed concentrations and the glucose uptake rate was observed, and a value of 3.9 g_{Glc} g_X^{-1} h^{-1} was achieved with the 16 mM_{Ace} h^{-1} feed, which was 50% higher in comparison

with a process without feed. The acetate concentration of the feed far exceeds the maintenance requirements for acetate. Based on the glucose maintenance (0.063 g_{Glc} g_X^{-1} h^{-1}) determined by Linton et al. (1977) and the CDW of 3.4 g_X L^{-1} obtained in a pyruvate production process without acetate feeding (PyrC_R1, Table 20), a feed of 2.4 $mmol_{Ace}$ L h^{-1} is required to meet the demand for acetate maintenance. The observation that higher feed concentrations resulted in increased glucose uptake rates indicates a higher glycolytic flux, possibly caused by an increased ATP consumption. The conversion of acetate to acetyl-CoA is catalyzed by the AcS and by the AckA and Pta, and both pathways require ATP (Figure 3). This results in a decreased overall availability of ATP, which could be compensated by a higher rate of glycolysis. Reducing the formation of ATP is a common strategy to enhance the metabolization of glucose (Zhu *et al.*, 2008; Maleki and Eiteman, 2017).

In addition to an elevated glucose uptake rate, acetate accumulation was also increased at higher feed concentrations, and around 12 g acetate L^{-1} were observed for the process with the 16 mM_{Ace} h^{-1} feed. Only half of the amount accumulated when a feed with 8 mM_{Ace} h^{-1} was applied, and the highest pyruvate titer was obtained. The CDW_{max} was reached after 6 h in all bioreactors when the initially given 2 g acetate L^{-1} were almost exhausted. It is not clear why biomass formation stopped, since acetate was provided throughout the process, but it seems that once the concentration of acetate falls below a critical value, a change in cellular metabolism is triggered and the cells enter the stationary phase. When the 8 mM_{Ace} h^{-1} feed was started at the beginning of the process, the CDW increased from 4 to 6 g_X L^{-1}, since more acetate was provided during the initial growth phase (PyrE, Table 20). Possibly, the cellular response to a low acetate concentration enables a great opportunity to adjust the CDW_{max} as desired via the initially supplied acetate.

The optimal provision of acetate for the acetate auxotrophic strain *V. natriegens* Δ*aceE* Δ*vnp12* was found to be a feed of 8 mM_{Ace} h^{-1} started at the beginning of the process. The achieved titer and volumetric productivity were approximately doubled compared to a process without feed. Another significant improvement of the application of an acetate feed was an elevated glucose uptake rate and overall glucose consumption. In the absence of a feed, 61.49 ± 1.80 g glucose L^{-1} were left when the maximum pyruvate concentration was reached, whereas only 14.05 ± 7.07 g glucose L^{-1} remained when a feed was applied. The early termination of glucose uptake and the subsequent cessation of production has already been observed in a succinate production process. The reasons for this are still unclear, but it is suspected that quorum sensing and the onset of the VBNC state could be possible causes. The addition of an acetate feed prolonged glucose consumption and pyruvate production, and furthermore, an outstandingly high glucose uptake rate of 3.46 ± 0.16 g_{Glc} g_X^{-1} h^{-1} was achieved with non-growing cells, which is about 80% higher as for *E. coli* grown at μ_{max} (Varma and Palsson, 1994). This high glucose uptake rate of *V. natriegens* surpasses typical industrial microorganisms and provides an excellent basis for achieving cost-efficient processes (Hoffart *et al.*, 2017). Furthermore, the high

glucose consumption is the perfect basis for low-cell density processes, as it enables high production rates, and thus high volumetric productivities.

Typically, high biomass concentrations are necessary to achieve high productivities, which wastes the carbon source as it is converted into the catalyst rather than the product (Sauer *et al.*, 2008). In addition, the accumulation of large amounts of biomass requires sterilization and disposal at the end of the process, thus adding to the production costs. In the pyruvate production process with *V. natriegens* Δ*aceE* Δ*vnp12*, a high volumetric productivity of 4.10 ± 0.18 g_{Pyr} L^{-1} h^{-1} was achieved with the low amount of 6.58 ± 0.42 g_X L^{-1}, placing this bacterium among one of the best pyruvate producers (Li *et al.*, 2001a; Maleki and Eiteman, 2017; Yuan *et al.*, 2022). However, the final titer (40.97 ± 1.83 g_{Pyr} L^{-1}) is not yet sufficient, and higher concentrations around 100 g pyruvate L^{-1} have been reported, especially for yeasts (Yuan *et al.*, 2022). It has been indicated that an extracellular concentration around 45 g pyruvate L^{-1} might inhibit further pyruvate formation, which is in the range of the titer achieved in this work (Zelić *et al.*, 2003; Zelić *et al.*, 2004). Therefore, processes with on-line product recovery would be ideal, as well as the implementation of continuous or repetitive fed-batch processes to investigate possible inhibitions. Zelić *et al.* (2004) tested different process strategies and obtained promising results for the *E. coli* strain YYC202 *ldhA::Kan*. A high productivity of 6.0 g_{Pyr} L^{-1} h^{-1} along with a remarkable yield of 1.78 mol_{Pyr} mol_{Glc}^{-1} were achieved by using a repetitive fed-batch process. A high (calculated) pyruvate titer of 79 g L^{-1} was obtained when an electrodialysis separation unit was used for in situ product recovery.

The product yield (1.05 ± 0.04 mol_{Pyr} mol_{Glc}^{-1}) obtained in this work for the pyruvate process with feed was about half of the theoretical maximum, which means that a high proportion of carbon from glucose is not sufficiently channeled into the desired product. However, hardly any byproducts were observed at the end of the process, although a large amount of carbon could not be recovered. When the pyruvate titer peaked at 10 h, only 74 ± 5% carbon could be recovered and this value, together with the pyruvate concentration, decreased drastically within the next 2 h to 40 ± 11% and 28.87 ± 8.46 g pyruvate L^{-1}. This indicates that a major part of the missing carbon is derived from pyruvate. Parapyruvate has been identified as an impurity in PA or PA salts, and it is assumed that the missing carbon has been channeled to this compound, which significantly reduces the titer, since two pyruvates are required to form one parapyruvate in an aldol condensation (Montgomery and Webb, 1956; Margolis and Coxon, 1986; Chang *et al.*, 2018). It is not clear whether the formation is driven by a chemical reaction or catalyzed by an enzyme. Parapyruvate formation appears to be promoted by high temperatures and pH values, as well as by ammonium salts (Margolis and Coxon, 1986). Lowering the concentration of the ammonia base from 25 to 10% to avoid local pH peaks during titration did not improve the titer or C-balance, whereas a reduction of the pH to 6.5 resulted in a 98% carbon recovery and an increased yield to 1.40 mol_{Pyr} mol_{Glc}^{-1}. Nevertheless, this strategy is not suitable as *V. natriegens* Δ*aceE* Δ*vnp12* did not tolerate the reduced pH, which significantly affected the growth rate and pyruvate formation. Only

14.6 g pyruvate L^{-1} were secreted within 12 h. Hence, a different approach with varying cultivation temperatures was tested.

At 30 °C, an equal titer of about 41 g pyruvate L^{-1} together with a slightly reduced productivity of 3.74 g_{Pyr} L^{-1} h^{-1} were obtained. The latter is probably caused by a reduced growth rate (0.64 h^{-1}) and the resulting slower biomass formation. The yield was increased to 1.18 mol_{Pyr} mol_{Glc}^{-1} and 78% carbon could be recovered when the pyruvate titer peaked. No significant changes in the pyruvate yield or the C-balance were obtained at 25 °C compared to the reference at 37 °C. Hence, no correlation was found between the cultivation temperature and the carbon recovery. When the temperature was further lowered to 20 °C, *V. natriegens* Δ*aceE* Δ*vnp12* was no longer able to grow. At 25 °C, the highest titer of 52.2 g pyruvate L^{-1} was achieved within 20 h, corresponding to a volumetric productivity of 2.61 g_{Pyr} L^{-1} h^{-1}. However, more data needs to be generated to determine the validity of the titers, since the processes with reduced cultivation temperatures were performed only once and, in particular, data points are missing for the 25 °C cultivation between 12 and 20 h, when the titer was still increasing. Nevertheless, a more promising approach seems to be the adjustment of the pH value and adaptive laboratory evolution experiments could help to accustom *V. natriegens* Δ*aceE* Δ*vnp12* to lower pH values.

In addition to process adjustments, *V. natriegens* Δ*aceE* Δ*vnp12* was further modified to investigate parapyruvate formation. The genome of *V. natriegens* annotates a parapyruvate aldolase and the corresponding gene *papA* was knocked out as well as overexpressed in the pyruvate strain background. No significant differences were observed between *V. natriegens* Δ*vnp12* Δ*aceE* and *V. natriegens* Δ*vnp12* Δ*aceE* Δ*papA* in a fed-batch process, whereas the overexpression of *papA* resulted in significant changes. The growth was impaired, which was reflected by a reduced growth rate, and the biomass curve was not well reproducible. Unusually high standard deviations were obtained for the course of the CDW, which might be due to the inhibitory effect of parapyruvate on the αKGDHC, and thus on the TCA. Further, the glucose uptake rate, the final titer and the volumetric productivity were reduced (2.06 ± 0.22 g_{Glc} g_X^{-1} h^{-1}, 20.06 ± 7.53 g pyruvate L^{-1}, and 1.34 ± 0.55 g_{Pyr} L^{-1} h^{-1}). In addition, the product yield was significantly decreased to 0.64 ± 0.16 mol_{Pyr} mol_{Glc}^{-1} and only 52 ± 9% of the carbon could be recovered when the maximum pyruvate titer was reached, indicating increased parapyruvate formation. This process demonstrates the tremendous burden that parapyruvate production places on cell growth and the negative impact on the overall pyruvate production. However, the additional knockout of *papA* in *V. natriegens* Δ*aceE* Δ*vnp12* had no significant effect, and therefore, the accumulation of parapyruvate at the end of the process along with the decreasing pyruvate concentration is probably caused by high pyruvate titers, leading to a shift in the chemical equilibrium towards parapyruvate, and thus the process needs to be adapted to change the thermodynamics more in favor of pyruvate. In addition, further investigation is needed to exclude the possibility that another aldolase exists that compensates for the *papA* deletion.

5. Conclusion

The aim of this work was the development of processes for anaerobic succinate and aerobic pyruvate production with the promising industrial host *V. natriegens*. First of all, a glucose-limited fed-batch process was established to achieve high biomass concentrations. During the development, EPS secretion accompanied by an increasing viscosity was observed, which negatively affected the operation of the bioreactors. To address this issue, several genes and gene clusters associated with EPS formation were targeted. The deletion of the biofilm regulator *cpsR* and of the EPS cluster *cps* resulted in consistently low viscosities and the strains maintained a wt-like growth phenotype. Transcriptomic data revealed that the deletion of *cps* had only a minimal effect on the expression of other genes, and it is therefore a sufficient target for the construction of future producer strains. However, the additional deletions did not result in an improved biomass formation, although the OTR was increased. Therefore, a first assumed oxygen limitation is unlikely and further process optimizations, such as systematic medium optimization, are required to overcome possible limitations. In addition, quorum sensing regulated biofilm formation or the transition to the VBNC state could also be possible reasons for the cessation of biomass formation, but only little information is available for *V. natriegens* yet. Thus, further studies are required.

Apart from the negative effects of EPS on bioprocesses, the formation of EPS as a main product is also desirable since many EPS exhibit attractive properties that are valuable for a variety of different industrial sectors. Therefore, *V. natriegens* Δ*sypK* would be an ideal candidate due to its high secretion of approximately 1 g EPS L^{-1} under glucose-limited conditions. Further research is required to learn more about the composition and the physicochemical properties of the EPS produced by *V. natriegens* and its EPS mutant strains to evaluate the potential for possible industrial applications.

Next, a two-stage succinate production process was performed to optimize succinate production with *V. natriegens* Succ1. Even under anaerobic conditions, EPS were secreted and the viscosity increased. Again, *cpsR* and *cps* were useful targets to overcome this issue. *V. natriegens* Succ1 Δ*cpsR* achieved a maximum productivity of 19.4 g_{Suc} L^{-1} h^{-1} with a product yield that represents 81% of the theoretical maximum.

Finally, a low-biomass fed-batch process was established for *V. natriegens* Δ*aceE* Δ*vnp12*. By adding an acetate feed, the titer was increased by 85% and the volumetric productivity was increased to 4.1 g_{Pyr} L^{-1} h^{-1}, although only 6.6 g_X L^{-1} were utilized as biocatalyst. In terms of volumetric productivities, the data obtained in this work place *V. natriegens* among the best performing succinate and pyruvate producer strains. However, the titers achieved for succinate (60 g L^{-1}) and pyruvate (41 g L^{-1}) need to be improved. At the beginning of a process, *V. natriegens* shows excellent production rates, which decline rapidly, as reflected, e.g., by the exceptionally high maximum productivity for the succinate

process, which then decreased to 8.6 g_{Suc} L^{-1} h^{-1}. Although this value still exceeds reported volumetric productivities of comparable processes, the cause must be identified in order to enhance the duration of *V. natriegens* and to enable higher titers. Furthermore, this phenomenon occurs in a variety of processes and is not limited to succinate production. *V. natriegens* owns a remarkable amount of genes associated with EPS formation and likely possesses a quorum sensing apparatus similar to *V. harveyi*. In addition, it cannot be excluded that cells undergo transformation to a VBNC state. These processes are all based on complex regulatory mechanisms that are not yet well understood, and it is not clear how they interfere with production processes. Thus, a deeper understanding of all the interrelationships is required to fully exploit the potential of *V. natriegens* as a host for industrial biotechnology.

6. References

Ahn, J.H., Jang, Y.-S., and Lee, S.Y. (2016) Production of succinic acid by metabolically engineered microorganisms. *Current Opinion in Biotechnology* **42:** 54–66.

Ahn, J.H., Seo, H., Park, W., Seok, J., Lee, J.A., Kim, W.J., *et al.* (2020) Enhanced succinic acid production by *Mannheimia* employing optimal malate dehydrogenase. *Nature Communications* **11** (1): 1970.

Albers, E., Larsson, C., Lidén, G., Niklasson, C., and Gustafsson, L. (1996) Influence of the nitrogen source on *Saccharomyces cerevisiae* anaerobic growth and product formation. *Applied and Environmental Microbiology* **62** (9): 3187–3195.

Ali, A., Johnson, J.A., Franco, A.A., Metzger, D.J., Connell, T.D., Morris, J.G., and Sozhamannan, S. (2000) Mutations in the extracellular protein secretion pathway genes (*eps*) interfere with rugose polysaccharide production in and motility of *Vibrio cholerae*. *Infection and Immunity* **68** (4): 1967–1974.

Asakura, H., Ishiwa, A., Arakawa, E., Makino, S., Okada, Y., Yamamoto, S., and Igimi, S. (2007) Gene expression profile of *Vibrio cholerae* in the cold stress-induced viable but non-culturable state. *Environmental Microbiology* **9** (4): 869–879.

Austin, B., Zachary, A., and Colwell, R.R. (1978) Recognition of *Beneckea natriegens* (Payne *et al*.) Baumann *et al*. as a member of the genus *Vibrio*, as previously proposed by Webb and Payne. *International Journal of Systematic and Evolutionary Microbiology* **28** (2): 315–317.

Ayrapetyan, M., Williams, T.C., and Oliver, J.D. (2014) Interspecific quorum sensing mediates the resuscitation of viable but nonculturable *Vibrios*. *Applied and Environmental Microbiology* **80** (8): 2478–2483.

Ball, A.S., Chaparian, R.R., and van Kessel, J.C. (2017) Quorum sensing gene regulation by LuxR/HapR master regulators in *Vibrios*. *Journal of Bacteriology* **199** (19): e00105-17.

Barcelos, M.C.S., Vespermann, K.A.C., Pelissari, F.M., and Molina, G. (2020) Current status of biotechnological production and applications of microbial exopolysaccharides. *Critical Reviews in Food Science and Nutrition* **60** (9): 1475–1495.

Bari, S.M.N., Roky, M.K., Mohiuddin, M., Kamruzzaman, M., Mekalanos, J.J., and Faruque, S.M. (2013) Quorum-sensing autoinducers resuscitate dormant *Vibrio cholerae* in environmental water samples. *Proceedings of the National Academy of Sciences of the United States of America* **110** (24): 9926–9931.

Basan, M., Hui, S., Okano, H., Zhang, Z., Shen, Y., Williamson, J.R., and Hwa, T. (2015) Overflow metabolism in *Escherichia coli* results from efficient proteome allocation. *Nature* **528** (7580): 99–104.

Bechthold, I., Bretz, K., Kabasci, S., Kopitzky, R., and Springer, A. (2008) Succinic acid: A new platform chemical for biobased polymers from renewable resources. *Chemical Engineering and Technology* **31** (5): 647–654.

Berardesca, E., Cameli, N., Primavera, G., and Carrera, M. (2006) Clinical and instrumental evaluation of skin improvement after treatment with a new 50% pyruvic acid peel. *Dermatologic Surgery* **32** (4): 526–531.

Biener, R., Horn, T., Komitakis, A., Schendel, I., König, L., Hauenstein, A., *et al.* (2023) High-cell-density cultivation of *Vibrio natriegens* in a low-chloride chemically defined medium. *Applied Microbiology and Biotechnology* **107** (23): 7043-7054.

Blombach, B., Buchholz, J., Busche, T., Kalinowski, J., and Takors, R. (2013) Impact of different CO_2/HCO_3^- levels on metabolism and regulation in *Corynebacterium glutamicum*. *Journal of Biotechnology* **168** (4): 331–340.

Blombach, B., and Takors, R. (2015) CO_2 - Intrinsic product, essential substrate, and regulatory trigger of microbial and mammalian production processes. *Frontiers in Bioengineering and Biotechnology* **3:** 108.

Bozell, J.J., and Petersen, G.R. (2010) Technology development for the production of biobased products from biorefinery carbohydrates—the US Department of Energy's "Top 10" revisited. *Green Chemistry* **12** (4): 539.

Bramhachari, P.V., and Dubey, S.K. (2006) Isolation and characterization of exopolysaccharide produced by *Vibrio harveyi* strain VB23. *Letters in Applied Microbiology* **43** (5): 571–577.

Bramhachari, P.V., Kishor, P.B.K., Ramadevi, R., Kumar, R., Rao, B.R., and Dubey, S.K. (2007) Isolation and characterization of mucous exopolysaccharide (EPS) produced by *Vibrio furnissii* strain VB0S3. *Journal of Microbiology and Biotechnology* **17** (1): 44–51.

Cao, Y., Zhang, R., Sun, C., Cheng, T., Liu, Y., and Xian, M. (2013) Fermentative succinate production: an emerging technology to replace the traditional petrochemical processes. *BioMed Research International* **2013:** 723412.

Casillo, A., Lanzetta, R., Parrilli, M., and Corsaro, M.M. (2018) Exopolysaccharides from marine and marine extremophilic bacteria: structures, properties, ecological roles and applications. *Marine Drugs* **16** (2): 69.

Cescutti, P. (2010) Bacterial capsular polysaccharides and exopolysaccharides. In *Microbial Glycobiology:* Elsevier, pp. 93–108.

Chang, S.-C., Lee, I., Ting, H., Chang, Y.-J., and Yang, N.-C. (2018) Parapyruvate, an impurity in pyruvate supplements, induces senescence in human fibroblastic Hs68 cells via inhibition of the α-ketoglutarate dehydrogenase complex. *Journal of Agricultural and Food Chemistry* **66** (28): 7504–7513.

Chen, G.-Q. (2012) New challenges and opportunities for industrial biotechnology. *Microbial Cell Factories* **11:** 111.

Cheng, K.-K., Wang, G.-Y., Zeng, J., and Zhang, J.-A. (2013) Improved succinate production by metabolic engineering. *BioMed Research International* **2013:** 538790.

Cheng, S., Lau, K.-T., Chen, S., Chang, X., Liu, T., and Yin, Y. (2010) Microscopical observation of the marine bacterium *Vibrio natriegens* growth on metallic corrosion. *Materials and Manufacturing Processes* **25** (5): 293–297.

Cybulski, K., Tomaszewska-Hetman, L., Rakicka, M., Juszczyk, P., and Rywińska, A. (2019) Production of pyruvic acid from glycerol by *Yarrowia lipolytica*. *Folia Microbiologica (Praha)* **64** (6): 809–820.

Dai, Z., Guo, F., Zhang, S., Zhang, W., Yang, Q., Dong, W., *et al.* (2020) Bio-based succinic acid: an overview of strain development, substrate utilization, and downstream purification. *Biofuels, Bioproducts and Biorefining* **14** (5): 965–985.

Dalia, T.N., Hayes, C.A., Stolyar, S., Marx, C.J., McKinlay, J.B., and Dalia, A.B. (2017) Multiplex genome editing by natural transformation (MuGENT) for synthetic biology in *Vibrio natriegens*. *ACS Synthetic Biology* **6** (9): 1650–1655.

Delbarre-Ladrat, C., Sinquin, C., Marchand, L., Bonnetot, S., Zykwinska, A., Verrez-Bagnis, V., and Colliec-Jouault, S. (2022) Influence of the carbon and nitrogen sources on diabolican production by the marine *Vibrio diabolicus* strain CNCM I-1629. *Polymers (Basel)* **14** (10): 1994

Dong, Y.H., Guo, N., Liu, T., Dong, L.H., and Yin, Y.S. (2016) Effect of extracellular polymeric substances isolated from *Vibrio natriegens* on corrosion of carbon steel in seawater. *Corrosion Engineering, Science and Technology* **51** (6): 455–462.

Drouillard, S., Jeacomine, I., Buon, L., Boisset, C., Courtois, A., Thollas, B., *et al.* (2015) Structure of an amino acid-decorated exopolysaccharide secreted by a *Vibrio alginolyticus* strain. *Marine Drugs* **13** (11): 6723–6739.

Drouillard, S., Jeacomine, I., Buon, L., Boisset, C., Courtois, A., Thollas, B., *et al.* (2018) Structure of the exopolysaccharide secreted by a marine strain *Vibrio alginolyticus*. *Marine Drugs* **16** (5): 164

Du, M., Chen, J., Zhang, X., Li, A., and Li, Y. (2007) Characterization and resuscitation of viable but nonculturable *Vibrio alginolyticus* VIB283. *Archives of Microbiology* **188** (3): 283–288.

Eagon, R.G. (1962) *Pseudomonas natriegens*, a marine bacterium with a generation time of less than 10 minutes. *Journal of Bacteriology* **83:** 736–737.

EFSA (2009) Calcium acetate, calcium pyruvate, calcium succinate, magnesium pyruvate magnesium succinate and potassium malate added for nutritional purposes to food supplements. *EFS2* **7** (6).

Ellis, G.A., Tschirhart, T., Spangler, J., Walper, S.A., Medintz, I.L., and Vora, G.J. (2019) Exploiting the feedstock flexibility of the emergent synthetic biology chassis *Vibrio natriegens* for engineered natural product production. *Marine Drugs* **17** (12): 679

Erian, A.M., Freitag, P., Gibisch, M., and Pflügl, S. (2020) High rate 2,3-butanediol production with *Vibrio natriegens*. *Bioresource Technology Reports* **10:** 100408.

Erian, A.M., Gibisch, M., and Pflügl, S. (2018) Engineered *E. coli* W enables efficient 2,3-butanediol production from glucose and sugar beet molasses using defined minimal medium as economic basis. *Microbial Cell Factories* **17** (1): 190.

Farmer, W.R., and Liao, J.C. (1997) Reduction of aerobic acetate production by *Escherichia coli*. *Applied and Environmental Microbiology* **63** (8): 3205–3210.

Fernández-Llamosas, H., Castro, L., Blázquez, M.L., Díaz, E., and Carmona, M. (2017) Speeding up bioproduction of selenium nanoparticles by using *Vibrio natriegens* as microbial factory. *Scientific Rep*orts **7** (1): 16046.

Finore, I., Di Donato, P., Mastascusa, V., Nicolaus, B., and Poli, A. (2014) Fermentation technologies for the optimization of marine microbial exopolysaccharide production. *Marine Drugs* **12** (5): 3005–3024.

Freitas, F., Alves, V.D., and Reis, M.A.M. (2011) Advances in bacterial exopolysaccharides: from production to biotechnological applications. *Trends in Biotechnology* **29** (8): 388–398.

Freitas, F., Torres, C.A.V., and Reis, M.A.M. (2017) Engineering aspects of microbial exopolysaccharide production. *Bioresource Technology* **245** (Pt B): 1674–1683.

Friedlander, R.S., Vlamakis, H., Kim, P., Khan, M., Kolter, R., and Aizenberg, J. (2013) Bacterial flagella explore microscale hummocks and hollows to increase adhesion. *Proceedings of the National Academy of Science of the United States of America* **110** (14): 5624–5629.

García, A., Fernández-Sandoval, M.T., Morales-Guzmán, D., Martínez-Morales, F., and Trejo-Hernández, M.R. (2022) Advances in exopolysaccharide production from marine bacteria. *Journal of Chemical Technology and Biotechnology* **97** (10): 2694–2705.

Gombert, A.K., Moreira dos Santos, M., Christensen, B., and Nielsen, J. (2001) Network identification and flux quantification in the central metabolism of *Saccharomyces cerevisiae* under different conditions of glucose repression. *Journal of Bacteriology* **183** (4): 1441–1451.

Gonzalez, J.E., Long, C.P., and Antoniewicz, M.R. (2017) Comprehensive analysis of glucose and xylose metabolism in *Escherichia coli* under aerobic and anaerobic conditions by ^{13}C metabolic flux analysis. *Metabolic Engineering* **39:** 9–18.

Goudenège, D., Boursicot, V., Versigny, T., Bonnetot, S., Ratiskol, J., Sinquin, C., *et al.* (2014) Genome sequence of *Vibrio diabolicus* and identification of the exopolysaccharide HE800 biosynthesis locus. *Applied Microbiology and Biotechnology* **98** (24): 10165–10176.

Güvener, Z.T., and McCarter, L.L. (2003) Multiple regulators control capsular polysaccharide production in *Vibrio parahaemolyticus*. *Journal of Bacteriology* **185** (18): 5431–5441.

Heidelberg, J.F., Eisen, J.A., Nelson, W.C., Clayton, R.A., Gwinn, M.L., Dodson, R.J., *et al.* (2000) DNA sequence of both chromosomes of the cholera pathogen *Vibrio cholerae*. *Nature* **406** (6795): 477–483.

Henke, J.M., and Bassler, B.L. (2004) Three parallel quorum-sensing systems regulate gene expression in *Vibrio harveyi*. *Journal of Bacteriology* **186** (20): 6902–6914.

Hoff, J., Daniel, B., Stukenberg, D., Thuronyi, B.W., Waldminghaus, T., and Fritz, G. (2020) *Vibrio natriegens*: an ultrafast-growing marine bacterium as emerging synthetic biology chassis. *Environmental Microbiology* **22** (10): 4394–4408.

Hoffart, E., Grenz, S., Lange, J., Nitschel, R., Müller, F., Schwentner, A., *et al.* (2017) High substrate uptake rates empower *Vibrio natriegens* as production host for industrial biotechnology. *Applied and Environmental Microbiology* **83** (22): e01614-17.

Holms, H. (1996) Flux analysis and control of the central metabolic pathways in *Escherichia coli*. *FEMS Microbiology Reviews* **19** (2): 85–116.

Jarman, T.R., and Pace, G.W. (1984) Energy requirements for microbial exopolysaccharide synthesis. *Archives of Microbiology* **137** (3): 231–235.

Jensen, R.V., Depasquale, S.M., Harbolick, E.A., Hong, T., Kernell, A.L., Kruchko, D.H., *et al.* (2013) Complete genome sequence of prepandemic *Vibrio parahaemolyticus* BB22OP. *Genome Announcements* **1** (1): e00002-12.

Jiang, M., Dai, W., Xi, Y., Wu, M., Kong, X., Ma, J., *et al.* (2014) Succinic acid production from sucrose by *Actinobacillus succinogenes* NJ113. *Bioresource Technology* **153:** 327–332.

Jiang, M., Liu, S.-W., Ma, J.-F., Chen, K.-Q., Yu, L., Yue, F.-F., *et al.* (2010) Effect of growth phase feeding strategies on succinate production by metabolically engineered *Escherichia coli*. *Applied and Environmental Microbiology* **76** (4): 1298–1300.

Johnson, T.L., Fong, J.C., Rule, C., Rogers, A., Yildiz, F.H., and Sandkvist, M. (2014) The Type II secretion system delivers matrix proteins for biofilm formation by *Vibrio cholerae*. *Jorunal of Bacteriology* **196** (24): 4245–4252.

Jung, S.A., Hawver, L.A., and Ng, W.-L. (2016) Parallel quorum sensing signaling pathways in *Vibrio cholerae*. *Current Genetics* **62** (2): 255–260.

Junker, B. (2009) Corrosion in bioprocessing applications. *Bioprocess Engineering* **32** (1): 1–29.

Kalburge, S.S., Carpenter, M.R., Rozovsky, S., and Boyd, E.F. (2017) Quorum sensing regulators are required for metabolic fitness in *Vibrio parahaemolyticus*. *Infection and Immunity* **85** (3): e00930-16.

Kawata, Y., Nishimura, T., Matsushita, I., and Tsubota, J. (2016) Efficient production and secretion of pyruvate from *Halomonas* sp. KM-1 under aerobic conditions. *AMB Express* **6** (1): 22.

Kenne, L., and Lindberg, B. (1983) Bacterial polysaccharides. In *The Polysaccharides:* Elsevier, pp. 287–363.

Kim, B.S., Lee, S.C., Lee, S.Y., Chang, Y.K., and Chang, H.N. (2004) High cell density fed-batch cultivation of *Escherichia coli* using exponential feeding combined with pH-stat. *Bioprocess and Biosystems Engineering* **26** (3): 147–150.

Lange, J., Takors, R., and Blombach, B. (2017) Zero-growth bioprocesses: A challenge for microbial production strains and bioprocess engineering. *Engineering in Life Science* **17** (1): 27–35.

Lebellenger, L., Verrez-Bagnis, V., Passerini, D., and Delbarre-Ladrat, C. (2018) Comparative genomics reveals a widespread distribution of an exopolysaccharide biosynthesis gene cluster among Vibrionaceae. *BMC Research Notes* **11** (1): 102.

Lee, H.H., Ostrov, N., Wong, B.G., Gold, M.A., Khalil, A.S., and Church, G.M. (2016) *Vibrio natriegens, a new genomic powerhouse*.

Lee, J., Lee, S.Y., Park, S., and Middelberg, A.P. (1999) Control of fed-batch fermentations. *Biotechnology Advances* **17** (1): 29–48.

Lee, J.A., Ahn, J.H., and Lee, S.Y. (2019) Organic acids: Succinic and malic acids. In *Comprehensive Biotechnology:* Elsevier, pp. 172–187.

Lee, J.-H., Rho, J.B., Park, K.-J., Kim, C.B., Han, Y.-S., Choi, S.H., *et al.* (2004) Role of flagellum and motility in pathogenesis of *Vibrio vulnificus*. *Infection and Immunity* **72** (8): 4905–4910.

Lee, S.J., Song, H., and Lee, S.Y. (2006) Genome-based metabolic engineering of *Mannheimia succiniciproducens* for succinic acid production. *Applied and Environmental Microbiology* **72** (3): 1939–1948.

Li, C., Wang, R., Wang, J., Liu, L., Li, H., Zheng, H., and Ni, J. (2023a) A highly compatible phototrophic community for carbon-negative biosynthesis. *Angewandte Chemie Internationale Edition in Englisch* **62** (2): e202215013.

Li, H.-H., Wu, J., Liu, J.-Q., Wu, Q.-Z., He, R.L., Cheng, Z.-H., *et al.* (2023b) Nonsterilized fermentation of crude glycerol for polyhydroxybutyrate production by metabolically engineered *Vibrio natriegens*. *ACS Synthetic Biology* **12** (11): 3454–3462.

Li, J., and Zhao, X. (2020) Effects of quorum sensing on the biofilm formation and viable but non-culturable state. *Food Research International* **137:** 109742.

Li, Y., Chen, J., and Lun, S.Y. (2001a) Biotechnological production of pyruvic acid. *Applied Microbiology and Biotechnology* **57** (4): 451–459.

Li, Y., Chen, J., Lun, S.Y., and Rui, X.S. (2001b) Efficient pyruvate production by a multi-vitamin auxotroph of *Torulopsis glabrata*: key role and optimization of vitamin levels. *Applied Microbiology and Biotechnology* **55** (6): 680–685.

Linton, J.D., Harrison, D.E., and Bull, A.T. (1977) Molar growth yields, respiration and cytochrome profiles of *Beneckea natriegens* when grown under carbon limitation in a chemostat. *Archives of Microbiology* **115** (2): 135–142.

Litsanov, B., Brocker, M., and Bott, M. (2012) Toward homosuccinate fermentation: metabolic engineering of *Corynebacterium glutamicum* for anaerobic production of succinate from glucose and formate. *Applied and Environmental Microbiology* **78** (9): 3325–3337.

Liu, X., Han, X., Peng, Y., Tan, C., Wang, J., Xue, H., *et al.* (2022) Rapid production of l-DOPA by *Vibrio natriegens*, an emerging next-generation whole-cell catalysis chassis. *Microbial Biotechnology* **15** (5): 1610–1621.

Long, C.P., Gonzalez, J.E., Cipolla, R.M., and Antoniewicz, M.R. (2017) Metabolism of the fast-growing bacterium *Vibrio natriegens* elucidated by ^{13}C metabolic flux analysis. *Metabolic Engineering* **44:** 191–197.

Lopes, B., Lopes Lessa, V., Silva, B., Carvalho, M.A., Schnitzler, E., and Lacerda, L. (2015) Xanthan gum: Properties, production conditions, quality and economic perspective. *Journal of Food and Nutrition Research* **54:** 185–194.

Maida, I., Bosi, E., Perrin, E., Papaleo, M.C., Orlandini, V., Fondi, M., *et al.* (2013) Draft genome sequence of the fast-growing bacterium *Vibrio natriegens* strain DSMZ 759. *Genome Announcements* **1** (4): e00648-13.

Maleki, N., and Eiteman, M. (2017) Recent progress in the microbial production of pyruvic acid. *Fermentation* **3** (1): 8.

Margolis, S.A., and Coxon, B. (1986) Identification and quantitation of the impurities in sodium pyruvate. *Analytical Chemistry* **58** (12): 2504–2510.

Martínez, I., Bennett, G.N., and San, K.-Y. (2010) Metabolic impact of the level of aeration during cell growth on anaerobic succinate production by an engineered *Escherichia coli* strain. *Metabolic Engineering* **12** (6): 499–509.

Martin-Pastor, M., Ferreira, A.S., Moppert, X., Nunes, C., Coimbra, M.A., Reis, R.L., *et al.* (2019) Structure, rheology, and copper-complexation of a hyaluronan-like exopolysaccharide from *Vibrio*. *Carbohydrate Polymers* **222:** 114999.

McDougald, D., Rice, S.A., Weichart, D., and Kjelleberg, S. (1998) Nonculturability: adaptation or debilitation? *FEMS Microbiology Ecology* **25** (1): 1–9.

McNeil, B., and Harvey, L.M. (1993) Viscous Fermentation Products. *Critical Reviews in Biotechnology* **13** (4): 275–304.

Meng, W., Zhang, Y., Ma, L., Lü, C., Xu, P., Ma, C., and Gao, C. (2022) Non-sterilized fermentation of 2,3-butanediol with seawater by metabolic engineered fast-growing *Vibrio natriegens*. *Frontiers in Bioengineering and Biotechnology* **10:** 955097.

Meyer, H.-P., Leist, C., and Fiechter, A. (1984) Acetate formation in continuous culture of *Escherichia coli* K12 D1 on defined and complex media. *Journal of Biotechnologyl* **1** (5-6): 355–358.

Michel, A., Koch-Koerfges, A., Krumbach, K., Brocker, M., and Bott, M. (2015) Anaerobic growth of *Corynebacterium glutamicum* via mixed-acid fermentation. *Applied and Environmental Microbiology* **81** (21): 7496–7508.

Milton, D.L. (2006) Quorum sensing in *vibrios*: complexity for diversification. *International Journal of Medical Microbiology* **296** (2-3): 61–71.

Miyashiro, T., Oehlert, D., Ray, V.A., Visick, K.L., and Ruby, E.G. (2014) The putative oligosaccharide translocase SypK connects biofilm formation with quorum signaling in *Vibrio fischeri*. *Microbiologyopen* **3** (6): 836–848.

Montgomery, C.M., and Webb, J.L. (1956) Metabolic studies on heart mitochondria. II. The inhibitory action of parapyruvate on the tricarboxylic acid cycle. *Journal of Biological Chemistry* **221** (1): 359–368.

Moorthy, S., and Watnick, P.I. (2004) Genetic evidence that the *Vibrio cholerae* monolayer is a distinct stage in biofilm development. *Molecular Microbiology* **52** (2): 573–587.

Moradali, M.F., and Rehm, B.H.A. (2020) Bacterial biopolymers: from pathogenesis to advanced materials. *Nature Reviews Microbiology* **18** (4): 195–210.

Muralidharan, J., and Jayachandran, S. (2003) Physicochemical analyses of the exopolysaccharides produced by a marine biofouling bacterium, *Vibrio alginolyticus*. *Process Biochemistry* **38** (6): 841–847.

Nakano, K., Rischke, M., Sato, S., and Märkl, H. (1997) Influence of acetic acid on the growth of *Escherichia coli* K12 during high-cell-density cultivation in a dialysis reactor. *Applied Microbiology and Biotechnology* **48** (5): 597–601.

Neiditch, M.B., Federle, M.J., Miller, S.T., Bassler, B.L., and Hughson, F.M. (2005) Regulation of LuxPQ receptor activity by the quorum-sensing signal autoinducer-2. *Molecular Cell* **18** (5): 507–518.

Nichols, C.A.M., Guezennec, J., and Bowman, J.P. (2005) Bacterial exopolysaccharides from extreme marine environments with special consideration of the southern ocean, sea ice, and deep-sea hydrothermal vents: a review. *Marine Biotechnology (NY)* **7** (4): 253–271.

Nimbalkar, P.R., Khedkar, M.A., Parulekar, R.S., Chandgude, V.K., Sonawane, K.D., Chavan, P.V., and Bankar, S.B. (2018) Role of trace elements as cofactor: an efficient strategy toward enhanced biobutanol production. *ACS Sustainable Chemistry and Engineering* **6** (7): 9304–9313.

Okino, S., Noburyu, R., Suda, M., Jojima, T., Inui, M., and Yukawa, H. (2008) An efficient succinic acid production process in a metabolically engineered *Corynebacterium glutamicum* strain. *Applied Microbiology and Biotechnology* **81** (3): 459–464.

Oliver, J.D. (1995) The viable but non-culturable state in the human pathogen *Vibrio vulnificus*. *FEMS Microbiology Letters* **133** (3): 203–208.

Oliver, J.D. (2005) The viable but nonculturable state in bacteria. *Journal of Microbiology* **43** Spec No: 93–100.

Payne, W.J. (1958) Studies on bacterial utilization of uronic acids. III. Induction of oxidative enzymes in a marine isolate. *Journal of Bacteriology* **76** (3): 301–307.

Payne, W.J. (1960) Effects of sodium and potassium ions on growth and substrate penetration of a marine pseudomonad. *Journal of Bacteriology* **80** (5): 696–700.

Payne, W.J., Eagon, R.G., and Williams, A.K. (1961) Some observations on the physiology of *Pseudomonas natriegens* nov. spec. *Antonie Van Leeuwenhoek* **27:** 121–128.

Pfeifer, E., Michniewski, S., Gätgens, C., Münch, E., Müller, F., Polen, T., *et al.* (2019) Generation of a prophage-free variant of the fast-growing bacterium *Vibrio natriegens*. *Applied and Environmental Microbiology* **85** (17): e00853-19.

Raab, A.M., and Lang, C. (2011) Oxidative versus reductive succinic acid production in the yeast *Saccharomyces cerevisiae*. *Bioengineered Bugs* **2** (2): 120–123.

Ramaiah, N., Ravel, J., Straube, W.L., Hill, R.T., and Colwell, R.R. (2002) Entry of *Vibrio harveyi* and *Vibrio fischeri* into the viable but nonculturable state. *Journal of Applied Microbiology* **93** (1): 108–116.

Riesenberg, D., and Guthke, R. (1999) High-cell-density cultivation of microorganisms. *Applied Microbiology and Biotechnology* **51** (4): 422-30.

Riesenberg, D., Schulz, V., Knorre, W.A., Pohl, H.-D., Korz, D., Sanders, E.A., *et al.* (1991) High cell density cultivation of *Escherichia coli* at controlled specific growth rate. *Journal of Biotechnology* **20** (1): 17–27.

Rougeaux, H., Kervarec, N., Pichon, R., and Guezennec, J. (1999) Structure of the exopolysaccharide of *Vibrio diabolicus* isolated from a deep-sea hydrothermal vent. *Carbohydrate Res*earch **322** (1-2): 40–45.

Ruby, E.G., Urbanowski, M., Campbell, J., Dunn, A., Faini, M., Gunsalus, R., *et al.* (2005) Complete genome sequence of *Vibrio fischeri*: a symbiotic bacterium with pathogenic congeners. *Proceedings of the National Academy of Sciences of the United States of America* **102** (8): 3004–3009.

Rühmann, B., Schmid, J., and Sieber, V. (2014) Fast carbohydrate analysis via liquid chromatography coupled with ultra violet and electrospray ionization ion trap detection in 96-well format. *Journal of Chromatography A* **1350:** 44–50.

Rühmann, B., Schmid, J., and Sieber, V. (2015) High throughput exopolysaccharide screening platform: from strain cultivation to monosaccharide composition and carbohydrate fingerprinting in one day. *Carbohydrate Polymers* **122:** 212–220.

Sambrook, J., and Russell, D.W. (2001) *Molecular cloning: A laboratory manual / Joseph Sambrook, David W. Russell. Vol. 1.* Cold Spring Harbor, N.Y.: Cold Spring Harbor laboratory Press.

Sánchez, A.M., Bennett, G.N., and San, K.-Y. (2005) Novel pathway engineering design of the anaerobic central metabolic pathway in *Escherichia coli* to increase succinate yield and productivity. *Metabolic Engineering* **7** (3): 229–239.

Sauer, M., Porro, D., Mattanovich, D., and Branduardi, P. (2008) Microbial production of organic acids: expanding the markets. *Trends in Biotechnology* **26** (2): 100–108.

Sauer, U., Hatzimanikatis, V., Hohmann, H.P., Manneberg, M., van Loon, A.P., and Bailey, J.E. (1996) Physiology and metabolic fluxes of wild-type and riboflavin-producing *Bacillus subtilis*. *Applied and Environmental Microbiology* **62** (10): 3687–3696.

Schilling, C., Badri, A., Sieber, V., Koffas, M., and Schmid, J. (2020) Metabolic engineering for production of functional polysaccharides. *Current Opinion in Biotechnology* **66:** 44–51.

Schulze, C., Hädrich, M., Borger, J., Rühmann, B., Döring, M., Sieber, V., *et al.* (2023) Investigation of exopolysaccharide formation and its impact on anaerobic succinate production with *Vibrio natriegens*. *Microbial Biotechnology* **17** (1): e14277.

Seviour, R.J., McNeil, B., Fazenda, M.L., and Harvey, L.M. (2011) Operating bioreactors for microbial exopolysaccharide production. *Critical Reviews in Biotechnology* **31** (2): 170–185.

Shime-Hattori, A., Iida, T., Arita, M., Park, K.-S., Kodama, T., and Honda, T. (2006) Two type IV pili of *Vibrio parahaemolyticus* play different roles in biofilm formation. *FEMS Microbiology Letters* **264** (1): 89–97.

Siebert, D., Altenbuchner, J., and Blombach, B. (2021) A timed off-switch for dynamic control of gene expression in *Corynebacterium glutamicum*. *Frontiers in Bioengineering and Biotechnology* **9:** 704681.

Smith, A.D., Tschirhart, T., Compton, J., Hennessa, T.M., VanArsdale, E., and Wang, Z. (2023) Rapid, high-titer biosynthesis of melanin using the marine bacterium *Vibrio natriegens*. *Frontiers in Bioengineering and Biotechnology* **11:** 1239756.

Souza Santos, M. de, Salomon, D., Li, P., Krachler, A.-M., and Orth, K. (2015) *Vibrio parahaemolyticus* virulence determinants. In *The comprehensive sourcebook of bacterial protein toxins:* Elsevier, pp. 230–260.

Stukenberg, D., Hoff, J., Faber, A., and Becker, A. (2021) *NT-CRISPR:* Combining natural transformation and CRISPR/Cas9 counterselection for markerless and scarless genome editing in *Vibrio natriegens*. *Communications Biology*, **5** (1): 265.

Sun, F., Chen, J., Zhong, L., Zhang, X.-H., Wang, R., Guo, Q., and Dong, Y. (2008) Characterization and virulence retention of viable but nonculturable *Vibrio harveyi*. *FEMS Microbiology Ecology* **64** (1): 37–44.

Teufel, M., Klein, C.A., Mager, M., and Sobetzko, P. (2022) A multifunctional system for genome editing and large-scale interspecies gene transfer. *Nature Communications* **13** (1): 3430.

Thiele, I., Gutschmann, B., Aulich, L., Girard, M., Neubauer, P., and Riedel, S.L. (2021) High-cell-density fed-batch cultivations of *Vibrio natriegens*. *Biotechnology Letters* **43** (9): 1723–1733.

Thoma, F., and Blombach, B. (2021) Metabolic engineering of *Vibrio natriegens*. *Essays in Biochemistry* **65** (2): 381-392.

Thoma, F., Schulze, C., Gutierrez-Coto, C., Hädrich, M., Huber, J., Gunkel, C., *et al.* (2021) Metabolic engineering of *Vibrio natriegens* for anaerobic succinate production. *Microbial Biotechnology* **15** (6): 1671-1684.

Thompson, B.G., Kole, M., and Gerson, D.F. (1985) Control of ammonium concentration in *Escherichia coli* fermentations. *Biotechnology and Bioengineering* **27** (6): 818–824.

Tian, J., Deng, W., Zhang, Z., Xu, J., Yang, G., Zhao, G., *et al.* (2023) Discovery and remodeling of *Vibrio natriegens* as a microbial platform for efficient formic acid biorefinery. *Nature Communications* **14** (1): 7758.

Tomar, A., Eiteman, M.A., and Altman, E. (2003) The effect of acetate pathway mutations on the production of pyruvate in *Escherichia coli*. *Applied Microbiology and Biotechnology* **62** (1): 76–82.

Utada, A.S., Bennett, R.R., Fong, J.C.N., Gibiansky, M.L., Yildiz, F.H., Golestanian, R., and Wong, G.C.L. (2014) *Vibrio cholerae* use pili and flagella synergistically to effect motility switching and conditional surface attachment. *Nature Communications* **5:** 4913.

Valgepea, K., Adamberg, K., Nahku, R., Lahtvee, P.-J., Arike, L., and Vilu, R. (2010) Systems biology approach reveals that overflow metabolism of acetate in *Escherichia coli* is triggered by carbon catabolite repression of acetyl-CoA synthetase. *BMC Systems Biology* **4:** 166.

Valley, G. (1928) The Effect of Carbon Dioxide on Bacteria. *The Quarterly Review of Biology* **3** (2): 209–224.

Van Maris, A.J.A., Geertman, J.-M.A., Vermeulen, A., Groothuizen, M.K., Winkler, A.A., Piper, M.D.W., *et al.* (2004) Directed evolution of pyruvate decarboxylase-negative *Saccharomyces cerevisiae*, yielding a C2-independent, glucose-tolerant, and pyruvate-hyperproducing yeast. *Applied and Environmental Microbiology* **70** (1): 159–166.

Varma, A., and Palsson, B.O. (1994) Stoichiometric flux balance models quantitatively predict growth and metabolic by-product secretion in wild-type *Escherichia coli* W3110. *Applied and Environmental Microbiology* **60** (10): 3724–3731.

Vemuri, G.N., Altman, E., Sangurdekar, D.P., Khodursky, A.B., and Eiteman, M.A. (2006) Overflow metabolism in *Escherichia coli* during steady-state growth: transcriptional regulation and effect of the redox ratio. *Applied and Environmental Microbiology.* **72** (5): 3653–3661.

Vemuri, G.N., Eiteman, M.A., and Altman, E. (2002) Succinate production in dual-phase *Escherichia coli* fermentations depends on the time of transition from aerobic to anaerobic conditions. *Journal of Industrial Microbiology and Biotechnology* **28** (6): 325–332.

Visick, K.L., and McFall-Ngai, M.J. (2000) An exclusive contract: specificity in the *Vibrio fischeri*-*Euprymna scolopes* partnership. *Journal of Bacteriology* **182** (7): 1779–1787.

Vuoristo, K.S., Mars, A.E., Sanders, J.P.M., Eggink, G., and Weusthuis, R.A. (2016) Metabolic engineering of TCA cycle for production of chemicals. *Trends in Biotechnology* **34** (3): 191–197.

Wang, D., Li, Q., Song, Z., Zhou, W., Su, Z., and Xing, J. (2011) High cell density fermentation via a metabolically engineered *Escherichia coli* for the enhanced production of succinic acid. *Journal of Chemical Technology and Biotechnology* **86** (4): 512–518.

Wang S, Wang B, You X, and Du L. (2023) Transcriptomic responses of the fast-growing bacterium *Vibrio natriegens* during cold-induced loss of culturability. *Applied Microbiology and Biotechnol*ogy **107** (9): 3009-3019.

Wang, Z., Lin, B., Hervey, W.J., and Vora, G.J. (2013) Draft genome sequence of the fast-growing marine bacterium *Vibrio natriegens* strain ATCC 14048. *Genome Announcements* **1** (4): e00589-13.

Wang, Z., Tschirhart, T., Schultzhaus, Z., Kelly, E.E., Chen, A., Oh, E., *et al.* (2020) Melanin produced by the fast-growing marine bacterium *Vibrio natriegens* through heterologous biosynthesis: characterization and application. *Applied and Environmental Microbiology* **86** (5): e02749-19

Waters, C.M., and Bassler, B.L. (2005) Quorum sensing: cell-to-cell communication in bacteria. *Annual Review of Cell and Developemental Biology* **21:** 319–346.

Watnick, P.I., Fullner, K.J., and Kolter, R. (1999) A role for the mannose-sensitive hemagglutinin in biofilm formation by *Vibrio cholerae* El Tor. *Journal of Bacteriology* **181** (11): 3606–3609.

Webb, C.D., and PAYNE, W.J. (1971) Influence of Na^+ on synthesis of macromolecules by a marine bacterium. *Applied Microbiology* **21** (6): 1080–1088.

Weinstock, M.T., Hesek, E.D., Wilson, C.M., and Gibson, D.G. (2016) *Vibrio natriegens* as a fast-growing host for molecular biology. *Nature Methods* **13** (10): 849–851.

Werpy, T., and Petersen, G. (2004) Top value added chemicals from biomass: Volume I—results of screening for potential candidates from sugars and synthesis gas.

Wieschalka, S., Blombach, B., and Eikmanns, B.J. (2012) Engineering *Corynebacterium glutamicum* for the production of pyruvate. *Applied Microbiology and Biotechnology* **94** (2): 449–459.

Wingender, J., Neu, T.R., and Flemming, H.-C. (ed.) (1999) *Microbial extracellular polymeric substances.* Berlin, Heidelberg: Springer Berlin Heidelberg.

Wolfaardt, G.M., Lawrence, J.R., and Korber, D.R. (1999) Function of EPS. In *Microbial extracellular polymeric substances.* Wingender, J., Neu, T.R., and Flemming, H.-C. (ed.). Berlin, Heidelberg: Springer Berlin Heidelberg, pp. 171–200.

Wong, H.-C., Wang, P., Chen, S.-Y., and Chiu, S.-W. (2004) Resuscitation of viable but non-culturable *Vibrio parahaemolyticus* in a minimum salt medium. *FEMS Microbiology Letters* **233** (2): 269–275.

Wu, B., Liang, W., Yan, M., Li, J., Zhao, H., Cui, L., *et al.* (2020) Quorum sensing regulation confronts the development of a viable but non-culturable state in *Vibrio cholerae*. *Environmental Microbiology* **22** (10): 4314–4322.

Wu, F., Wang, S., Peng, Y., Guo, Y., and Wang, Q. (2023) Metabolic engineering of fast-growing *Vibrio natriegens* for efficient pyruvate production. *Microbial Cell Factories* **22** (1): 172.

Wuisan, Z.G., Kresna, I.D.M., Böhringer, N., Lewis, K., and Schäberle, T.F. (2021) Optimization of heterologous Darobactin A expression and identification of the minimal biosynthetic gene cluster. *Metabolic Engineering* **66:** 123–136.

Xu, H.S., Roberts, N., Singleton, F.L., Attwell, R.W., Grimes, D.J., and Colwell, R.R. (1982) Survival and viability of nonculturable *Escherichia coli* and *Vibrio cholerae* in the estuarine and marine environment. *Microbial Ecology* **8** (4): 313–323.

Yang, Q., Wu, M., Dai, Z., Xin, F., Zhou, J., Dong, W., *et al.* (2020) Comprehensive investigation of succinic acid production by *Actinobacillus succinogenes*: a promising native succinic acid producer. *Biofuels, Bioproducts and Biorefining* **14** (5): 950–964.

Yao, Z.-Y., Qin, J., Gong, J.-S., Ye, Y.-H., Qian, J.-Y., Li, H., *et al.* (2021) Versatile strategies for bioproduction of hyaluronic acid driven by synthetic biology. *Carbohydrate Polymers* **264:** 118015.

Yildiz, F.H., Dolganov, N.A., and Schoolnik, G.K. (2001) VpsR, a member of the response regulators of the two-component regulatory systems, is required for expression of *vps* biosynthesis genes and EPS(ETr)-associated phenotypes in *Vibrio cholerae* O1 El Tor. *Journal of Bacteriology* **183** (5): 1716–1726.

Yildiz, F.H., and Visick, K.L. (2009) *Vibrio* biofilms: so much the same yet so different. *Trends in Microbiology* **17** (3): 109–118.

Yin, J., Chen, J.-C., Wu, Q., and Chen, G.-Q. (2015) Halophiles, coming stars for industrial biotechnology. *Biotechnology Advances* **33** (7): 1433–1442.

Yip, E.S., Grublesky, B.T., Hussa, E.A., and Visick, K.L. (2005) A novel, conserved cluster of genes promotes symbiotic colonization and sigma-dependent biofilm formation by *Vibrio fischeri*. *Molecular Microbiology* **57** (5): 1485–1498.

Yuan, W., Du, Y., Yu, K., Xu, S., Liu, M., Wang, S., *et al.* (2022) The production of pyruvate in biological technology: A critical review. *Microorganisms* **10** (12).

Yuan, W., Lin, X., Zhong, S., Chen, J., Wang, Z., and Sun, J. (2020) Enhanced pyruvic acid yield in an osmotic stress-resistant mutant of *Yarrowia lipolytica*. *Electronic Journal of Biotechnology* **44:** 19–24.

Zanchetta, P., Lagarde, N., and Guezennec, J. (2003) A new bone-healing material: a hyaluronic acid-like bacterial exopolysaccharide. *Calcified Tissue International* **72** (1): 74–79.

Zelić, B., Gerharz, T., Bott, M., Vasić-Rački, Đ., Wandrey, C., and Takors, R. (2003) Fed-batch process for pyruvate production by recombinant *Escherichia coli* YYC202 Strain. *Engineering in Life Science* **3** (7): 299–305.

Zelić, B., Gostović, S., Vuorilehto, K., Vasić-Racki, D., and Takors, R. (2004) Process strategies to enhance pyruvate production with recombinant *Escherichia coli*: from repetitive fed-batch to in situ product recovery with fully integrated electrodialysis. *Biotechnology and Bioengineering* **85** (6): 638–646.

Zhang, X.-H., Ahmad, W., Zhu, X.-Y., Chen, J., and Austin, B. (2021a) Viable but nonculturable bacteria and their resuscitation: implications for cultivating uncultured marine microorganisms. *Marine Life Science and Technology* **3** (2): 189–203.

Zhang, Y., Liu, D., and Chen, Z. (2023) Genome-scale modeling and systems metabolic engineering of *Vibrio natriegens* for the production of 1,3-propanediol. *Methods in Molecular Biology* **2553:** 209–220.

Zhang, Y., Sun, Q., Liu, Y., Cen, X., Liu, D., and Chen, Z. (2021b) Development of a plasmid stabilization system in *Vibrio natriegens* for the high production of 1,3-propanediol and 3-hydroxypropionate. *Bioresources and Bioprocessing* **8** (1): 125.

Zhu, J., Thakker, C., San, K.-Y., and Bennett, G. (2011) Effect of culture operating conditions on succinate production in a multiphase fed-batch bioreactor using an engineered *Escherichia coli* strain. *Applied Microbiology and Biotechnology* **92** (3): 499–508.

Zhu, N., Xia, H., Yang, J., Zhao, X., and Chen, T. (2014) Improved succinate production in *Corynebacterium glutamicum* by engineering glyoxylate pathway and succinate export system. *Biotechnology Letters* **36** (3): 553–560.

Zhu, Y., Eiteman, M.A., Altman, R., and Altman, E. (2008) High glycolytic flux improves pyruvate production by a metabolically engineered *Escherichia coli* strain. *Applied and Environmental Microbiology* **74** (21): 6649–6655.

Appendix

Table A1: List of genes potentially involved in quorum sensing in *V. natriegens* ATCC 14048 as annotated by KEGG (Schulze *et al.*, 2023).

Identifier	Name	Length | bp
PN96_19855	*cqsS*	2055
PN96_03880	*luxN*	2538
PN96_17980	*luxQ*	2574
PN96_03290	*luxU*	339
PN96_03285	*luxO*	1407
PN96_04645		1461
PN96_01350	*hapR*	615
PN96_01245	*luxS*	519

Table A2: List of chemicals

Chemical	Manufacturer
ß-Alanine	VWR International GmbH, Darmstadt, Germany
Acetonitrile	VWR International GmbH, Darmstadt, Germany
Agar-Agar, Kobe 1	Carl Roth GmbH & Co. KG, Karlsruhe, Germany
Ammonia water (25%)	Carl Roth GmbH & Co. KG, Karlsruhe, Germany
Ammonium sulfate	Carl Roth GmbH & Co. KG, Karlsruhe, Germany
Bacto™ Tryptone	BD Biosciences, Heidelberg, Germany
Bacto™ Yeast extract	BD Biosciences, Heidelberg, Germany
Boric acid	Carl Roth GmbH & Co. KG, Karlsruhe, Germany
Calcium carbonate	Carl Roth GmbH & Co. KG, Karlsruhe, Germany
Calcium chloride dihydrate	VWR International GmbH, Darmstadt, Germany
Citric acid	Carl Roth GmbH & Co. KG, Karlsruhe, Germany
Cobalt chloride hexahydrate	Carl Roth GmbH & Co. KG, Karlsruhe, Germany
Copper(II)sulfate pentahydrate	Merck KGaA, Darmstadt, Germany
D(+)-glucose monohydrate	Carl Roth GmbH & Co. KG, Karlsruhe, Germany
Dipotassium hydrogen phosphate	Carl Roth GmbH & Co. KG, Karlsruhe, Germany
Disodium succinate	ThermoFischer Scientific, Waltham, United States
Ethylenediaminetetraacetic acid	Carl Roth GmbH & Co. KG, Karlsruhe, Germany
Glycerol	Carl Roth GmbH & Co. KG, Karlsruhe, Germany
Hydrochloric acid	VWR International GmbH, Darmstadt, Germany
Iron(III) citrate monohydrate	Carl Roth GmbH & Co. KG, Karlsruhe, Germany
Iron sulfate heptahydrate	Carl Roth GmbH & Co. KG, Karlsruhe, Germany
Isopropyl β-D-1-thiogalactopyranosid	Carl Roth GmbH & Co. KG, Karlsruhe, Germany
Kanamycin sulfate	Carl Roth GmbH & Co. KG, Karlsruhe, Germany
Magnesium chloride hexahydrate	VWR International GmbH, Darmstadt, Germany
Magnesium sulfate heptahydrate	VWR International GmbH, Darmstadt, Germany
Manganese sulfate monohydrate	Merck KGaA, Darmstadt, Germany
Methanol	SIGMA-ALDRICH Chemie GmbH, Steinheim, Germany
Nickel chloride hexahydrate	Carl Roth GmbH & Co. KG, Karlsruhe, Germany
Norvaline	SIGMA-ALDRICH Chemie GmbH, Steinheim, Germany
Phosphoric acid	Carl Roth GmbH & Co. KG, Karlsruhe, Germany
Potassium acetate	Carl Roth GmbH & Co. KG, Karlsruhe, Germany

Potassium dihydrogen phosphate	Carl Roth GmbH & Co. KG, Karlsruhe, Germany
Potassium hydrogen carbonate	VWR International GmbH, Darmstadt, Germany
Potassium hydroxide	VWR International GmbH, Darmstadt, Germany
Potassium iodate	Carl Roth GmbH & Co. KG, Karlsruhe, Germany
Sodium chloride	Carl Roth GmbH & Co. KG, Karlsruhe, Germany
Sodium L-lactate	SIGMA-ALDRICH Chemie GmbH, Steinheim, Germany
Sodium molybdate dihydrate	Carl Roth GmbH & Co. KG, Karlsruhe, Germany
Sodium pyruvate	Carl Roth GmbH & Co. KG, Karlsruhe, Germany
Sodium selenite	Merck KGaA, Darmstadt, Germany
Sodium sulfate	Merck KGaA, Darmstadt, Germany
Sodium tetraborate	SIGMA-ALDRICH Chemie GmbH, Steinheim, Germany
Sodium tungstate dihydrate	Carl Roth GmbH & Co. KG, Karlsruhe, Germany
Struktol® J 647	Schill+Seilacher GmbH, Hamburg, Germany
Sulfuric acid	Carl Roth GmbH & Co. KG, Karlsruhe, Germany
Water for HPLC	VWR International GmbH, Darmstadt, Germany
Bacto™ Yeast extract	BD Biosciences, Heidelberg, Germany
Zinc sulfate heptahydrate	Carl Roth GmbH & Co. KG, Karlsruhe, Germany
3-(N-morpholino)propanesulfonic acid	SIGMA-ALDRICH Chemie GmbH, Steinheim, Germany

Table A3: Devices and materials

Name	Device/Material	Manufacturer
0.5 L Shaking flasks with appropriate cellulose plugs	Culture vessels	VWR International GmbH, Darmstadt, Germany
1 L Shaking flasks with appropriate cellulose plugs	Culture vessels	VWR International GmbH, Darmstadt, Germany
1260 Infinity II system	HPLC equipped with RID	Agilent Technologies, Waldbronn, Germany
1260 Infinity II system	HPLC equipped with FLD	Agilent Technologies, Waldbronn, Germany
AdvanceBio AAA column	HPLC column for amino acid analysis; 4.6 x 100 mm, 2.7 µm	Agilent Technologies, Waldbronn, Germany
AdvanceBio AAA guard column	Guard column for HPLC column; 4.6 x 5.0 mm, 2.7 µm	Agilent Technologies, Waldbronn, Germany
Centrifuge 5425	Benchtop centrifuge	Eppendorf SE, Hamburg, Germany
Centrifuge 5910R	Refrigerated high-capacity centrifuge	Eppendorf SE, Hamburg, Germany
DASGIP® parallel bioreactor system	DASGIP®: DASGIP Bioblock / DASGIP CWD4 / DASGIP PH4PO4L / DASGIP MX4/4 / DASGIP MP8 / DASGIP TC4SC4 / DASGIP GA4 / DASGIP process control module	Eppendorf AG, Jülich, Germany
DO Sensor InPro®6800	DO electrode for DASGIP®	Mettler-Toledo GmbH, Gießen, Germany
Entris® 124i-1S	Balance	Sartorius AG, Göttingen, Germany
Entris® 420i-1S	Analytical balance	Sartorius AG, Göttingen, Germany
Filtropur S plus 0.2	Sterile filter (pore size 0.2 µm)	SARSTEDT, Nümbrecht, Germany
FiveEasy pH meter F20	pH meter	Mettler Toledo GmbH, Gießen, Germany
Heraeus® Multifuge® 4KR	Refrigerated high-capacity centrifuge	Thermo Electron LED GmbH, Osterode am Harz, Germany
Herasafe™ 2030i	Clean bench	ThermoFischer Scientific, Waltham, United States

Hi-Plex H column	HPLC column for carbohydrate analysis; 7.7 x 300 mm, 8 µm	Agilent Technologies, Waldbronn, Germany
Hi-Plex H guard cartridge	Guard cartridge for HPLC column; 3.0 x 5.0 mm, 8 µm	Agilent Technologies, Waldbronn, Germany
Medi-Test Glucose	Test strips for glucose analysis	MACHEREY-NAGEL GmbH & Ko.KG, Düren, Germany
Modell BD 115	Incubator	BINDER GmbH, Tuttlingen, Germany
Multitron Standard SU252	Orbital shaker (Ø 25 mm)	INFORS AG, Bottmingen, Switzerland
NanoPhotometer® NP80	Small volume spectrophotometer	Implen GmbH, Munich, Germany
pH Electrode LE407	pH electrode for pH meter	Mettler-Toledo GmbH, Gießen, Germany
pH Sensor 405-DPAS-SC-K8S/325	pH electrode for DASGIP®	Mettler-Toledo GmbH, Gießen, Germany
Rheometer MCR302	Rotational rheometer with TEK150 chamber and CP50-1 measuring cell	Anton-Paar, Graz, Austria
Ultrospec® 10 Cell Density Meter	Hand-held spectrophotometer	Biochrom Ltd, Cambridge, United Kingdom
Vortex-Genie 2	Vortex mixer	Scientific Industries, Inc., Bohemia, United States

Table A4: Software

Name	Purpose	Manufacturer
BioRender	Scientific image and illustration software	Science Suite Inc., Toronto, Canada
DASware® control	Bioreactor regulation and data collection	Eppendorf, Hamburg, Germany
Inkscape	Vector graphics editor	Inkscape Project, New York, United States
OpenLab CDS – Chemstation Edition	Acquisition and analysis of HPLC data	Agilent Technologies, Waldbronn, Germany

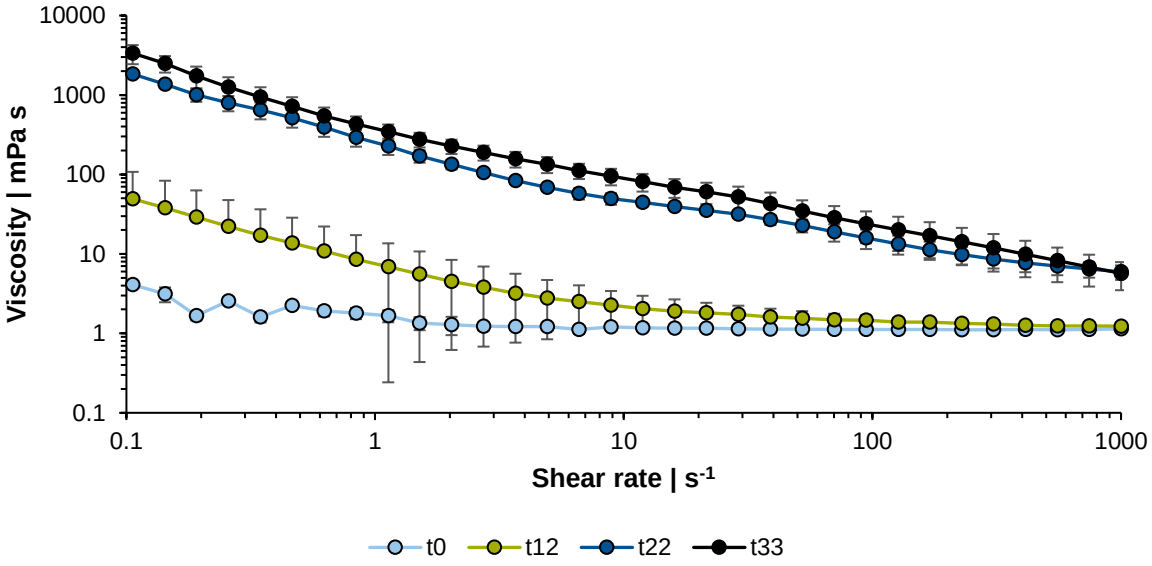

Figure A1: Viscosity of the bioreactor broth of a *V. natriegens* wildtype cultivation measured at different shear rates. Light blue, green, dark blue, and black lines indicate samples taken at 0, 12, 22, and 33 h, respectively.

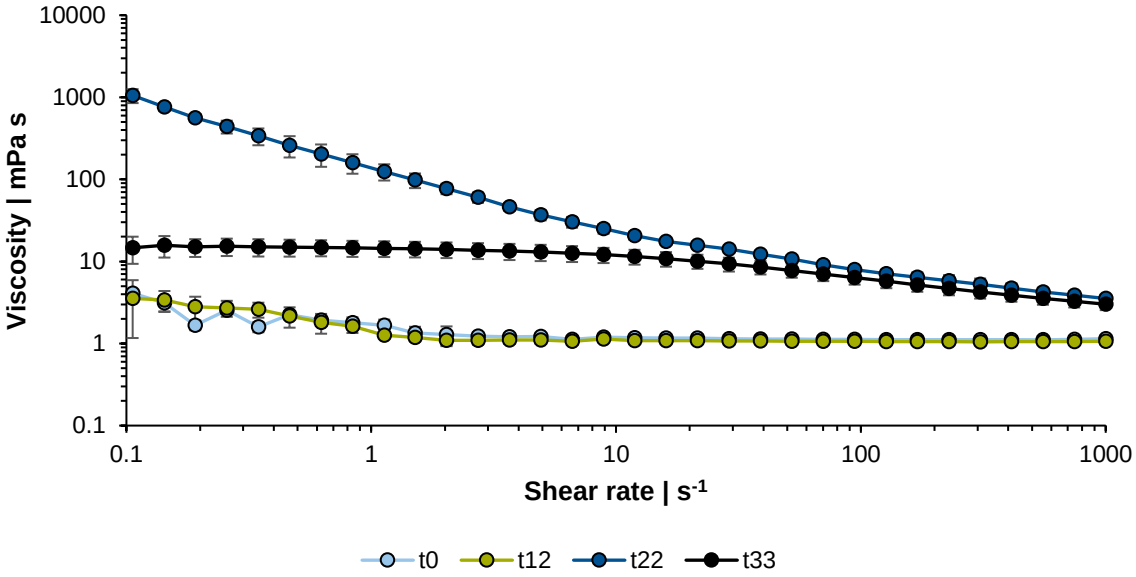

Figure A2: Viscosity of the bioreactor broth of a *V. natriegens* Δ*wbfF* cultivation measured at different shear rates. Light blue, green, dark blue, and black lines indicate samples taken at 0, 12, 22, and 33 h, respectively.

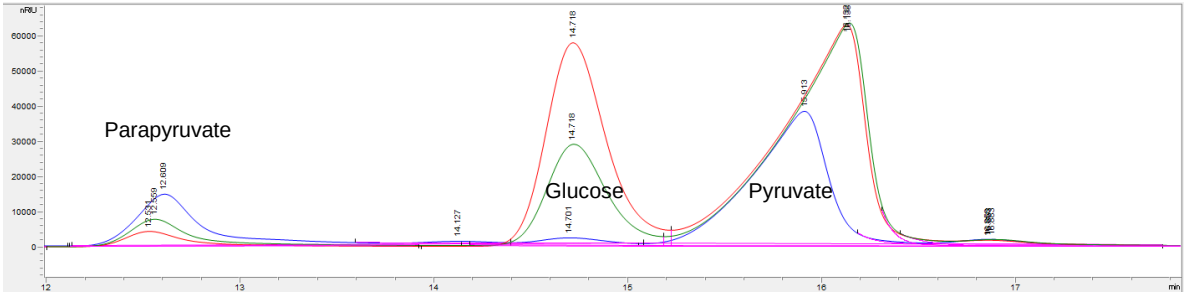

Figure A3: HPLC RI signal for a pyruvate process performed at 37 °C with a feed of 8 mM_{Ace} h^{-1}. The samples were taken at the following times: 10 h (red), 12 h (green), and 20 h (blue).